SANDIA REPORT

SAND98–2034
Unlimited Release
Printed September 1998

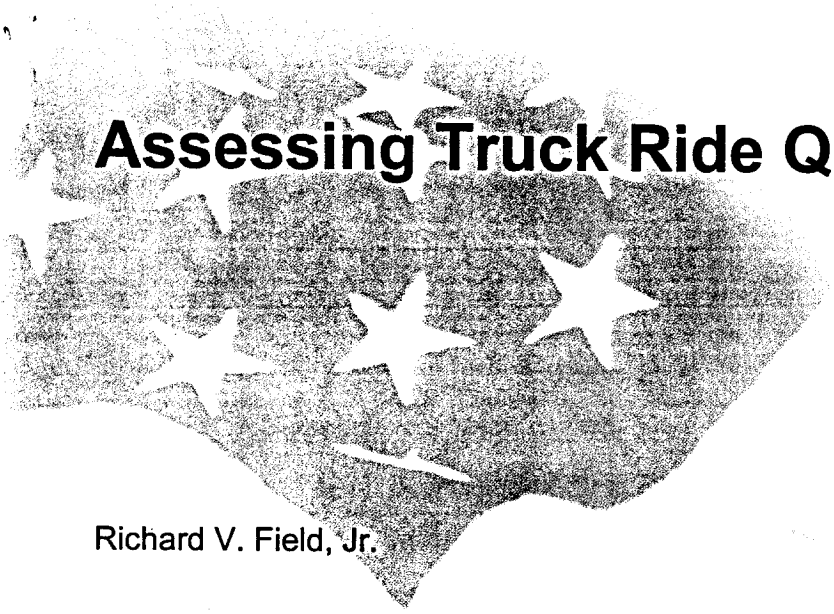

Assessing Truck Ride Quality for Design

Richard V. Field, Jr.

Prepared by
Sandia National Laboratories
Albuquerque, New Mexico 87185 and Livermore, California 94550

Sandia is a multiprogram laboratory operated by Sandia Corporation, a Lockheed Martin Company, for the United States Department of Energy under Contract DE-AC04-94AL85000.

Sandia National Laboratories

Issued by Sandia National Laboratories, operated for the United States Department of Energy by Sandia Corporation.

Available to DOE and DOE contractors from
Office of Scientific and Technical Information
P.O. Box 62
Oak Ridge, TN 37831

Prices available from (615) 576-8401, FTS 626-8401

Available to the public from
National Technical Information Service
U.S. Department of Commerce
5285 Port Royal Rd
Springfield, VA 22161

NTIS price codes
Printed copy: A05
Microfiche copy: A01

SAND98-2034
Unlimited Release
Printed September 1998

Assessing Truck Ride Quality for Design

Richard V. Field, Jr.

Structural Dynamics and Vibration Control Dept.
Sandia National Laboratories
P.O. Box 5800
Albuquerque, NM 87185-0439

ABSTRACT

This report summarizes a three-year project to characterize and improve the ride quality of the Department of Energy (DOE) tractor/trailer. A high-fidelity computer model was used to simulate the vibrational response in the passenger compartment of the truck due to a common roadway environment. It is the intensity of this response that is indicative of the ride quality of the vehicle. The computational model was then validated with experimental tests using a novel technique employing both lab-based modal tests and modal data derived using the Natural Excitation Technique (NExT). The validated model proved invaluable as a design tool. Utilizing the model in a predictive manner, modifications to improve ride quality were made to both the existing vehicle and the next-generation design concept. As a result, the next-generation fleet of tractors (procurement process begins in FY98) will incorporate elements of a successful model-based design for improved truck ride.

Acknowledgements

The work presented here summarizes a three-year project to characterize and understand heavy truck dynamics and heavy truck ride. Many individuals made significant contributions to this effort, and the author would like to acknowledge them at this time:

Clark Dohrmann (Structural Dynamics and Vibration Control, Org. 9234) helped with model validation issues

Tom Carne, John Hurtado (Experimental Structural Dynamics, Org. 9119) performed all laboratory and road experiments and provided valuable modeling insight

Robert Baca (TSD Transportation Engineering, Org. 6313) and Barry Boughton (High Consequence Assess and Technology, Org. 6314) provided the funding, were able to obtain vehicles from the fleet for experimental work, provided feedback, and kept us on schedule

Table of Contents

This page intentionally left blank.

Nomenclature

c	viscous damping coefficient
g	acceleration of gravity
k	stiffness coefficient
rms	root mean square
DOE	Department of Energy
FRF	Frequency Response Function
$L(f)$	insertion loss function
MAC	Modal Assurance Criterion
MIF	Modal Indicator Function
NExT	Natural Excitation Technique
RSI	Ride Severity Index
$S(f)$	Power Spectral Density (PSD) function
SST	Safe Secure Trailer
ϕ_a, ϕ_t	Eigenvector from analysis (a) and test (t)
$(\ )^T$	matrix transpose
$E[\ ]$	expected value operator

This page intentionally left blank.

Introduction

Designing tractor/trailer style trucks that exhibit good ride characteristics has been a challenge to automotive engineers for decades [4,5]. Historical methods to improve cab-ride quality have included: altering the frame bending stiffness, introducing softer primary suspensions, and improving tire stability and driver seats [2]. The idea of a cab suspension system was first employed in heavy truck design more than two decades ago and consisted of an independent leaf spring assembly placed at each of the four corners of the cab [3]. Since then, the design of the typical cab suspension system has evolved into a fixed-front pivot combined with a spring/damper rear mount. It is this configuration that is commonly seen on the road today and will be analyzed for use with the Department of Energy (DOE) Transportation Safeguards Division (TSD) tractor.

The DOE is committed to researching ideas for improved heavy truck ride, because a smoother ride is less fatiguing to the operators and, hence, safer to everyone on the road. Previous work funded by Sandia internal DP R&D funds in this area (see Appendix) demonstrated that the addition of a cab isolation system may provide considerable ride improvements to DOE's existing fleet of tractors, as well as be a key ingredient for the next-generation of DOE vehicles to be purchased starting in late FY98.

The purpose of this report is to summarize all "lessons learned" about heavy truck modeling and design for ride quality over the three-year history of this project. At the beginning of the project, some DOE couriers complained of fatigue experienced during a mission, due to the fact that it was difficult to sleep in the bunk. This project was initiated to identify the cause of this and prevent it from propagating into future designs. The ingredients necessary for improved ride quality were discovered through continued use of a computational model. Results were passed on to the next-generation tractor design team. This report summarizes those ingredients and will show how the validated model was an essential part of the preliminary design of the next-generation tractor.

Computational Model Development

Figure 1 illustrates a schematic of the current DOE tractor, including some of the terminology commonly used in the heavy truck community. The driver is located in the cab, and any off-duty personnel lie on the bunk in the sleeper compartment. The vehicle is currently configured in a separate cab / sleeper arrangement, meaning that there is no structural member connecting the cab and sleeper compartments.

The MSC/NASTRAN computational model of the DOE tractor is shown in Fig. 2. A two-axle trailer connected to the tractor at the fifth wheel is also modeled, representing the Safe Secure Trailer (SST) used by DOE to transfer defense cargo. Novel system identification approaches were used to validate this model, employing both lab-based modal tests and modal data derived using the Natural Excitation Technique (NExT) [6], a scheme that utilizes the roadway surface as a natural forcing function. Please see the Appendix for a detailed description of the computational model development and validation process.

Throughout the project, experimental testing proved an essential element in creating a valid model of the vehicle. Private vendors that supplied DOE with hardware on the tractor (suspension systems, tires, bushings, etc.) were unable or unwilling to provide information on how to properly

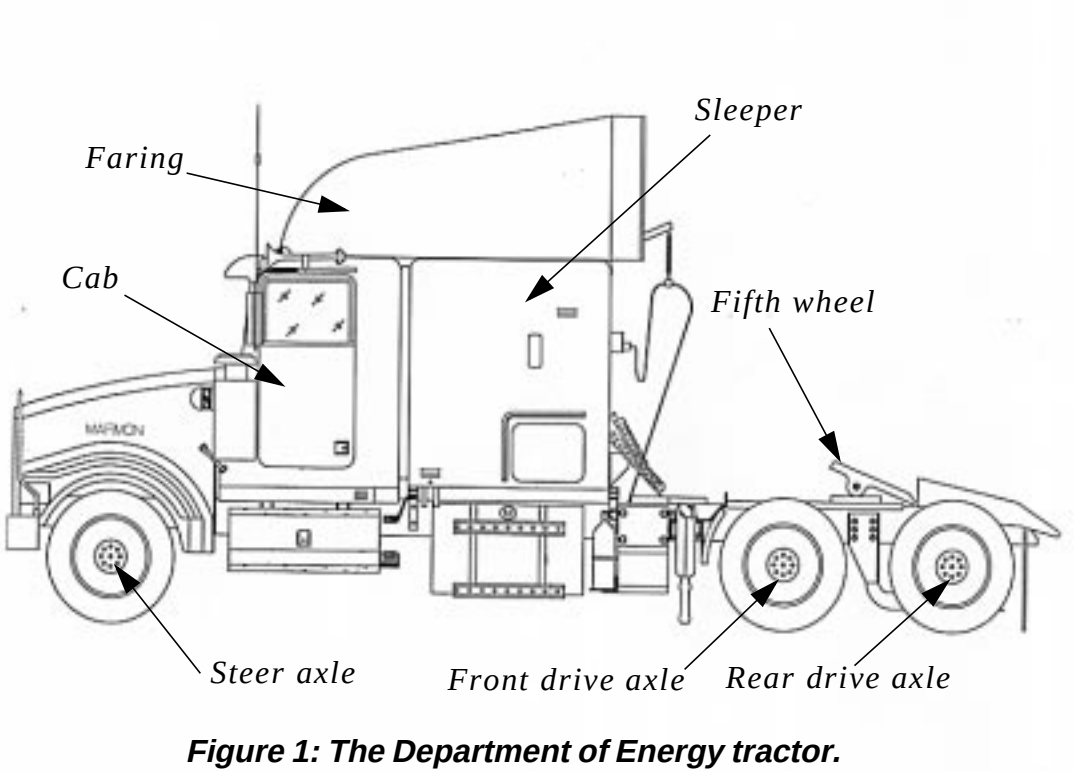

Figure 1: The Department of Energy tractor.

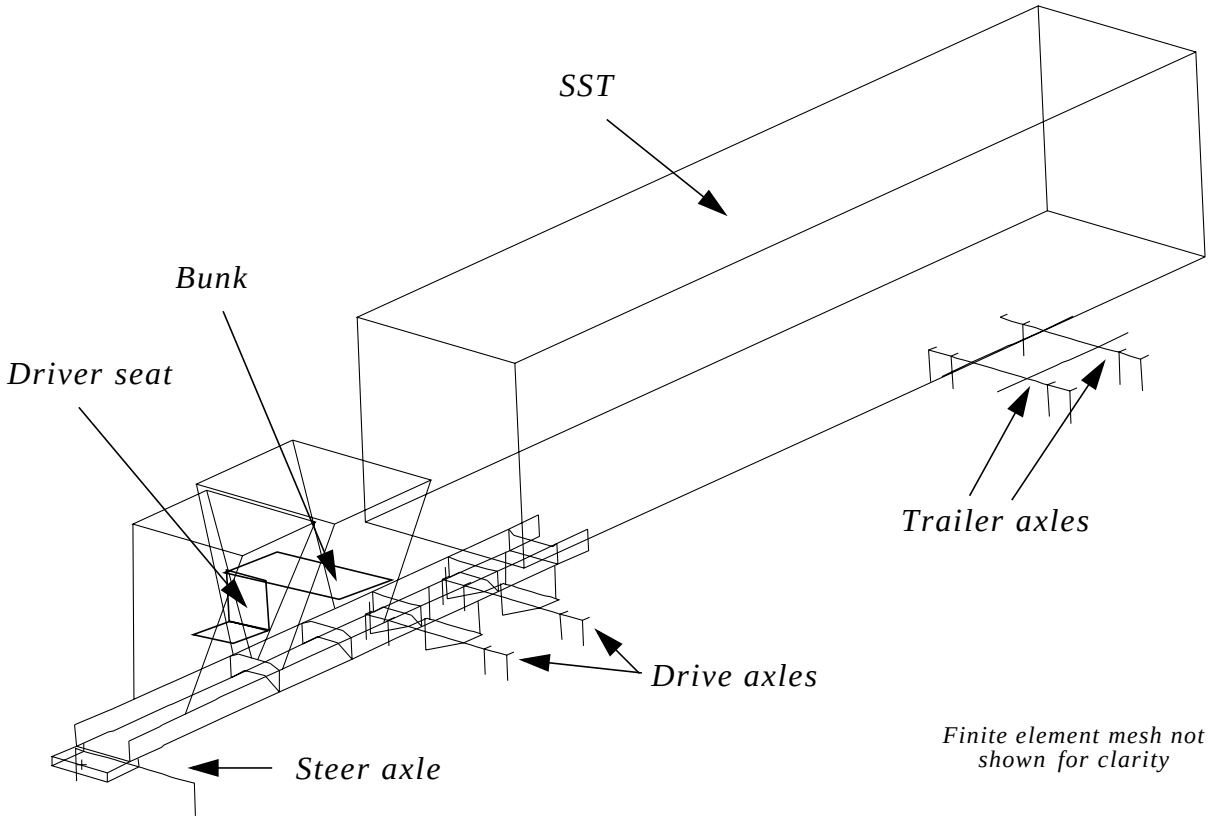

Figure 2: Computational model of the Department of Energy tractor.

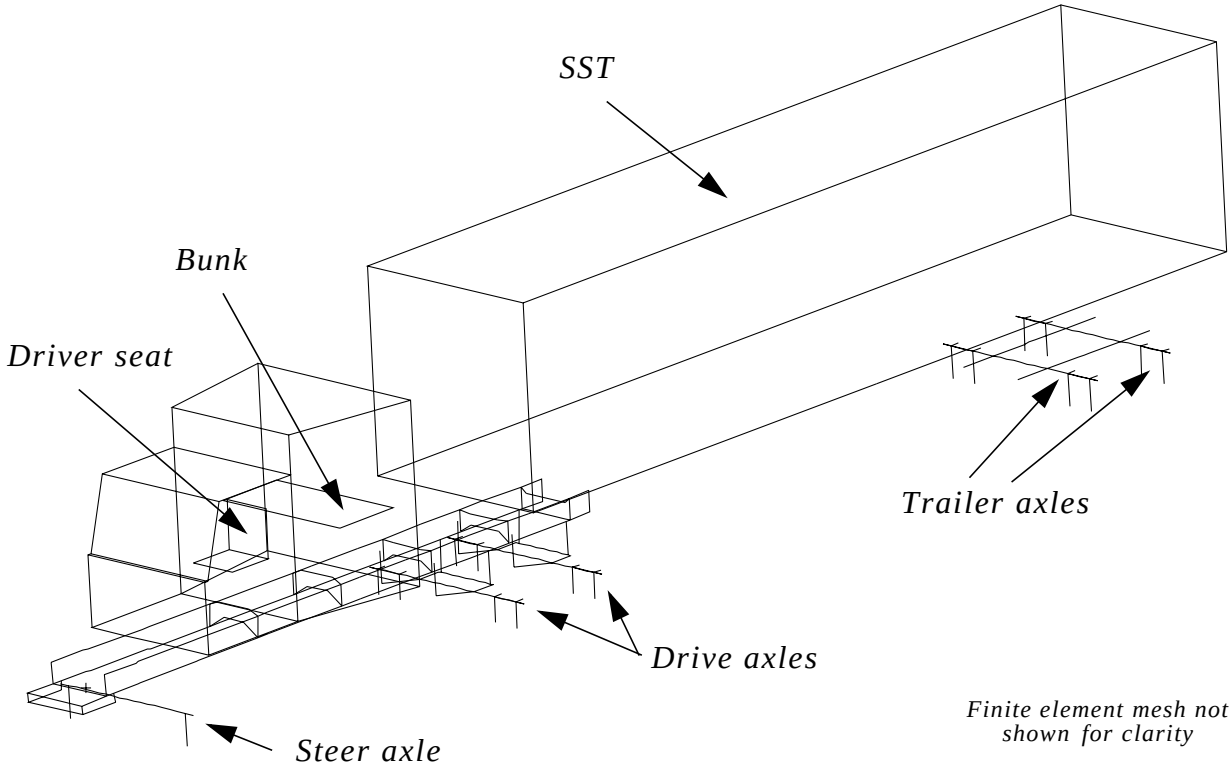

Figure 3: Computational model of the next-generation tractor design.

model their product. As a result, the huge uncertainty in predicted response would have rendered the model useless without experimental validation testing.

Utilizing the "lessons learned" from modeling the existing vehicle, a computational model was constructed of the next-generation design, as shown in Fig. 3. Note that when constructing the new model, the original model was used as the starting point, with most major modifications listed in Table 1. Because of the numerous validation efforts performed on the original model, one can be confident of the predictive capabilities of this new next-generation vehicle model.

Ride Quality Predictions for Next-Generation Design

To predict ride quality, excitation from a simulated road surface is supplied as input to the computational model. This is formulated as a random vibration problem, and it is the severity of vibration at key locations on the vehicle that is of interest.

The ride severity index (RSI), a weighted measure of the power of the output response, is indicative of the ride quality at a particular point

$$RSI = \sqrt{\int_{f_1}^{f_2} L(f)^2 S(f) df}, \qquad \text{(EQ 1)}$$

Table 1: Parameters from original model and next-generation model

Parameter	Original vehicle	Next-generation vehicle
cab mass	4968 *lb*	3012 *lb*
cab front mount stiffness	50 *kip/in* (vertical) 20 *kip/in* (radial)	29 *kip/in* (vertical) 6 *kip/in* (radial)
cab isolation system	N/A	200 *lb/in* (x 2)
steer axle stiffness	7067 *lb/in* (each axle end)	1500 *lb/in* (each axle end)
steer axle location	25.75 *in* aft of cm #1	36 *in* aft of cm #1
wheelbase	231 *in*	224 *in*

where $S(f)$ is the output power spectral density function and $f \in [f_1, f_2]$ denotes the frequency band of interest. Note that the RSI is a scalar quantity that is simply a weighted sum of the output PSD. The insertion loss factor, $L(f)$, is a quantity indicative of the human body's sensitivity to vibration and is applied as a filter to the output response. The higher the loss factor, the more sensitive the human is to the excitation [1]. For a detailed discussion of the specifics on calculating the RSI, refer to the Appendix.

One simulated output PSD is shown in Fig. 4, where the solid and dashed lines represent the response of the current design and next-generation design, respectively. The dotted lines indicate the frequencies at which symmetric structural modes occur. Peaks in the PSD response indicate that a particular mode was excited by the road surface input. Note the peak introduced around 1.75 *Hz*. This is due to excitation of the mode created with the addition of the cab isolation system. By definition, the isolation system isolates the cab from the tractor frame above its resonant frequency. Here, this leads to a significant reduction of the response of the original vehicle near 3 *Hz*. With this in mind, one would expect a significant improvement in ride quality moving from the original to the next-generation vehicle.

The ride severity was analytically calculated for both the current vehicle and the next-generation design. These predictions, along with experimental measurements of the RSI for the current vehicle, are shown in Table 2. First, note that there is good agreement between the analytical predictions and experimental measurements of ride quality for the current vehicle. The ride is a little less severe at the bunk than at the driver seat. Second, the numbers illustrate that the next-generation design will likely exhibit superior ride quality at the driver seat. This can be attributed to three things: (1) the addition of the cab isolation system, (2) the cab weight decreased by nearly 40%, and (3) the old steel leaf spring suspension at the steer axle has been replaced with a composite spring assembly that exhibits nearly 80% lower spring rate.

There is no doubt that adding an isolation system under the cab will improve ride quality, but previous studies in this area met with limited success. Previously, stiff air springs in the isolation system were required to support the static load of the much heavier cab, placing its resonant frequency too high and thereby limiting its ability to "isolate" the cab from the other modes of the

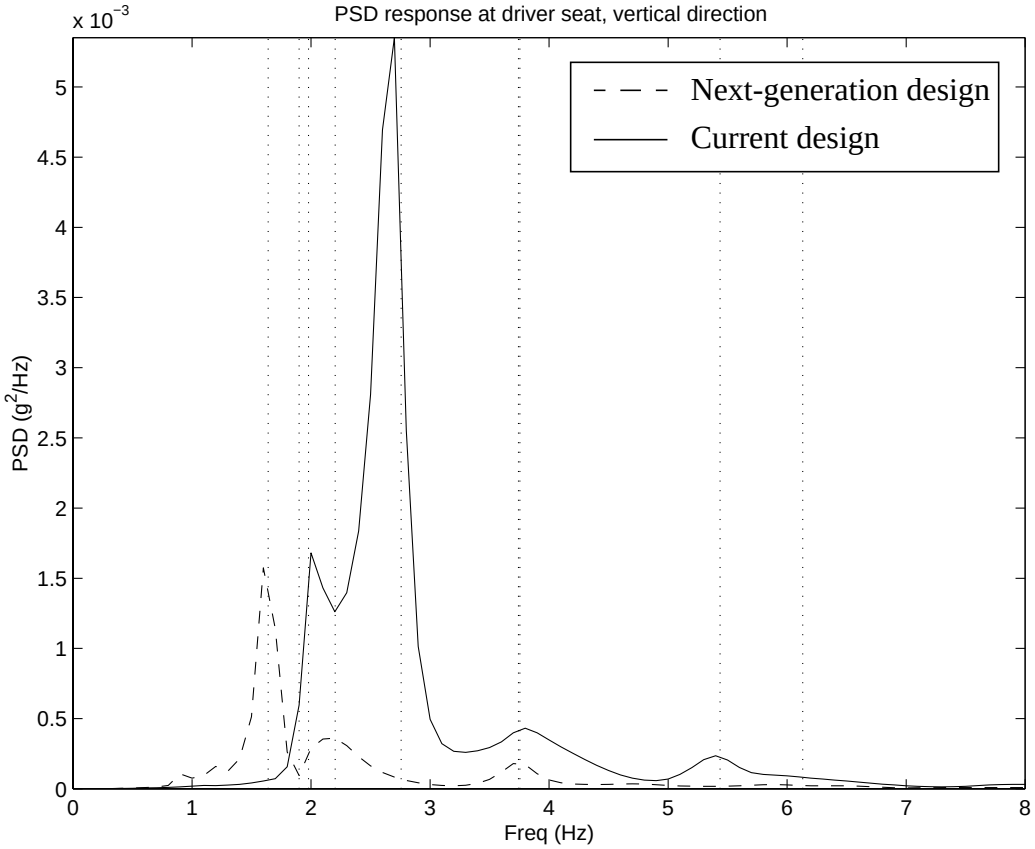

Figure 4: PSD response at driver seat for the current design and next-generation design.

vehicle. The reduced weight in the next-generation design allows for softer springs which can further separate the cab isolation modes from the vehicle modes, allowing it to "isolate" the cab to its full potential.

It is important to note that the computational model of the next-generation vehicle has not been correlated with experimental data. There has been, however, an extensive effort to validate the model of the current vehicle, which proved quite successful (see Appendix). Because this new model contains, in most instances, only slight modifications from the original validated model, one

Table 2: Ride Severity for current vehicle and next-generation design

	RSI at driver seat (*mg rms*)	RSI at bunk (*mg rms*)
Current vehicle (experimental)	59.32	50.99
Current vehicle (analytical)	61.16	52.56
Next-generation vehicle (analytical)	45.08	*

can place a high degree of confidence in its predictive capabilities. Nevertheless, the model of the next-generation vehicle will be validated with experimental data when it becomes available.

One inadequacy of the model must be addressed at this time. In all cases, the cab was represented as a rigid body. While this may be adequate when modeling the current vehicle, the flexibility of the much longer and more compliant unicab can no longer be ignored when modeling the next-generation design. Therefore, missing from Table 2 is the RSI for the new design at the bunk because it is expected that the response at the bunk will largely be effected by the flexing of the cab. This inadequacy of the model will be addressed in the future, if funding allows.

Summary and Conclusions

A computer model of the DOE tractor/trailer has been validated using a combination of modal and road test data. The computer model proved useful in explaining many complex features of heavy truck dynamics and proved to be an invaluable tool when considering the design of the next-generation tractor. With this tool, an un-validated computational model of the next-generation vehicle was also constructed and used to perform ride quality predictions. Results show that one can expect superior ride in the new design. Future work will look at validating these predictions with experimental data.

References

1. Evaluation of Human Exposure to Whole-Body Vibration," International Organization for Standardization, ISO 2631/1-1985(E).

2. Flower, W., "Analytical and Subjective Ride Quality Comparison of Front and Rear Cab Isolation Systems on a COE Tractor," *Society of Automotive Engineers*, No. 780411, pp. 1917-1929, 1978.

3. Foster, A.W., "A Heavy Truck Cab Suspension for Improved Ride," *Society of Automotive Engineers*, No. 780408, pp. 1899-1916, 1978.

4. Gillespie, T.D., *Fundamentals of Vehicle Dynamics*, Society of Automotive Engineers, 1992.

5. Gillespie, T.D., "Heavy Truck Ride", Society of Automotive Engineers, The Thirty-First L. Ray Buckendale Lecture, SP-607, 1985.

6. James, G.H., T.G. Carne, and J.P. Lauffer, "The Natural Excitation Technique (NExT) for Modal Parameter Extraction from Operating Structures," *International Journal of Analytical and Experimental Modal Analysis*, Society of Experimental Mechanics, Vol. 10, No. 4, October, 1995, pp. 260-277.

Appendix

1) DOE Tractor Trailer Modal Test / Analysis Reconciliation
2) DOE Tractor Trailer Rough Road Simulation
3) Optimal Cab Suspension for Next-Generation Armored Tractor
4) Structural Dynamics Modeling and Testing of the DOE Tractor Trailer
5) Analytical and Experimental Assessment of Heavy Truck Ride
6) Analytical Assessment of Proposed Four-Point Cab Isolation System

date: October 22, 1996

Albuquerque, New Mexico 87185

to: Distribution

from: R. V. Field, Jr. and C. R. Dohrmann, Dept. 9234, MS0439

subject: DOE Tractor Trailer Modal Test/Analysis Reconciliation

1. Summary

The preliminary model presented here is the second phase in a combined analytical and experimental effort to investigate possible improvements in the ride quality of the DOE armored tractors. The focus herein is to augment the experimental test results, as presented in [1-2], with the use of a high quality computer model. This report will discuss finite element modeling of the frame, cab, suspension systems, and other major components contributing to the overall dynamics of the vehicle. The techniques employed to update the model so that it correlates with modal test results will also be presented. Preliminary results indicate that the predictions from the finite element model agree well with results from the experimental modal tests.

2. Finite Element Model

Figure 2 illustrates the MSC/NASTRAN finite element model of the DOE Armored Tractor with Safe Secure Trailer (SST).

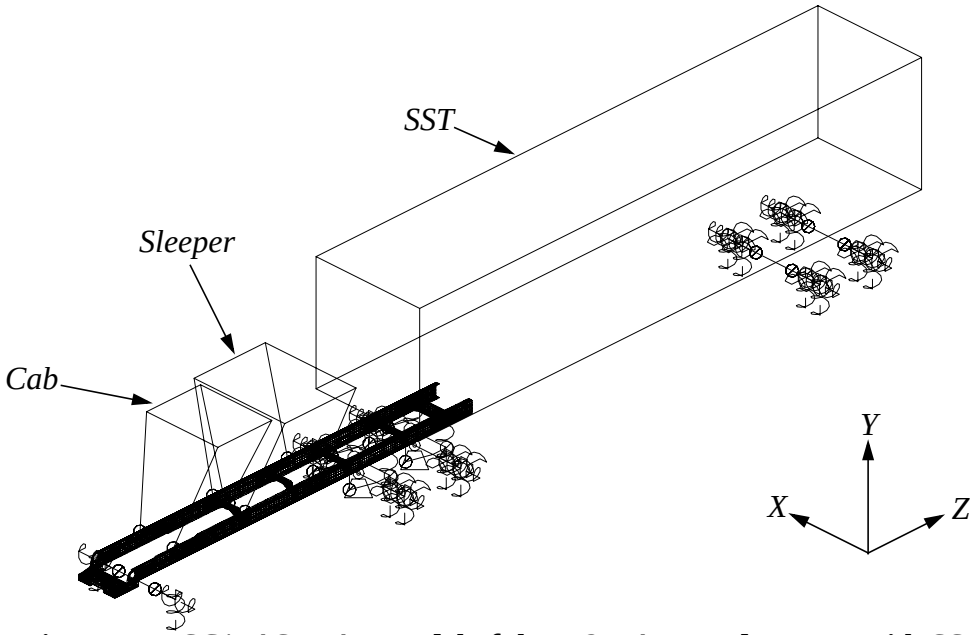

Figure 2: MSC/NASTRAN model of the DOE Armored Tractor with SST.

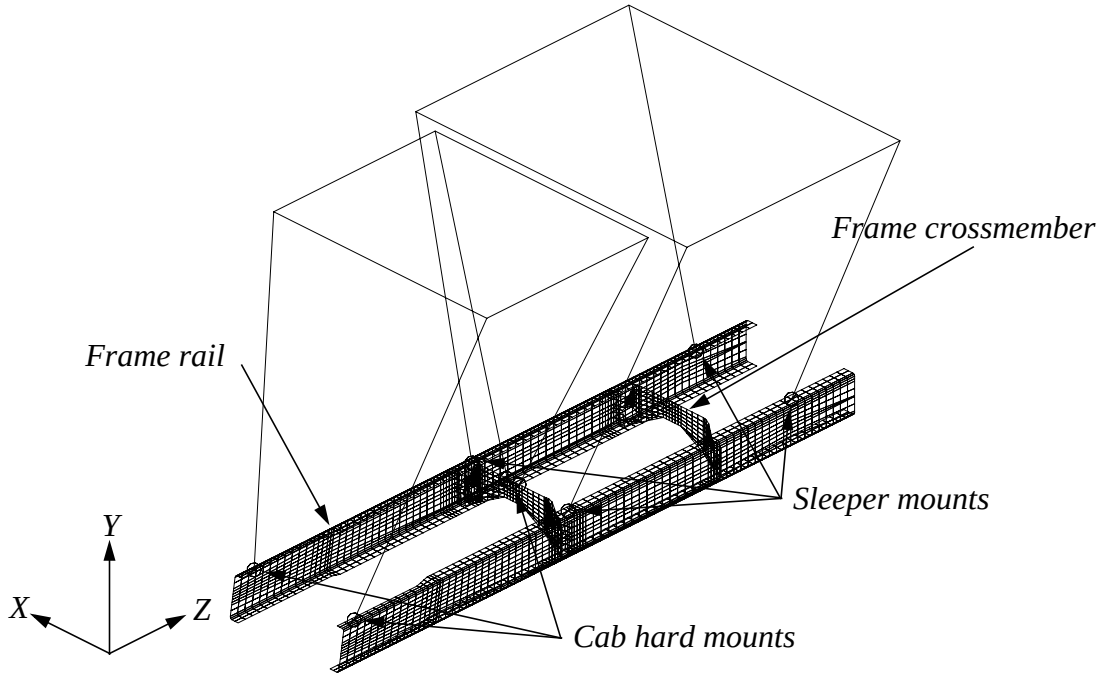

Figure 3: Cab and sleeper mount models.

Currently, the cab, sleeper, and SST are modeled as rigid body elements; each has a concentrated mass element associated with it located at the center-of-mass, and appropriate rigid element connections join these point masses to the remainder of the vehicle. One particular interface is located at the fifth wheel, where the tractor and SST connect. The fifth wheel itself is modeled as a point mass, including the effects of the steel mounting plate that adds significant stiffness to the tractor frame. At the top of the fifth wheel is the king pin, which allows relative rotation in the X and Y directions between the tractor and trailer. Another interface is shown in Fig. 3, where linear springs model the cab and sleeper "hard-mounts" to the truck frame. These mounts exhibit stiffness in the three translational directions, and are situated in a 3-point and 4-point configuration, respectively. The tractor frame and crossmembers are modeled with a large number of QUAD elements that capture the frame elastic modes.

A detailed view of the steer axle suspension system is illustrated in Fig. 4, where the leaf spring is modeled as a simple linear spring in the vertical direction, and "very stiff" in the remaining five directions. The leaf spring is rigidly connected to both the steer axle and the truck frame. A linear tire model is used here, consisting of two spring elements that represent the effective stiffness in the vertical and lateral directions. Note that this is valid since only small displacements are expected in a modal test. There is no fore/aft stiffness for the tire because there are no brakes on the steer axle. Lastly, the axle model is a series of NASTRAN BEAM elements.

Figure 5 contains a detailed view of the Neway AD-246 suspension system used on both the front and rear tractor drive axles. Each suspension system utilizes a trailing arm, modeled as a rigid link, an airbag, modeled as a linear spring in the axial direction only, and

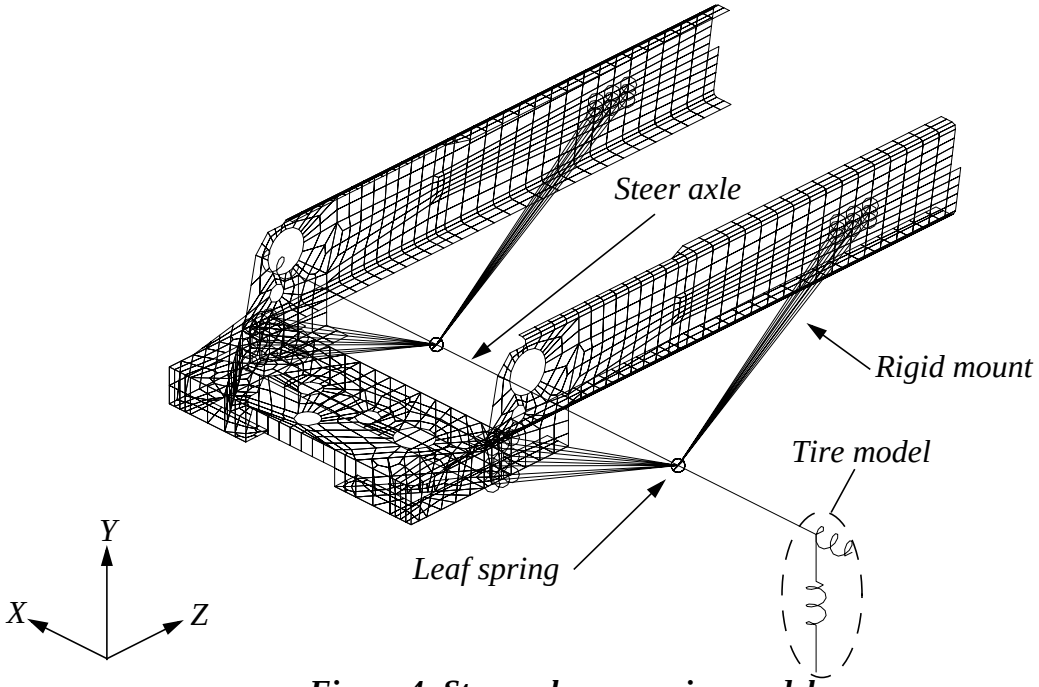

Figure 4: Steer axle suspension model.

anti-roll bar, modeled as a series of BEAM elements. The AD-246 also contains two shock absorbers (just in-board of the airbags) that connect the anti roll-bar to the frame cross-members. These were not modeled, however, since the experimental modal tests were performed with them disconnected. The tires (each axle contains four) are modeled identical to those on the steer axle, with one exception - an additional spring can be included to model the combined brake/tire stiffness in the fore/aft direction. This allows the NASTRAN model to simulate the vehicle modal response with and without the brakes applied. As before, the front and rear axles were modeled as a series of BEAM elements.

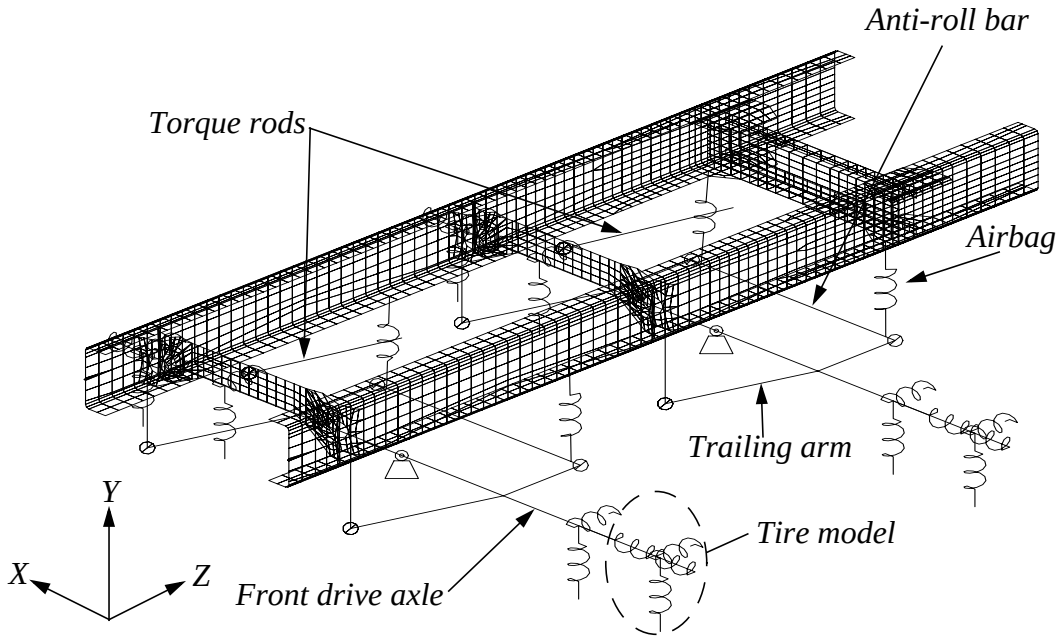

Figure 5: Drive axle suspension model.

The suspension systems on the SST also utilize leaf springs, but with a much higher spring rate. Similarly, modal testing was performed with and without the brakes on the trailer, leading to a tire model identical to that on the tractor drive axles.

3. Test/Analysis Correlation

In order to obtain good agreement between a finite element model and modal test results, it is often necessary to change the values of some uncertain parameters in the model. Six of the parameters that were updated in this study are shown in Table 3. The original parameter values lead to large errors in the frequencies of the model. In addition, the mode shapes did not correlate well, as indicated by poor initial MAC values. These rather large discrepancies can be attributed to a lack of information needed to provide estimates for initial stiffnesses of the various suspensions and tire/wheel assemblies. Updated parameter values were obtained using the in-house code PESTDY (Parameter Estimation for STructural DYnamics). Six frequencies from the brakes-on test and five frequencies from the brakes-off were used by PESTDY to determine the updated parameter values.

A few comments concerning the results of the test/analysis correlation are in order. Because the correlation was performed using modal test data, the updated parameters are associated with small amplitude motions. It is expected that some stiffnesses, such as those of the leaf springs, would be reduced in over-the-road environments where stiction effects are overcome. Efforts are currently underway to obtain stiffness and damping estimates directly from the transient response of driving the vehicle over a prescribed bump. Finally, it is noted that there remains some uncertainty as to the specific values of the tire vertical and suspension stiffnesses because these stiffness elements act together in series.

Table 3: Parameter changes due to model update

Parameter	Original	Updated
Tire vertical stiffness	4568 lb/in	11750 lb/in
Tire lateral stiffness	1500 lb/in	2080 lb/in
Tire fore-aft stiffness	2015 lb/in	2580 lb/in
Tractor leaf spring stiffness	2050 lb/in	8340 lb/in
Airbag stiffness	2100 lb/in	1040 lb/in
Trailer leaf spring stiffness	14000 lb/in	16350 lb/in

4. Results

Comparisons of analysis and test results for the brakes-on and brakes-off modal tests are shown in Tables 4 and 5, respectively. In addition to comparing the modal frequencies, the final column in the tables includes the Modal Assurance Criterion (MAC) values for the mode shapes. The MAC value between test mode shape ϕ_t and analysis mode shape ϕ_a is defined as

$$MAC(\phi_t, \phi_a) = \frac{(\phi_t \bullet \phi_a)^2}{(\phi_t \bullet \phi_t)(\phi_a \bullet \phi_a)} \quad (2)$$

MAC values are bounded between zero and unity. Values close to unity indicate good agreement between the test and analysis mode shapes. That is, the mode shapes are nearly parallel. MAC values close to zero indicate that the mode shapes are nearly perpendicular and not in good agreement.

It is evident from Tables 4 and 5 that the analysis frequencies and mode shapes are in good agreement with both the brakes-on and brakes-off modal tests. Visual comparisons of the analysis and test mode shapes are given in Figures 6-18. As was mentioned earlier, six frequencies from the brakes-on test and five frequencies from the brakes-off test were used to update parameter values. It is reassuring that the updated model accurately predicts the roll/twist #2 modal frequencies in both configurations (see final rows of Tables 4 and 5) even though these frequencies were not used in the test/analysis correlation.

Table 4: Test/Analysis comparison for brakes on.

Mode Description	Test Frequency (Hz)	Analysis Frequency (Hz)	Percent Error	MAC
roll/twist #1	1.10	1.08	-1.8	0.985
bounce	1.76	1.79	1.7	0.812
fore-aft	2.58	2.56	-0.8	0.786
pitch	3.40	3.32	-2.4	0.952
counter pitch	4.26	4.26	0	0.752
bending	6.28	6.17	-1.8	0.838
roll/twist #2	1.84	1.85	0.5	not available

Table 5: Test/Analysis comparison for brakes off.

Mode Description	Test Frequency (Hz)	Analysis Frequency (Hz)	Percent Error	MAC
roll/twist #1	1.09	1.08	-0.9	0.980
bounce	2.04	2.01	-1.5	0.867
pitch	3.19	3.22	0.9	0.939
counter pitch	4.16	4.12	-1.0	0.835

Table 5: Test/Analysis comparison for brakes off.

Mode Description	Test Frequency (Hz)	Analysis Frequency (Hz)	Percent Error	MAC
bending	5.96	6.06	1.7	0.830
roll/twist #2	1.76	1.76	0	not available

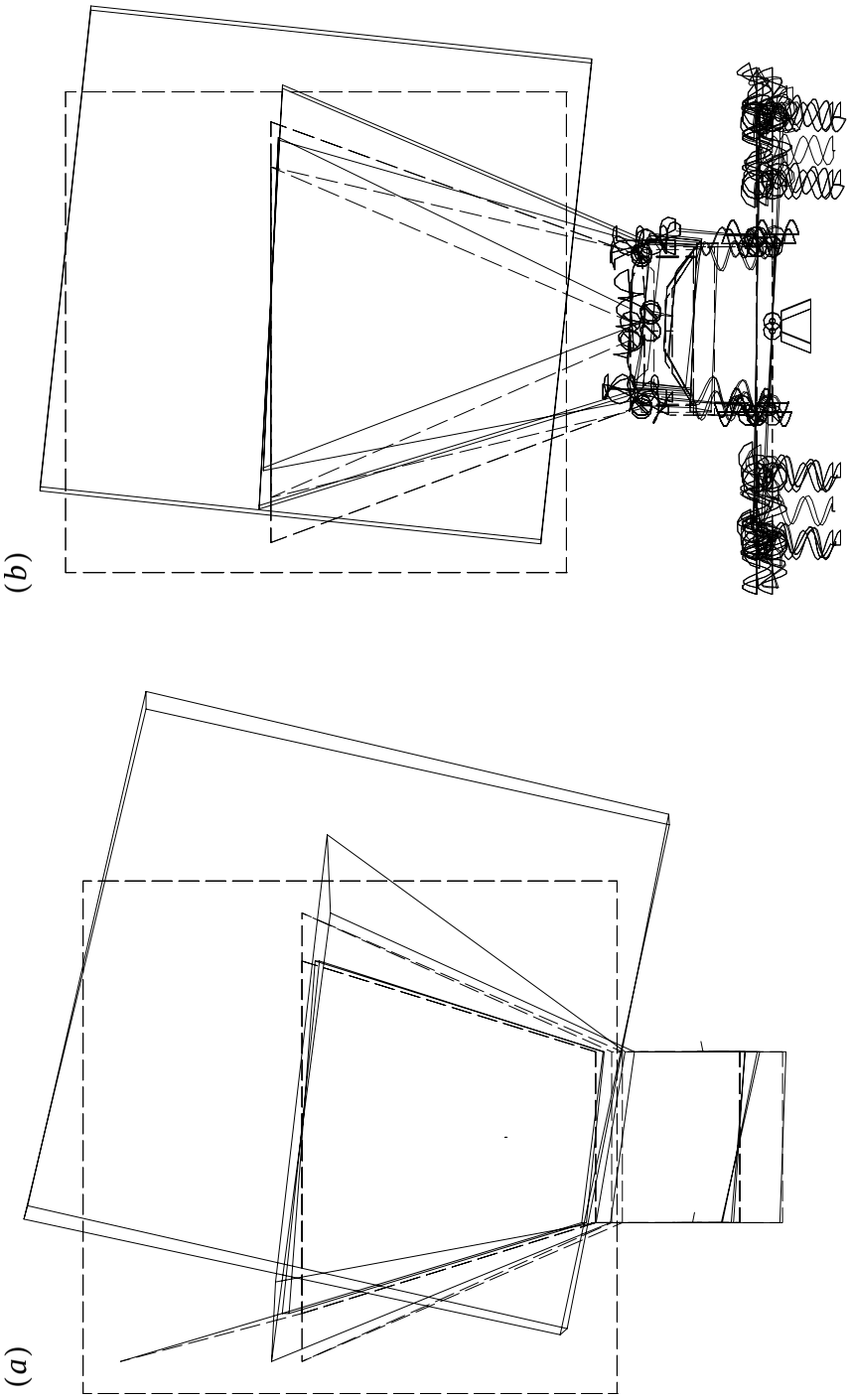

Figure 6: Roll/twist mode #1 (brakes on), experimental, (a), and analytical, (b).

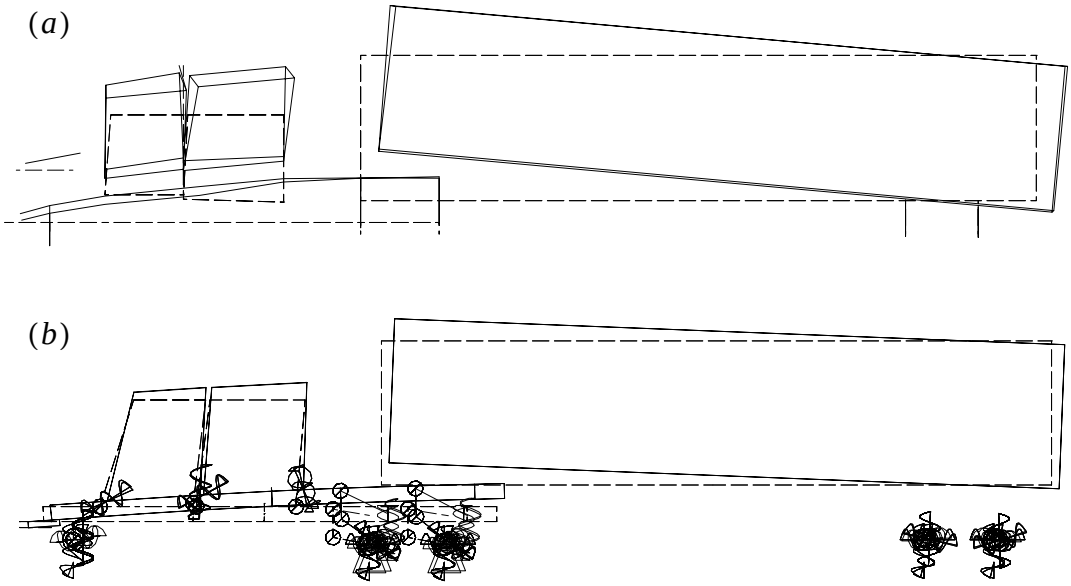

Figure 7: Bounce mode (brakes on), experimental, (a), and analytical, (b).

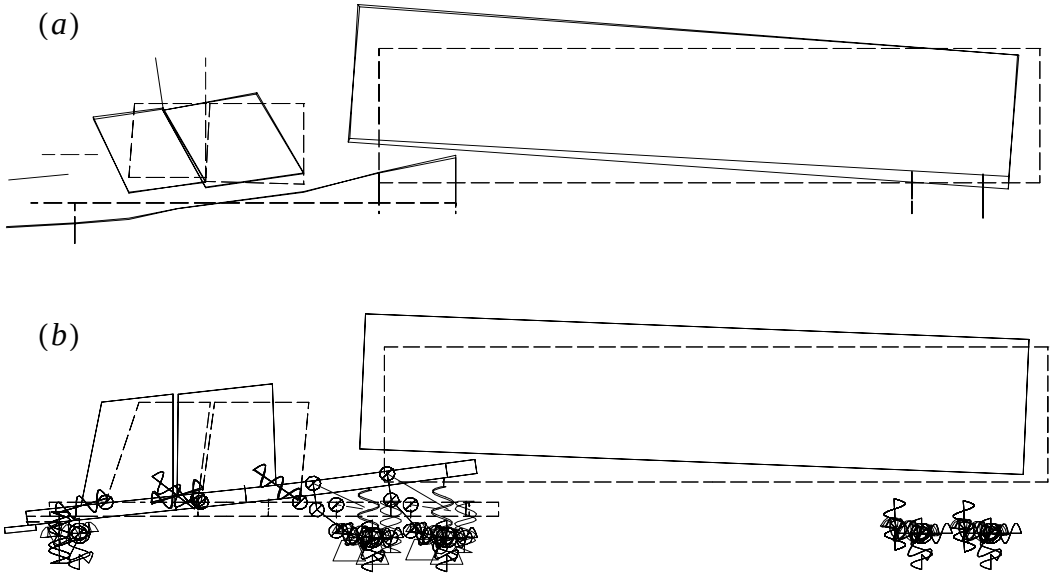

Figure 8: Fore-aft mode (brakes on), experimental, (a), and analytical, (b).

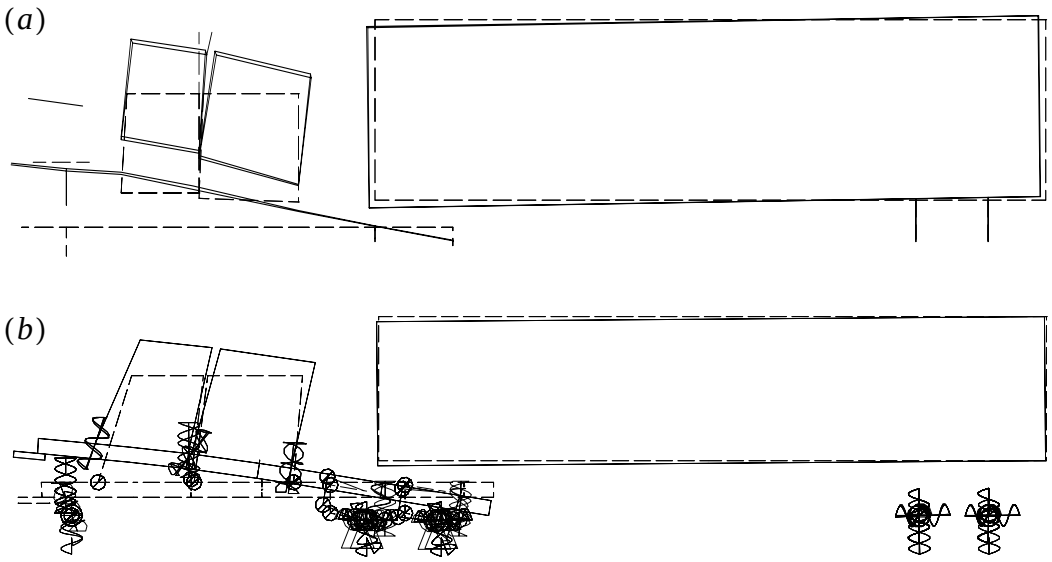

Figure 9: Pitch mode (brakes on), experimental, (a), and analytical, (b).

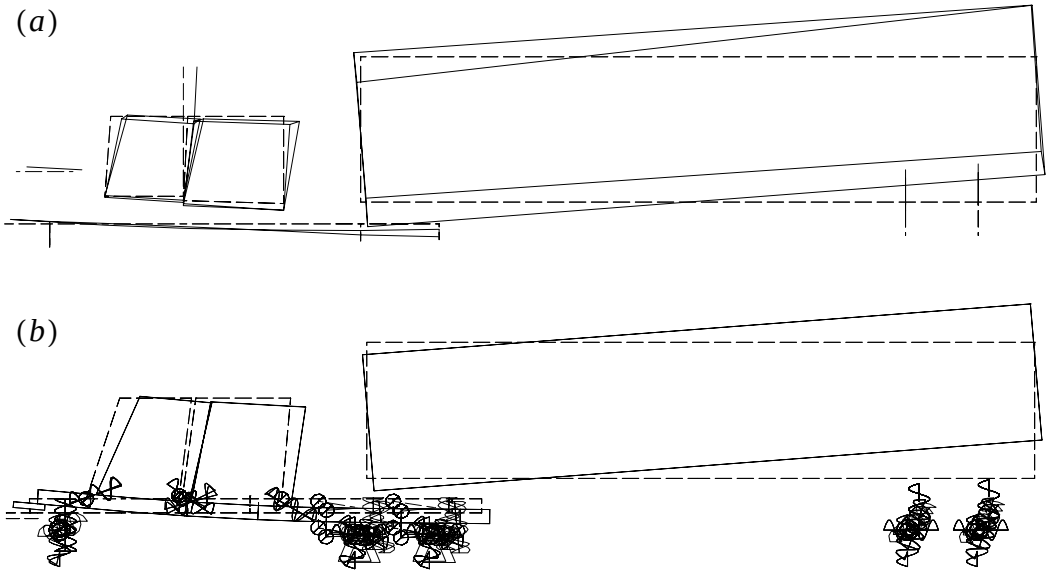

Figure 10: Counter-pitch mode (brakes on), experimental, (a), and analytical, (b).

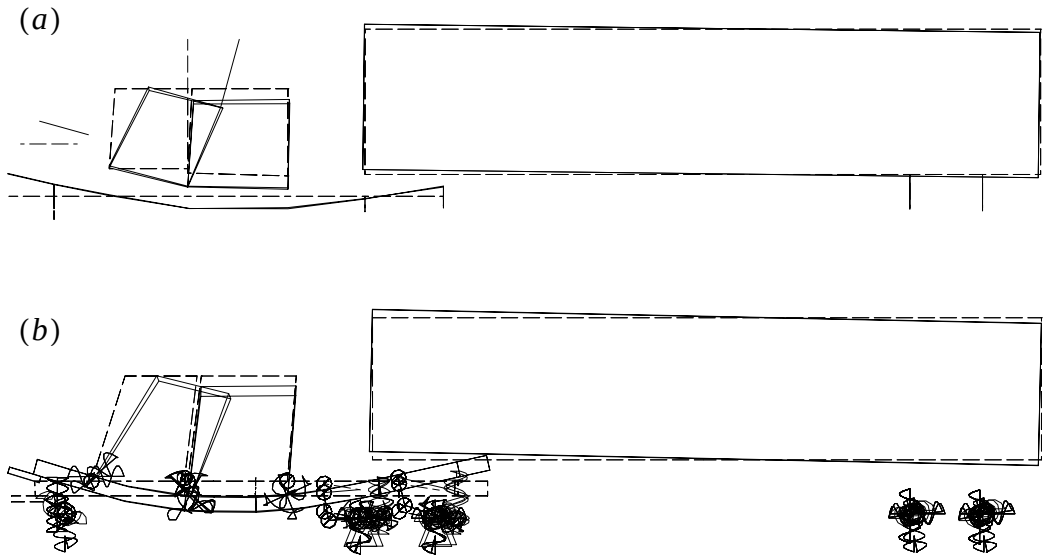

Figure 11: Frame bending mode (brakes on), experimental, (a), and analytical, (b).

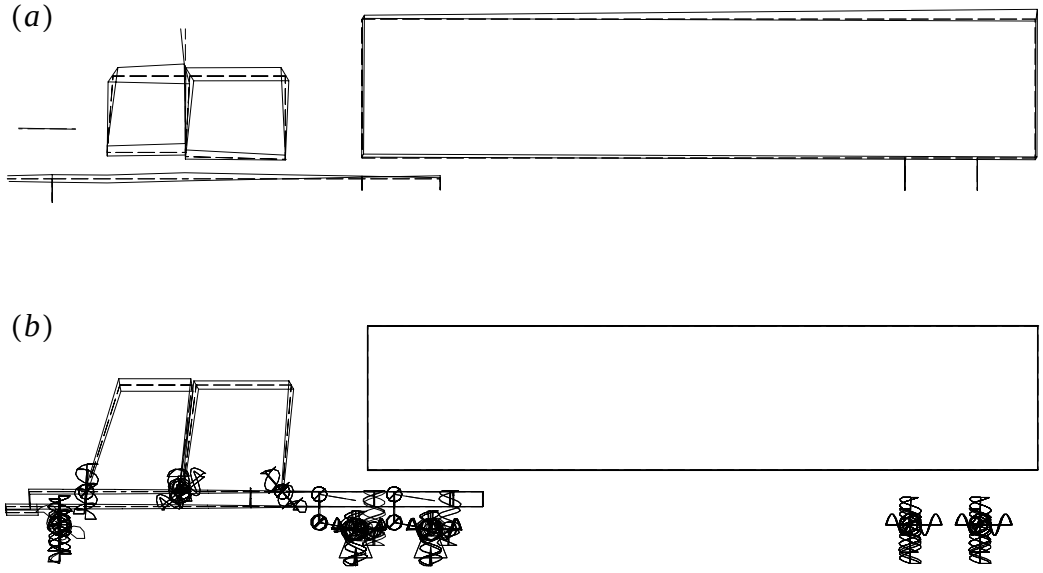

Figure 12: Roll/twist mode #2 (brakes on), experimental, (a), and analytical, (b).

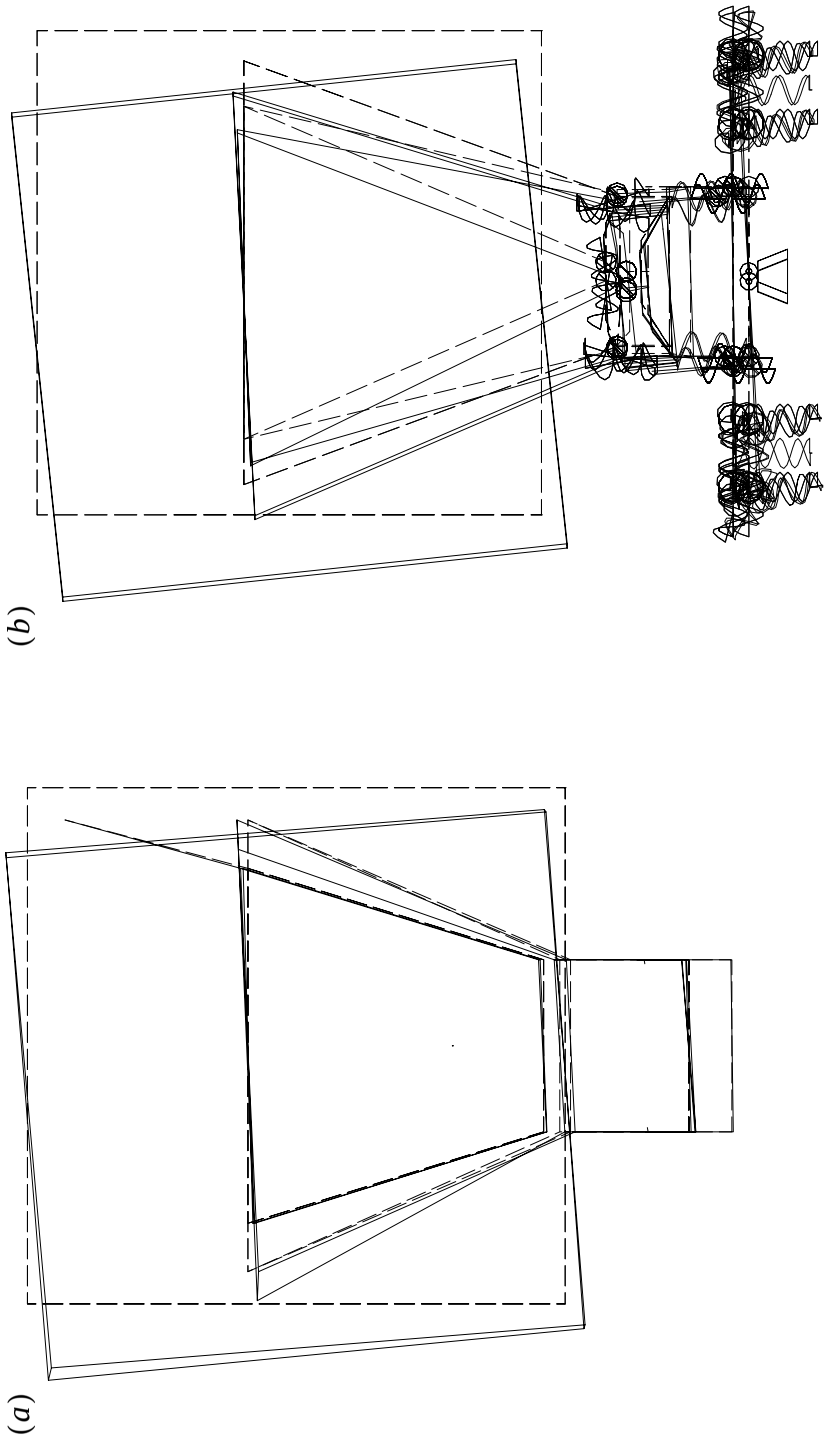

Figure 13: Roll/twist mode #1 (brakes off), experimental, (a), and analytical, (b).

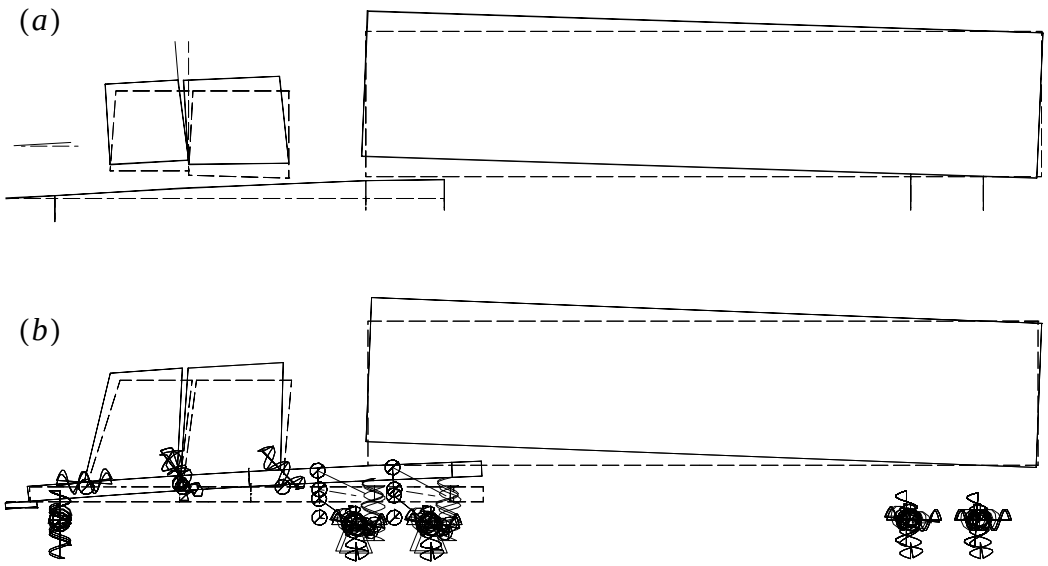

Figure 14: Bounce mode (brakes off), experimental, (a), and analytical, (b).

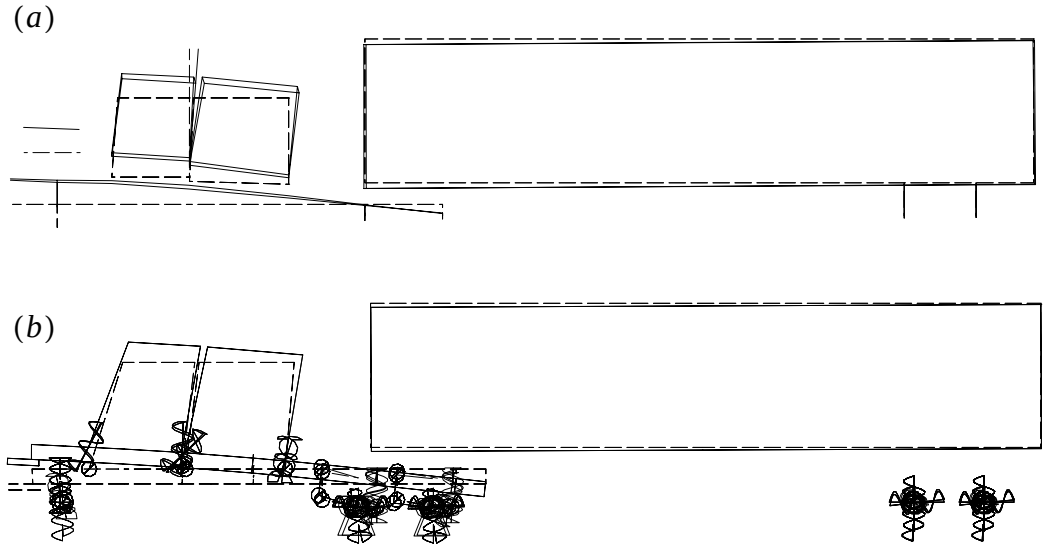

Figure 15: Pitch mode (brakes off), experimental, (a), and analytical, (b).

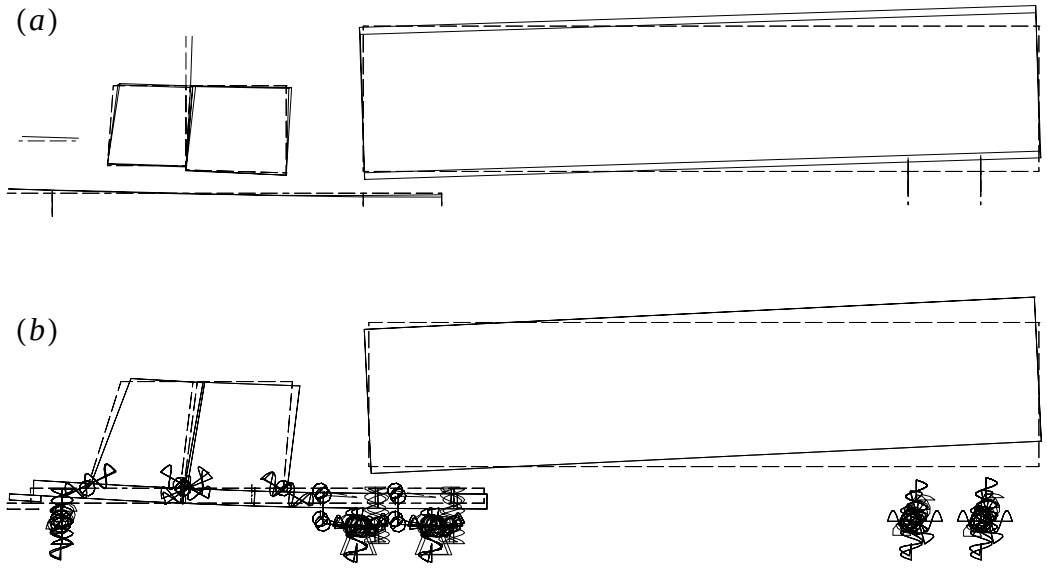

Figure 16: Counter-pitch mode (brakes off), experimental, (a), and analytical, (b).

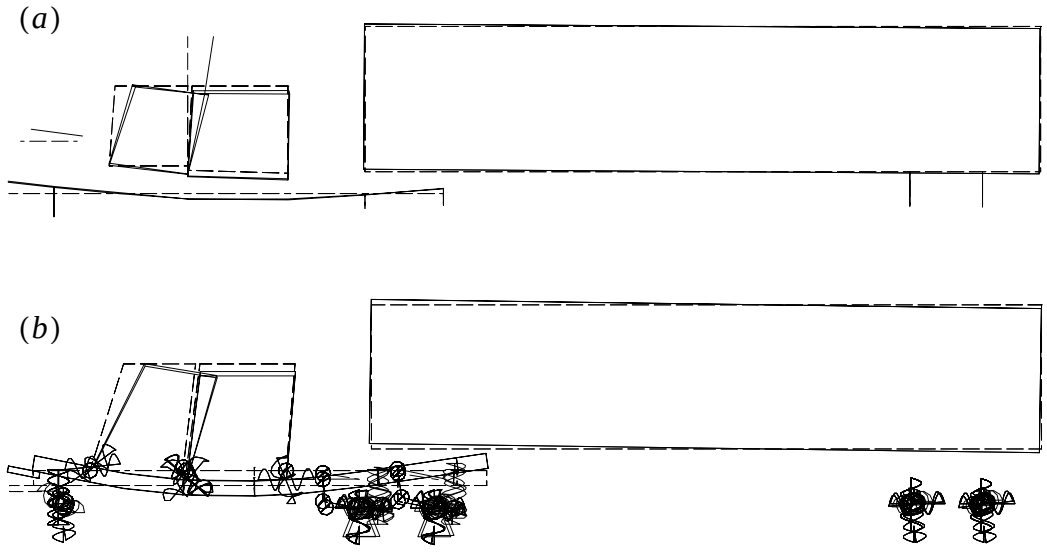

Figure 17: Frame bending mode (brakes off), experimental, (a), and analytical, (b).

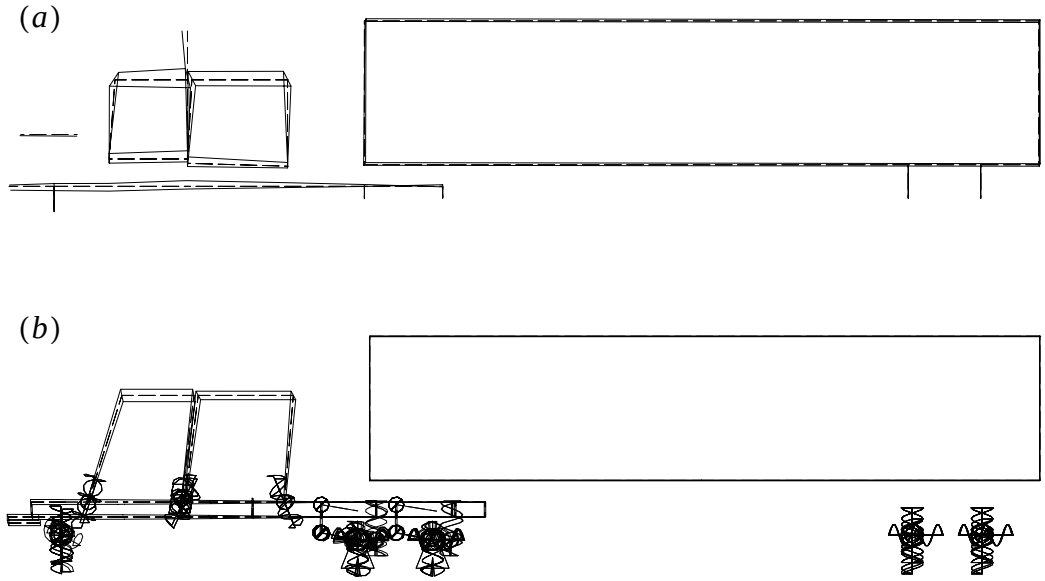

Figure 18: Roll/twist mode #2 (brakes off), experimental, (a), and analytical, (b).

5. Conclusions

The preliminary dynamic model of the DOE armored tractor with SST trailer correlates well with the characteristics seen during the experimental modal tests. As the model is refined, it is clear that it will be an integral tool in determining the design of the next-generation armored tractor. Any possible benefits to be gained from the use of available passive cab vibration suppression methods will be researched. In addition, the computer model can be used to examine any improvements utilizing active vibration control techniques.

References

7. Hurtado, J.E. and L.R. Dorrell, “Modal Testing of SST Armored Tractor Trailer,” memo to Distribution, Sandia National Laboratories, Albuquerque, NM, July 5, 1996.

8. Hurtado, J.E. and T.G. Carne, “Addendum to Modal Testing of SST Armored Tractor Trailer,” memo to Distribution, Sandia National Laboratories, Albuquerque, NM, July 10, 1996.

RVF: 9234

Copies To:

5503	A.K. Moonka	MS 0767
5512	B.D. Boughton	MS 0790
5513	R.G. Baca	MS 0790
5513	J.J. Roesch	MS 0790
9117	H.S. Morgan	MS 0443
9118	E.P. Chen	MS 0437
9215	P.D. Heermann	MS 0318
9234	C.R. Dohrmann	MS 0439
9234	G.R. Eisler	MS 0439
9234	R.V. Field, Jr.	MS 0439
9234	D.R. Martinez	MS 0439
9234	T.J. Baca	MS 0557
9741	T.G. Carne	MS 0557
9741	L.R. Dorrell	MS 0557
9741	J.E. Hurtado	MS 0557

Sandia National Laboratories

Albuquerque, New Mexico 87185

date: October 17, 1996

to: Distribution

from: R. V. Field, Jr., Dept. 9234, MS 0439

subject: DOE Tractor Trailer Rough Road Simulation

1. Summary

Frequency response and power spectral density analyses can be utilized to assess the vibratory response of automotive vehicles. This report contains preliminary results from such a study that simulates the DOE Armored Tractor with Safe Secure Trailer driving at 55 *m.p.h.* over a “rough road”. Some theoretical concepts are presented, and analytical results using the MSC/NASTRAN finite element program are discussed. Special emphasis is given to the issue of random loading and the cross-spectral density matrix that simulates the road input to an 18-wheel vehicle.

2. Finite Element Model

Figure 19 illustrates the MSC/NASTRAN 46,000 degree-of-freedom finite element model of the DOE Armored Tractor with Safe Secure Trailer (SST). For a detailed discussion of this model, see [11].

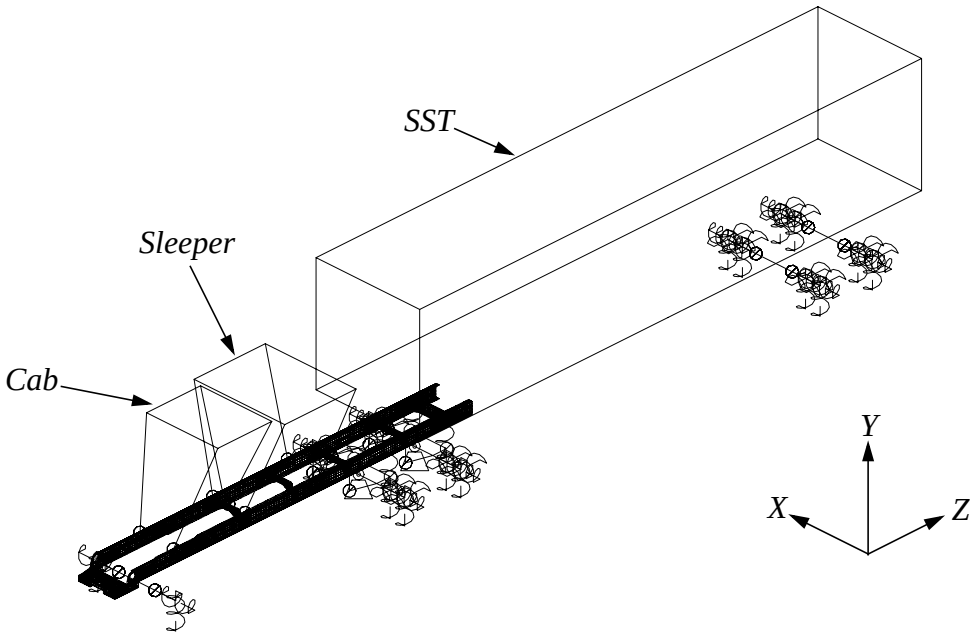

Figure 19: MSC/NASTRAN model of the DOE Armored Tractor with SST.

3. Input Spectrum Description

Most road surfaces have irregularities that are best described as random processes, and many can be accurately represented under an additional assumption of stationarity [13]. It is therefore relevant to study the vehicle response due to a stationary random "rough road" input at several key locations of the truck.

To apply this input PSD, knowledge of the cross-spectral density matrix of input forces is required. Assuming the vehicle is following a straight, constant speed trajectory, let W_1 and W_2 represent the amplitude seen by the left and right tires, respectively, due to the excitation of the road. For the studies presented here, it is assumed that the left and right tires experience the same road surface, but the two are not perfectly correlated. Define

$$\phi_{11}(\tau) = E[W_1(\tau)W_1(t+\tau)], \qquad \textit{(EQ 3)}$$

$$\phi_{22}(\tau) = E[W_2(\tau)W_2(t+\tau)], \qquad \textit{(EQ 4)}$$

$$\phi_{12}(\tau) = E[W_1(\tau)W_2(t+\tau)], \qquad \textit{(EQ 5)}$$

where $E[\cdot]$ is the expectation operator, $\phi_{11}(\tau)$ and $\phi_{22}(\tau)$ are the autocorrelation functions, and $\phi_{12}(\tau)$ is the crosscorrelation function representing the interaction between the left and right sides of the vehicle.

The schematic shown in Fig. 20. illustrates the 10 locations in which the "rough road" will excite the vehicle, assuming the dual wheel locations at stations 3 through 10 act together. The complete input power spectra is therefore characterized by a ten-by-ten matrix, where the elements of this matrix involve the Fourier transforms of Eqs. (3)-(5). Specifically, the two-by-two blocks on the diagonal of this matrix are of the form

$$\Phi_{2x2}(f) = \begin{bmatrix} k_{eff}^2\phi_{11}(f) & k_{eff}^2\phi_{12}(f) \\ k_{eff}^2\phi_{12}(f) & k_{eff}^2\phi_{22}(f) \end{bmatrix}, \qquad \textit{(EQ 6)}$$

where k_{eff} is the effective stiffness at the particular station of interest (*i.e.*, the collective vertical tire stiffness), and $\phi_{11}(f)$, $\phi_{12}(f)$, and $\phi_{22}(f)$ are the Fourier transforms of Eqs. (3)-(5). Note that by scaling Eq. (6) by the stiffness terms, the input is now a *force* power spectral density [10].

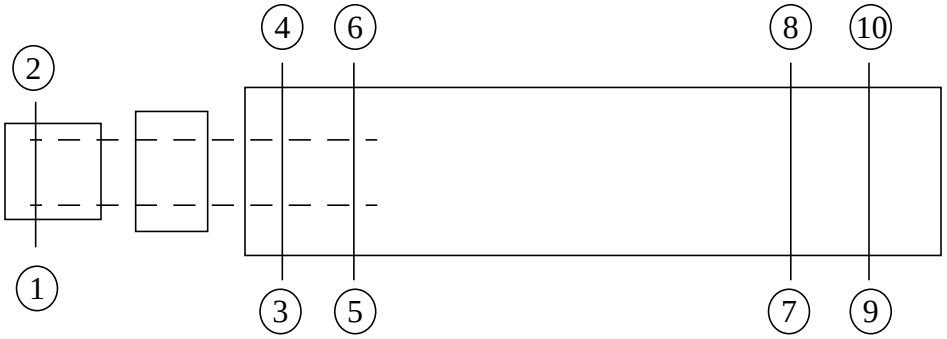

Figure 20: Input stations for the DOE Armored Tractor with SST.

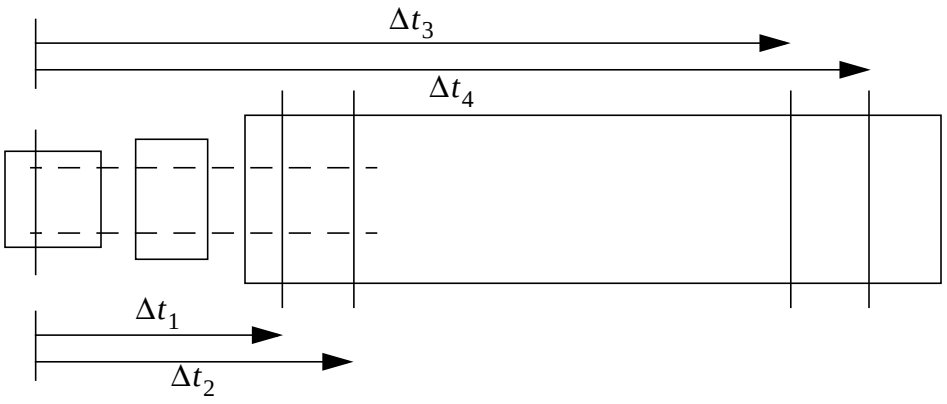

Figure 21: Input time delays for the DOE Armored Tractor with SST.

The remaining terms involve various degrees of correlation between the different axles. Since the vehicle is at a constant speed, this can be accomplished by delaying the input to the tractor front drive axle, as well as those behind it, as illustrated in Fig. 21.

To apply this in the frequency domain, recall the Time-Shifting Property of the Fourier transform

$$\textit{If } f(t) \Leftrightarrow F(\omega)\textit{, then } f(t-\tau) \Leftrightarrow F(\omega)e^{-i\omega\tau} \qquad \textit{(EQ 7)}$$

Therefore, for example, it is evident that to describe the crosscorrelation function for steer axle and front drive axle input force, the corresponding terms in the matrix must resemble

$$\Phi_{2x2}(f) = \begin{bmatrix} k_{eff}^{SA}k_{eff}^{DA}e^{-a}\phi_{11}(f) & k_{eff}^{SA}k_{eff}^{DA}e^{-a}\phi_{12}(f) \\ k_{eff}^{SA}k_{eff}^{DA}e^{-a}\phi_{12}(f) & k_{eff}^{SA}k_{eff}^{DA}e^{-a}\phi_{22}(f) \end{bmatrix}, \qquad \textit{(EQ 8)}$$

where k_{eff}^{SA} and k_{eff}^{DA} are the effective stiffnesses at the steer axle and drive axle, respectively, and $a = i2\pi f\Delta t_1$.

The full force input power spectral density matrix, $\Phi(f)$, is given by

$$\begin{bmatrix}
k^2\phi_{11} & k^2\phi_{12} & 2k^2e^{-a}\phi_{11} & 2k^2e^{-a}\phi_{12} & 2k^2e^{-f}\phi_{11} & 2k^2e^{-f}\phi_{12} & 2k^2e^{-g}\phi_{11} & 2k^2e^{-g}\phi_{12} & 2k^2e^{-h}\phi_{11} & 2k^2e^{-h}\phi_{12} \\
k^2\phi_{12} & k^2\phi_{22} & 2k^2e^{-a}\phi_{12} & 2k^2e^{-a}\phi_{22} & 2k^2e^{-f}\phi_{12} & 2k^2e^{-f}\phi_{22} & 2k^2e^{-g}\phi_{12} & 2k^2e^{-g}\phi_{22} & 2k^2e^{-h}\phi_{12} & 2k^2e^{-h}\phi_{22} \\
2k^2e^{a}\phi_{11} & 2k^2e^{a}\phi_{12} & 4k^2\phi_{11} & 4k^2\phi_{12} & 4k^2e^{-b}\phi_{11} & 4k^2e^{-b}\phi_{12} & 4k^2e^{-k}\phi_{11} & 4k^2e^{-k}\phi_{12} & 4k^2e^{-l}\phi_{11} & 4k^2e^{-l}\phi_{12} \\
2k^2e^{a}\phi_{12} & 2k^2e^{a}\phi_{22} & 4k^2\phi_{12} & 4k^2\phi_{22} & 4k^2e^{-b}\phi_{12} & 4k^2e^{-b}\phi_{22} & 4k^2e^{-k}\phi_{12} & 4k^2e^{-k}\phi_{22} & 4k^2e^{-l}\phi_{12} & 4k^2e^{-l}\phi_{22} \\
2k^2e^{f}\phi_{11} & 2k^2e^{f}\phi_{12} & 4k^2e^{b}\phi_{11} & 4k^2e^{b}\phi_{12} & 4k^2\phi_{11} & 4k^2\phi_{12} & 4k^2e^{-c}\phi_{11} & 4k^2e^{-c}\phi_{12} & 4k^2e^{-m}\phi_{11} & 4k^2e^{-m}\phi_{12} \\
2k^2e^{f}\phi_{12} & 2k^2e^{f}\phi_{22} & 4k^2e^{b}\phi_{12} & 4k^2e^{b}\phi_{22} & 4k^2\phi_{12} & 4k^2\phi_{22} & 4k^2e^{-c}\phi_{12} & 4k^2e^{-c}\phi_{22} & 4k^2e^{-m}\phi_{12} & 4k^2e^{-m}\phi_{22} \\
2k^2e^{g}\phi_{11} & 2k^2e^{g}\phi_{12} & 4k^2e^{k}\phi_{11} & 4k^2e^{k}\phi_{12} & 4k^2e^{c}\phi_{11} & 4k^2e^{c}\phi_{12} & 4k^2\phi_{11} & 4k^2\phi_{12} & 4k^2e^{-d}\phi_{11} & 4k^2e^{-d}\phi_{12} \\
2k^2e^{g}\phi_{12} & 2k^2e^{g}\phi_{22} & 4k^2e^{k}\phi_{12} & 4k^2e^{k}\phi_{22} & 4k^2e^{c}\phi_{12} & 4k^2e^{c}\phi_{22} & 4k^2\phi_{12} & 4k^2\phi_{22} & 4k^2e^{-d}\phi_{12} & 4k^2e^{-d}\phi_{22} \\
2k^2e^{h}\phi_{11} & 2k^2e^{h}\phi_{12} & 4k^2e^{l}\phi_{11} & 4k^2e^{l}\phi_{12} & 4k^2e^{m}\phi_{11} & 4k^2e^{m}\phi_{12} & 4k^2e^{d}\phi_{11} & 4k^2e^{d}\phi_{12} & 4k^2\phi_{11} & 4k^2\phi_{12} \\
2k^2e^{h}\phi_{12} & 2k^2e^{h}\phi_{22} & 4k^2e^{l}\phi_{12} & 4k^2e^{l}\phi_{22} & 4k^2e^{m}\phi_{12} & 4k^2e^{m}\phi_{22} & 4k^2e^{d}\phi_{12} & 4k^2e^{d}\phi_{22} & 4k^2\phi_{12} & 4k^2\phi_{22}
\end{bmatrix}$$

where $a = i\omega\Delta t_1$, $b = i\omega(\Delta t_2 - \Delta t_1)$, $c = i\omega(\Delta t_3 - \Delta t_2)$, $d = i\omega(\Delta t_4 - \Delta t_3)$, $f = i\omega\Delta t_2$, $g = i\omega\Delta t_3$

$h = i\omega\Delta t_4$, $k = i\omega(\Delta t_3 - \Delta t_1)$, $l = i\omega(\Delta t_4 - \Delta t_1)$, $m = i\omega(\Delta t_4 - \Delta t_2)$. *(EQ 9)*

This assumes that the vertical tire stiffness of each tire is identical and equal to k. Please note that the f-dependency of the ϕ 's in Eq. (9) is implied.

It has been found that terrain roughness can be represented in the frequency domain by power spectral density functions of the form

$$\Psi(\Omega) = c\Omega^{-n}, \qquad \textit{(EQ 10)}$$

where Ω is the spatial frequency, in units of *cycles/length*, and n and c are constants. As discussed in [9] and [13], $n = 2.0$ is typical. Therefore, for a vehicle traveling at a constant speed of v_o, the power spectral density that describes the input displacement seen at the road surface can be given by

$$\Phi(f) = \frac{1}{v_o}\Psi(\frac{2\pi f}{v_o}) = \frac{v_o c}{(2\pi f)^2}, \qquad \textit{(EQ 11)}$$

where f is now the temporal frequency, in units of *cycles/sec*. In addition, plots of Ψ *vs.* Ω are presented in [9] for several road surface types. Assuming a "rough road" terrain, $c = 3.24e\text{-}6$ *in-cycles*.

Figure 22 illustrates $\phi_{11}(f)$, $\phi_{22}(f)$, and $\phi_{12}(f)$ vs. frequency, where plot (a) is directly from Eq. (11) for $v_o = 55\ mph$. To estimate the correlation of the terrain between the left and right tire tracks of the vehicle, consider the coherency function

$$g^2(\Omega) = \frac{\left|\Psi_{12}(\Omega)\right|^2}{\Psi_{11}(\Omega)\Psi_{22}(\Omega)}, \qquad \textit{(EQ 12)}$$

where $0 \le g^2(\Omega) \le 1$. Typically, as discussed in [16], $g^2(\Omega)$ is near unity at low frequencies (*i.e.*, high correlation for hills or dips in the road surface), and much lower at

the higher frequencies (*i.e.*, low correlation for cracks in the pavement, potholes, etc.). Utilizing this assumption, Eq. (12) can be used to determine $\phi_{12}(f)$, as illustrated in Fig. 22(b).

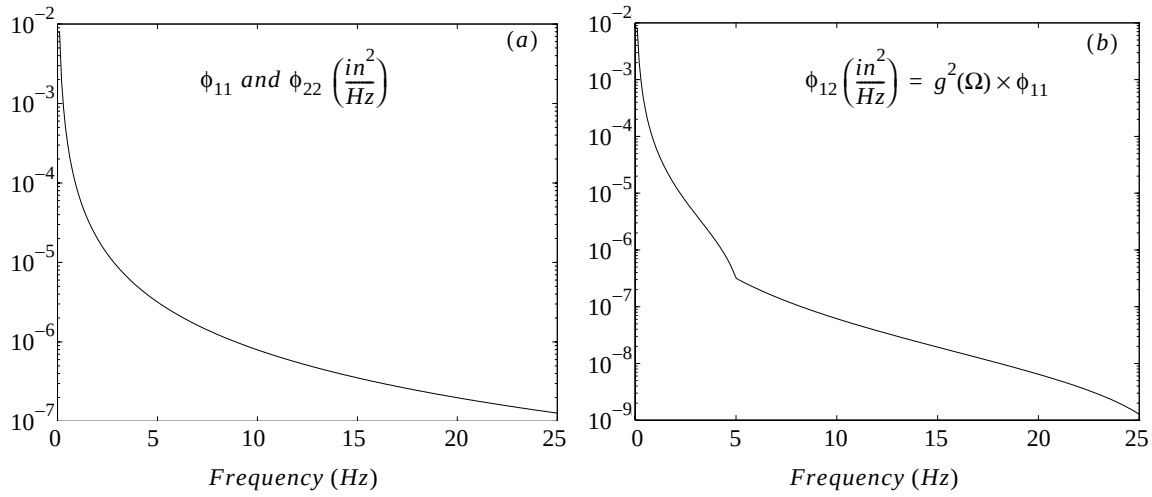

Figure 22: Input autopower and crosspower spectral density functions.

4. Results

To complete the rough road analysis, the input force PSD matrix of Eq. (9) was applied to the finite element model of the DOE Armored Tractor with SST. Experimental modal damping values from [14] and [15] were used in this model. This is most likely insufficient for on-road applications, however, since damping in the suspension systems and tires will be greater when the vehicle response is no longer constrained to the small displacements of a modal test. In addition, the shock absorbers at the steer and drive axles are not included in these calculations because the dynamic characteristics of the shocks remain unknown at this time.

The root-mean-square (*RMS*) values of the response at several locations on the vehicle are listed in Table 1. Note that the highest response levels are recorded at the axles (*i.e.*, the input locations), and the presence of the frame and cab/sleeper mounts help to diminish the vibrational response at the driver's seat, sleeper bunk, and fifth wheel.

Plots of the output power spectra at these same points of interest are shown in Figs. 23 through 31. The response of the cab and sleeper, indicative of the vibrational loading felt by the driver and sleeper bunk occupant, is illustrated in Figs. 23 through 28. When considering the vehicle's response in the vertical (Y) direction, the pitch mode, occurring at $f = 3.19\ Hz$, dominates the response of the cab, while the sleeper is most susceptible to the counter-pitch mode at $f = 4.16\ Hz$. In the fore/aft (Z) direction, the counter-pitch mode is the dominant dynamic mode for both the cab and sleeper, neglecting information above $10\ Hz$, where the finite element model remains un-correlated with any test data [11]. Furthermore, it is evident that the tractor cab and sleeper are most susceptible to the pitch and counter-pitch modes, which occur in a frequency range that is most irritating and debilitating to the human body [17]. Note the presence of a very low frequency mode (*i.e.*,

$f < 0.02\ Hz$) in the fore/aft response plots. This is due to the rigid-body motion of the entire vehicle rolling front and back on the tires.

Also shown is the response of the fifth wheel (the connection point between the tractor and trailer). It is evident that the response in the vertical direction is more pronounced than in the fore/aft direction, since the excitation from the road surface is up-and-down only. As illustrated in Figs. 29 and 30, the fifth wheel is most excited by the bounce ($f = 2.04\ Hz$) and counter-pitch ($f = 4.16\ Hz$) modes.

Figures 31 and 32 represent the vibrational response of the vehicle at the steer axle, where all six of the vehicle modes discussed in [11] are visible in the response spectrum. Also present is a high frequency mode in the vertical direction (near $f = 23.5\ Hz$), which can be attributed to the steer axle "hop" mode described in [13]. Overall, note the close resemblance between the displacement response with the input PSD, shown in Fig. 22. This is to be expected since the steer axle is one of the input locations. Furthermore, the acceleration response PSD of Fig. 31 appears to resemble two time-differentiations of the displacement input of Fig. 22. This trend of increasing magnitude with increasing frequency causes the large *RMS* values at the steer axle presented in Table 1.

The Ride Severity Index (RSI), discussed in [12], is given by

$$RSI = \left[\int_{f_1}^{f_2} L(f)^2 S_{out}(f) df\right]^{\frac{1}{2}}, \qquad \textit{(EQ 13)}$$

where $S_{out}(f)$ is the output power spectral density function and $f \in [f_1, f_2]$ denotes the frequency band of interest. As shown, the RSI is a scalar quantity that is just a weighted sum of the output PSD. The insertion loss factor, $L(f)$, is a quantity indicative of the human body's sensitivity to low frequency vibration. The higher the loss factor, the more sensitive the human is to the excitation [17]. $L(f)$ is greatest from one to two *Hz* in the fore/aft direction (normal to the driver's chest) and from four to eight *Hz* in the vertical direction

Location	Z-disp, *in-rms*	Z-accel, *mg-rms*	Y-disp, *in-rms*	Y-accel, *mg-rms*
C.G. of cab	0.01578	18.53	0.04338	34.81
C.G. of sleeper	0.01526	46.29	0.04305	22.47
Steer axle	0.01194	16.14	0.04140	406.9
Front drive axle	0.01366	42.69	0.03764	160.6
Fifth wheel	0.01264	6.712	0.04591	13.68

Table 1: Root-mean-square (RMS) response of vehicle.

(along his/her spine). As part of this study, the RSI for the DOE Armored Tractor with SST was computed at the c.g. of the cab and sleeper. Results are listed in Table 2.

Note that the ride is more severe in the sleeper, even though the PSD plots to follow indicate that the vibrational environment of the sleeper is less than that of the cab. The reason for this is the different orientations of the human body; seated upright in the cab, and laying down in the sleeper (see [12] for a more detailed discussion).

Location	RSI, *mg-rms*
Cab c.g.	20.42
Sleeper c.g.	23.53

Table 2: Ride severity index for DOE truck.

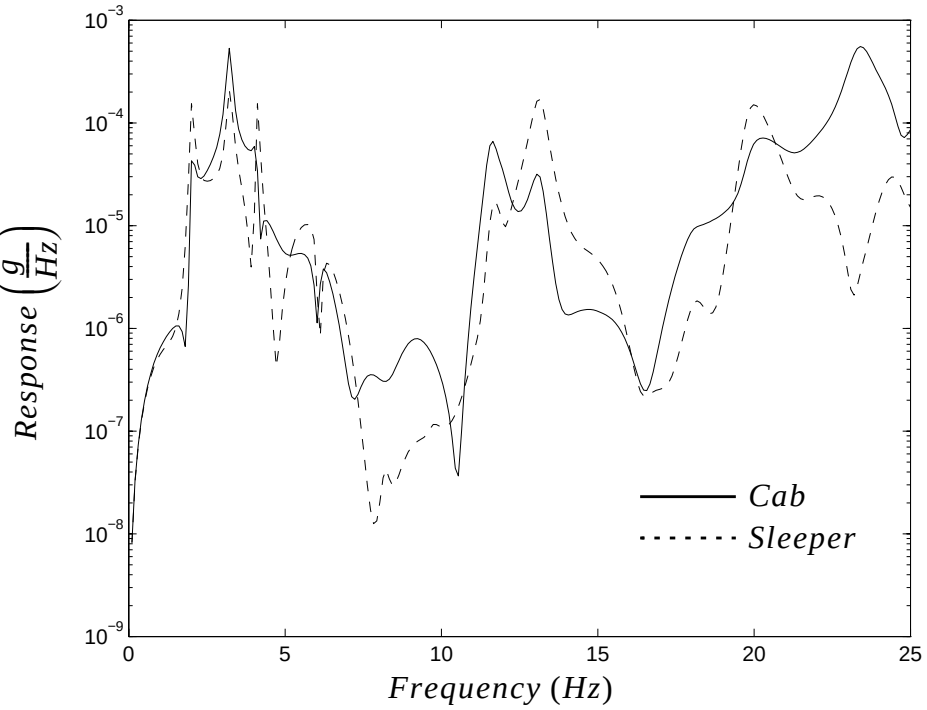

Figure 23: Vertical PSD acceleration response of cab and sleeper.

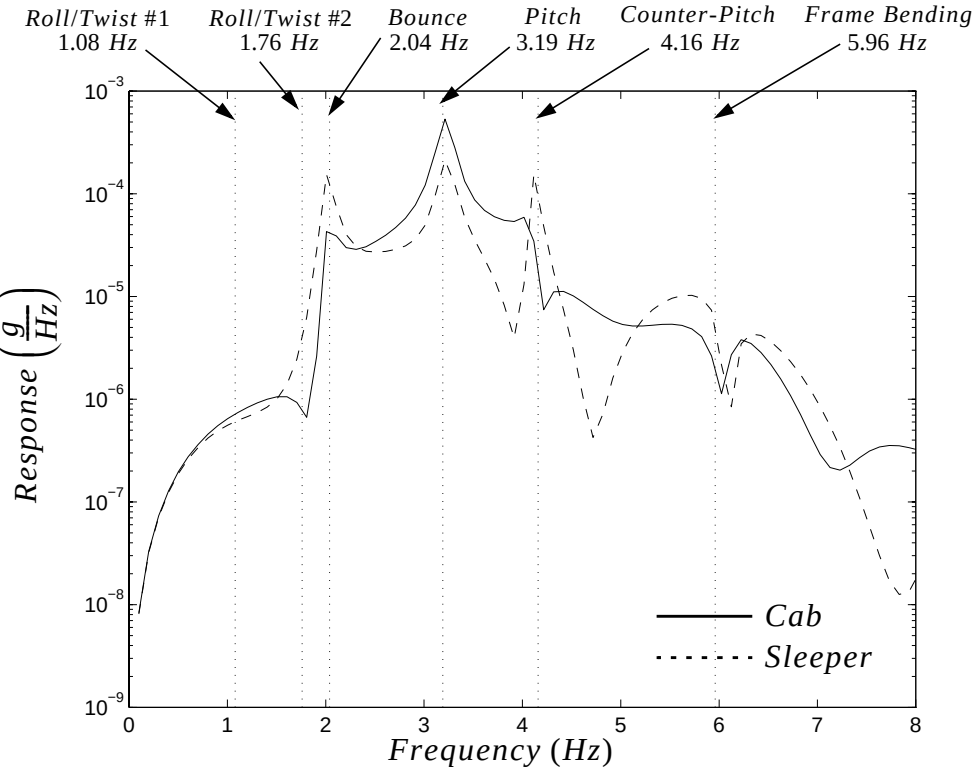

Figure 24: Close-up of cab and sleeper vertical response.

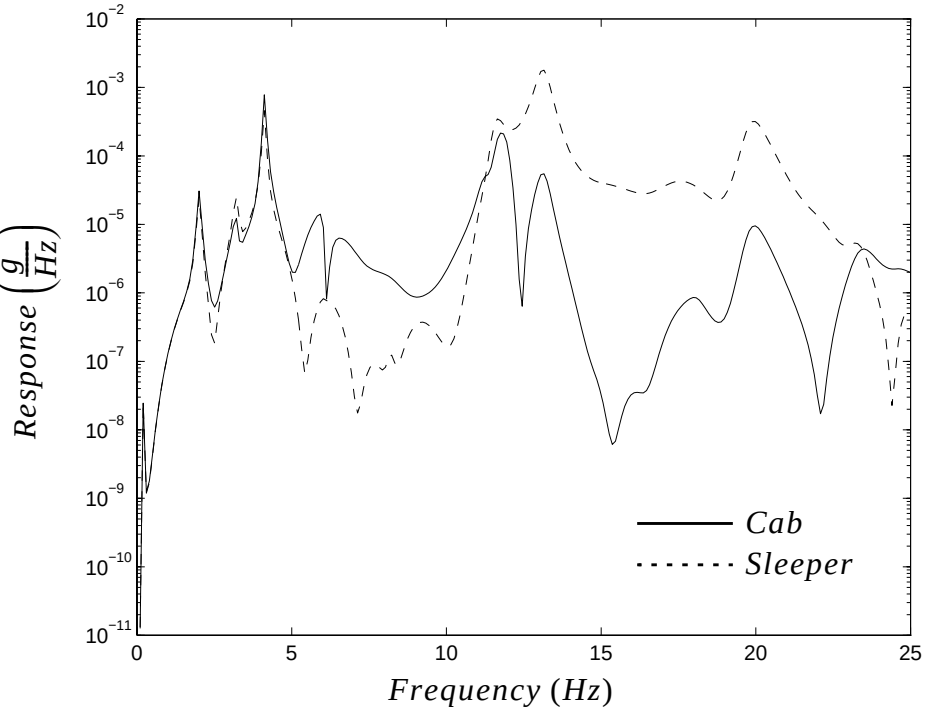

Figure 25: Fore/aft PSD acceleration response of cab and sleeper.

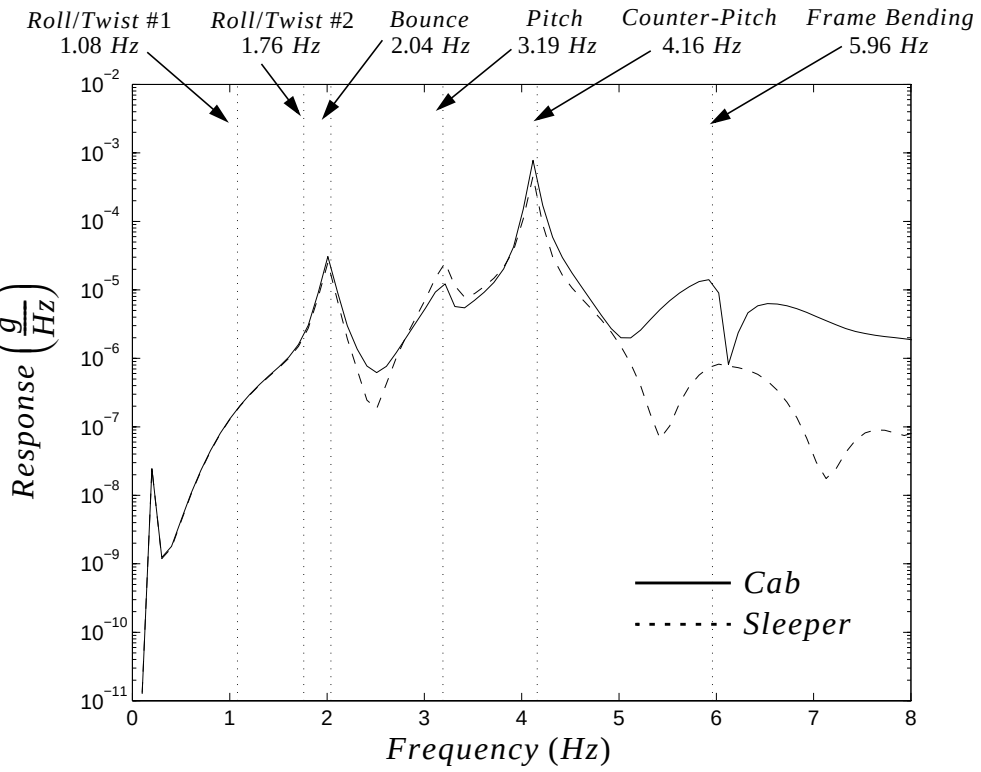

Figure 26: Close-up of cab and sleeper fore/aft response.

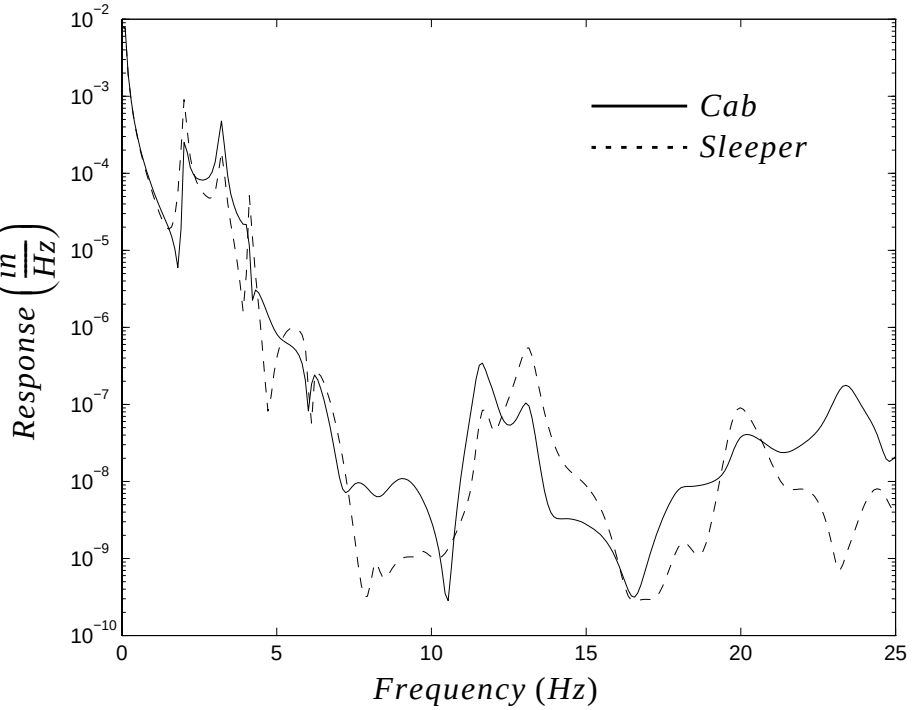

Figure 27: Vertical PSD displacement response of cab and sleeper.

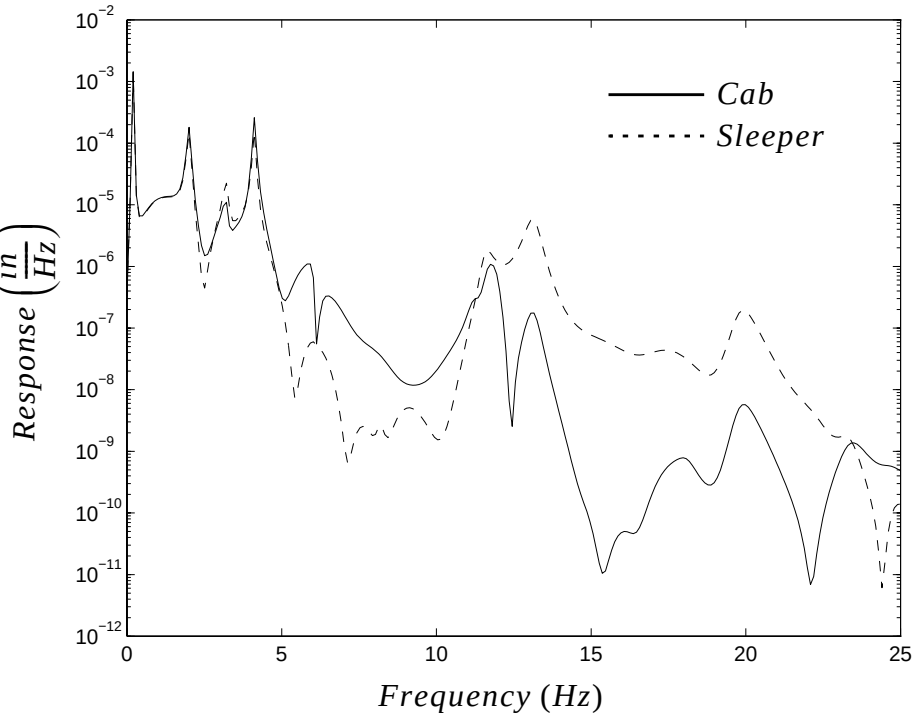

Figure 28: Fore/aft PSD displacement response of cab and sleeper.

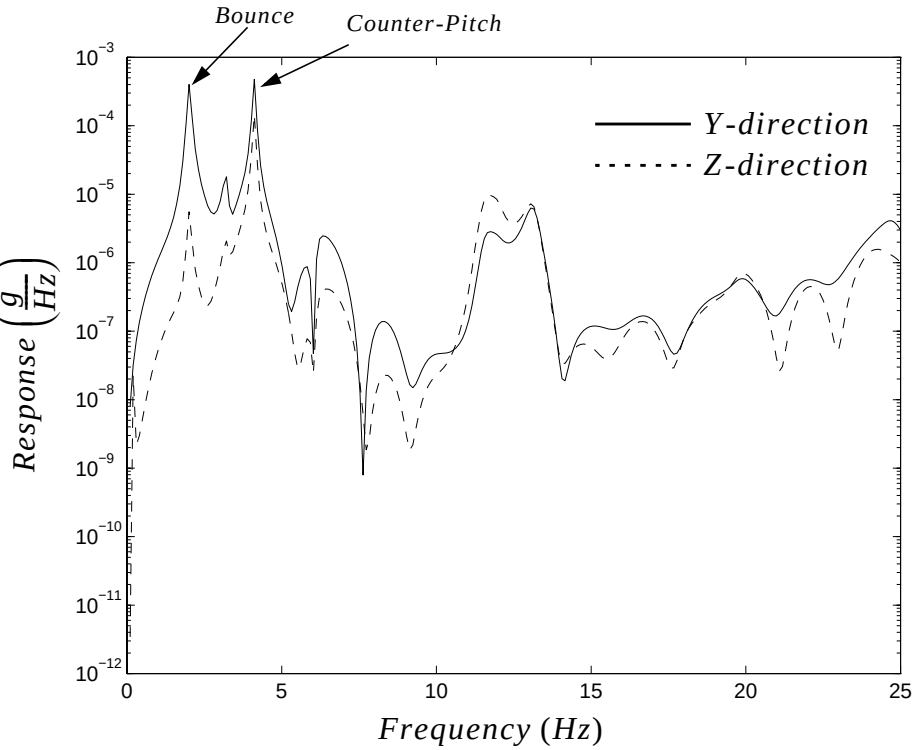

Figure 29: PSD acceleration response of fifth wheel.

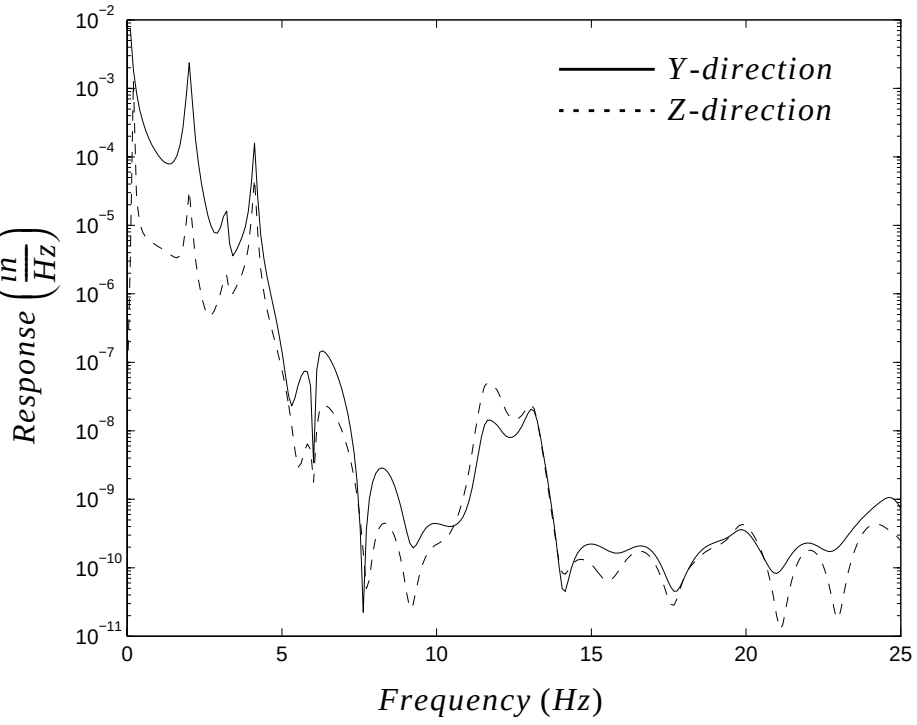

Figure 30: PSD displacement response of fifth wheel.

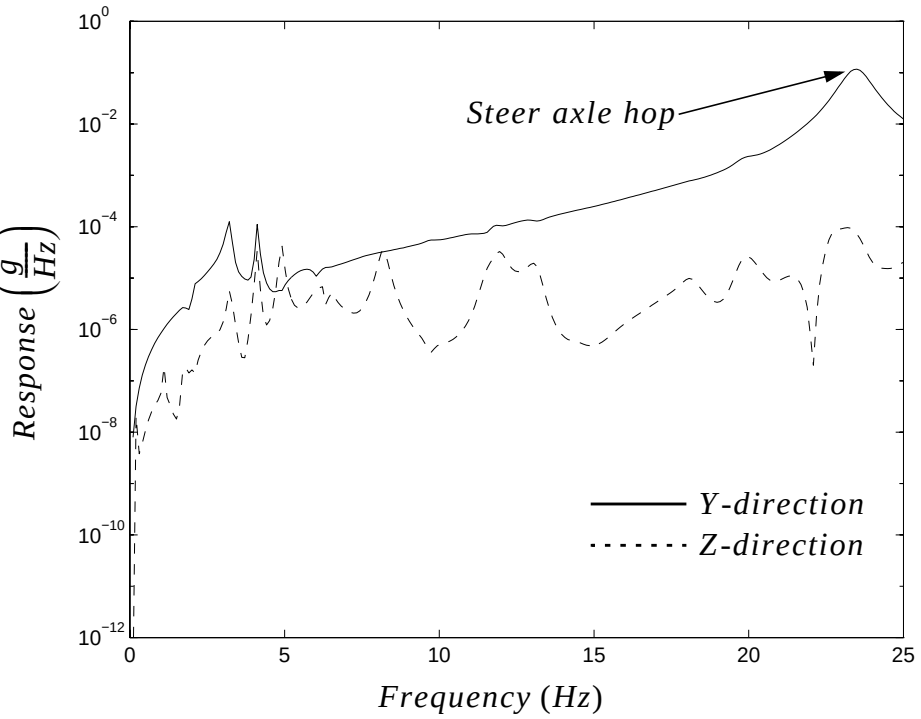

Figure 31: PSD acceleration response of steer axle.

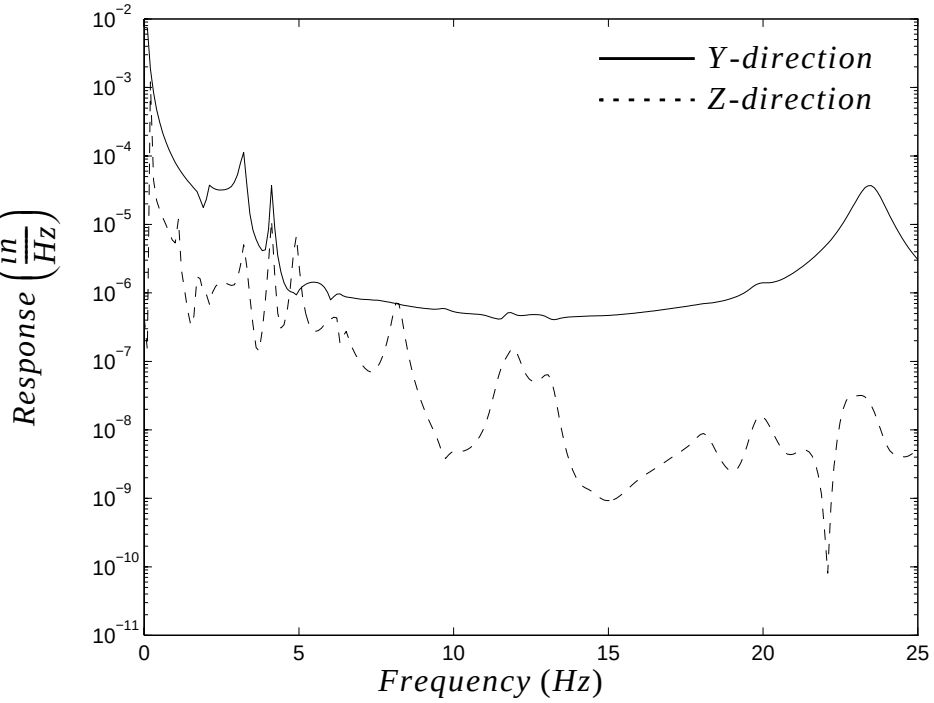

Figure 32: PSD displacement response of steer axle.

5. Conclusions

The vibratory response of the DOE Armored Tractor with Safe Secure Trailer traveling over a rough road at 55 *m.p.h.* has been presented. The preliminary results presented here agree with general trends seen in experimental rough road testing. Before more precise vibrational response data of this type can be extracted from the model, however, an improved description of the damping in the vehicle suspension systems, tires, and shock absorbers is required. This may be accomplished through the use of time-domain model reconciliation techniques.

It is evident that the tractor cab and sleeper are most susceptible to the pitch and counter-pitch modes, which occur in a frequency range that is most irritating and debilitating to the human body. It may be possible to diminish the amount of vibrational loading transmitted from the road surface to the passenger compartments by modifying the existing interface from the truck frame to the cab and sleeper. Therefore, to make possible improvements in ride quality for the next-generation vehicle, the concept of a cab suspension system should be investigated.

References

9. Baum, J.M., J.A. Bennett, and T.G. Carne, "Truck Ride Improvement Using Analytical and Optimization Methods," General Motors Research Laboratories, GMR-2324-R, December, 1978.

10. Carne, T.G. and J.E. Hurtado, "On the Numerical Application of Road Inputs to a Finite Element Vehicle Model," memo to Distribution, Sandia National Laboratories, Albuquerque, NM, September 3, 1996.

11. Dohrmann, C.R. and R.V. Field, Jr., "DOE Tractor Trailer Modal Test/Analysis Reconciliation," memo to Distribution, Sandia National Laboratories, Albuquerque, NM, October, 1996.

12. Field, R.V. Jr., "Optimal Cab Suspension for Next-Generation Armored Tractor," memo to Distribution, Sandia National Laboratories, Albuquerque, NM, October, 1996.

13. Gillespie, T.D., *Fundamentals of Vehicle Dynamics*, Society of Automotive Engineers, 1992.

14. Hurtado, J.E. and L.R. Dorrell, "Modal Testing of SST Armored Tractor Trailer," memo to Distribution, Sandia National Laboratories, Albuquerque, NM, July 5, 1996.

15. Hurtado, J.E. and T.G. Carne, "Addendum to Modal Testing of SST Armored Tractor Trailer," memo to Distribution, Sandia National Laboratories, Albuquerque, NM, July 10, 1996.

16. Soong, T.T. and M. Grigoriu, *Random Vibration of Mechanical and Structural Systems*, Prentice-Hall, Inc., 1993.

17. Evaluation of Human Exposure to Whole-Body Vibration," International Organization for Standardization, ISO 2631/1-1985(E).

RVF: 9234

Copies To:

5503	E.R. Hoover	MS 0767	9234	G.R. Eisler	MS 0439
5512	B.D. Boughton	MS 0790	9234	R.V. Field, Jr.	MS 0439
5513	R.G. Baca	MS 0790	9234	D.R. Martinez	MS 0439
5513	J.J. Roesch	MS 0790	9741	T.J. Baca	MS 0557
9117	H.S. Morgan	MS 0443	9741	T.G. Carne	MS 0557
9118	E.P. Chen	MS 0437	9741	L.R. Dorrell	MS 0557
9215	P.D. Heermann	MS 0318	9741	J.E. Hurtado	MS 0557
9234	C.R. Dohrmann	MS 0439			

Sandia National Laboratories

date: October 17, 1996

Albuquerque, New Mexico 87185

to: Distribution

from: R. V. Field, Jr., Dept. 9234, MS 0439

subject: Optimal Cab Suspension for Next-Generation Armored Tractor

1. Summary

The design of a next-generation DOE Armored Tractor is to be completed in the next few years. This new vehicle will most likely exhibit significant modifications from the current design. One such change may be the addition of a tractor cab suspension system, such as the Cab-Mate™ system manufactured by Link, Inc., to improve the vibrational response of the truck at the driver seat. This report contains a description of the finite element model of the next-generation tractor, which includes an integrated cab/sleeper with an optimized cab suspension system. This cab suspension system is optimal in the sense that it provides the maximum protection to the driver from vibration due to road surface input.

2. Finite Element Model

Figure 33 illustrates the MSC/NASTRAN 46,000 degree-of-freedom finite element model of the next-generation DOE Armored Tractor with Safe Secure Trailer (SST).

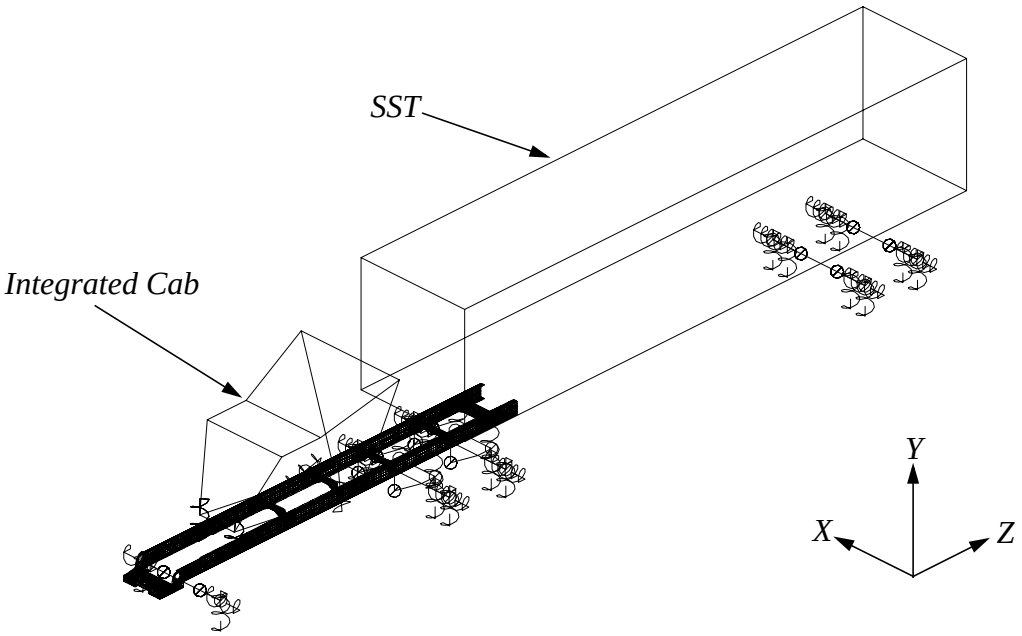

Figure 33: MSC/NASTRAN model of the next-generation DOE Armored Tractor with SST.

Most of the finite element model presented here is identical to the model of the current vehicle [19]. The integrated cab and SST are still modeled as rigid elements, but the geometry of the cab structure is taken from modal test results performed on the Marmon vehicle. In addition, the mass properties of the integrated cab used in the model presented here are a combination of the current armored cab/sleeper arrangement. The result is a "best guess" at the dynamic qualities of an armored integrated cab system. Table 3 presents the analytical modal data of this new model.

Table 3: Modal results for next-generation vehicle.

Mode Description	Brakes-on Frequency (Hz)	Brakes-off Frequency (Hz)
cab suspension	1.34	1.34
roll/twist #1	1.10	1.10
roll/twist #2	1.47	1.47
bounce	1.82	2.12
fore/aft	2.62	0.231
pitch	3.43	3.32
counter pitch	4.30	4.13
frame bending	7.01	6.85

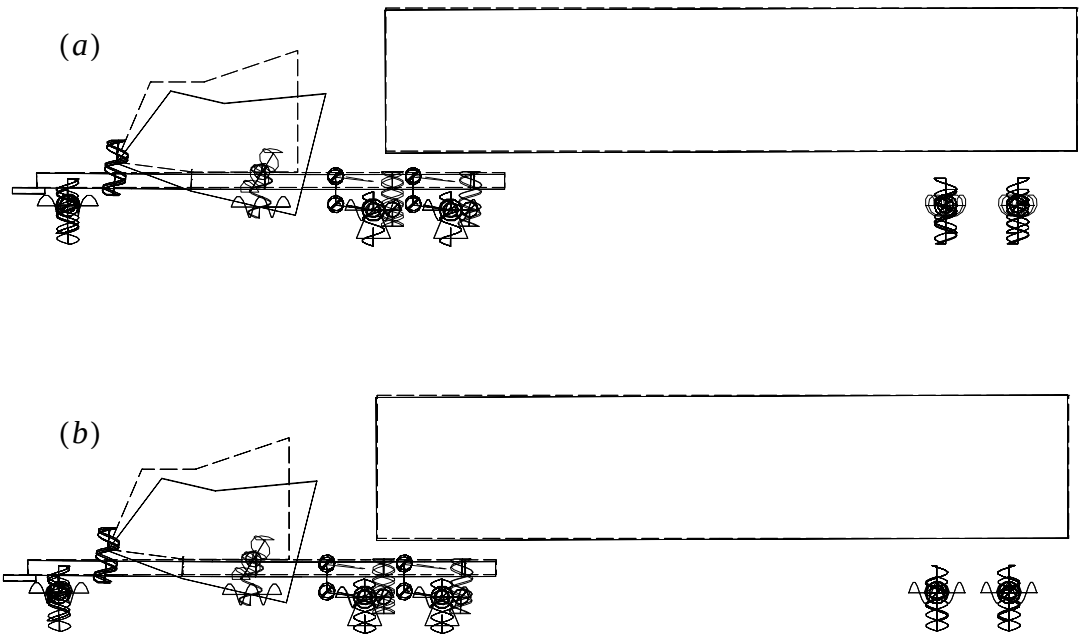

Figure 34: Cab-mate suspension mode with brakes on, (a), and brakes off, (b).

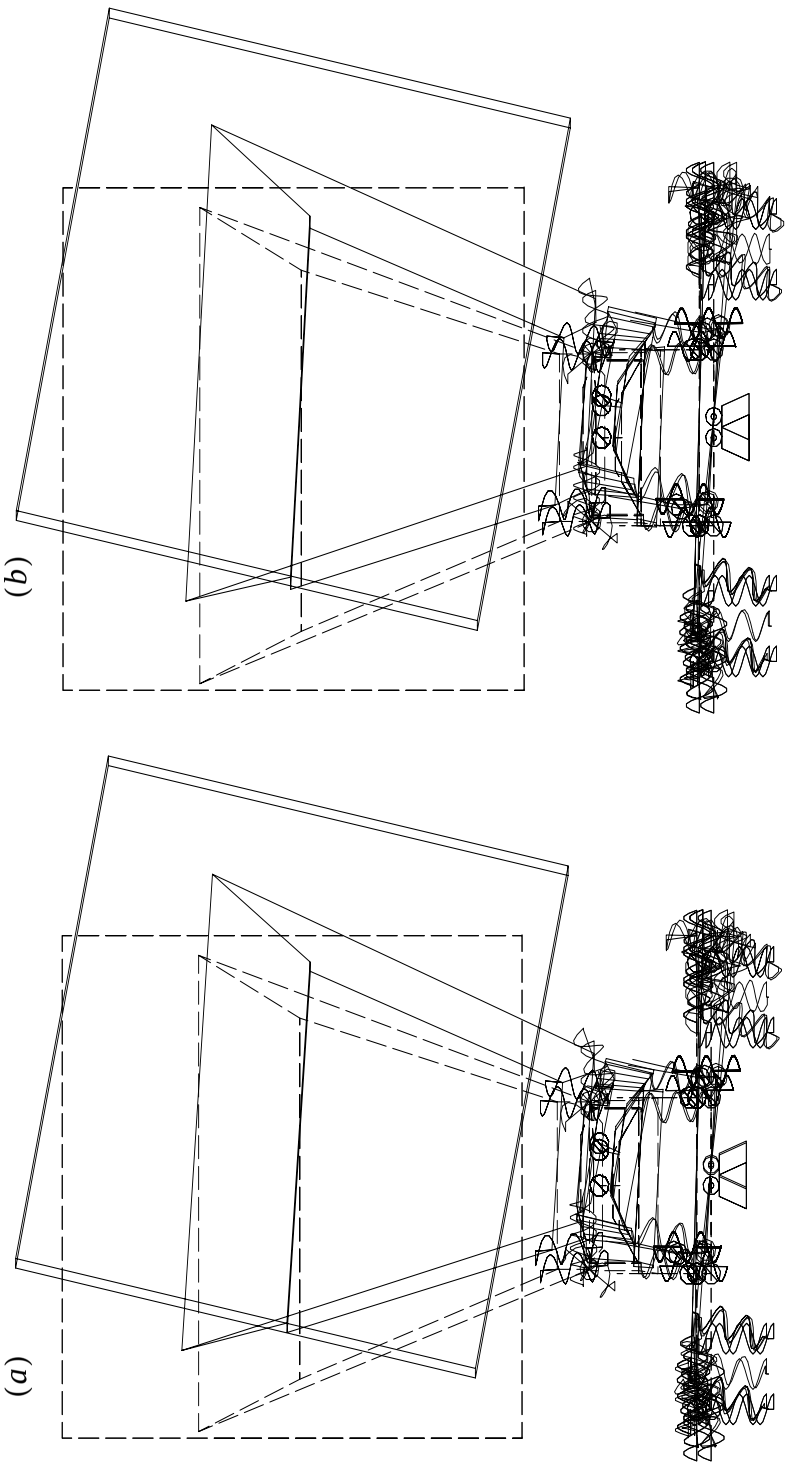

Figure 35: Roll/twist mode #1 with brakes on, (a), and with brakes off, (b).

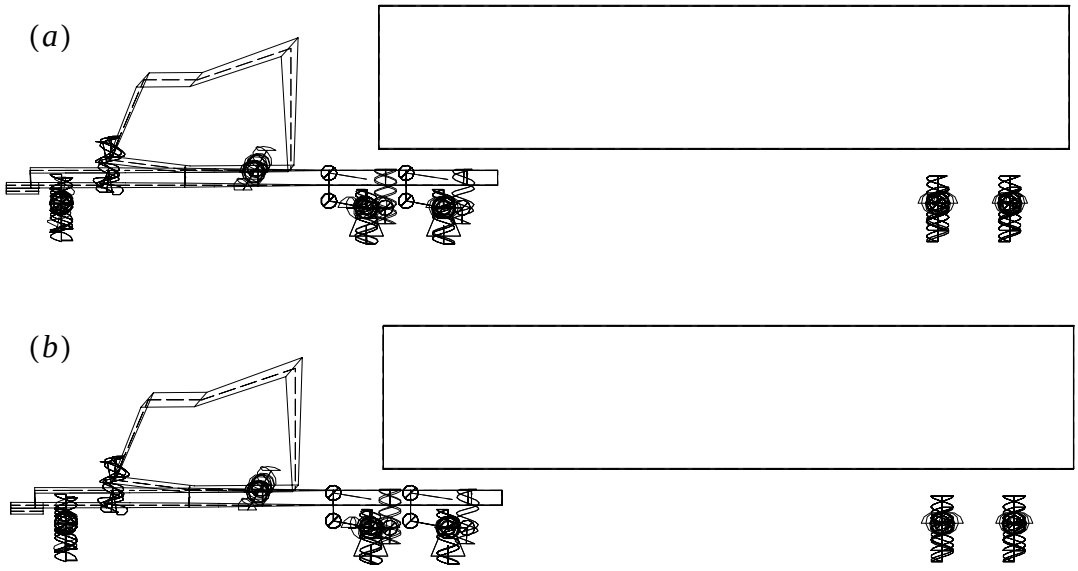

Figure 36: Roll/twist mode #2 with brakes on, (a) and brakes off, (b).

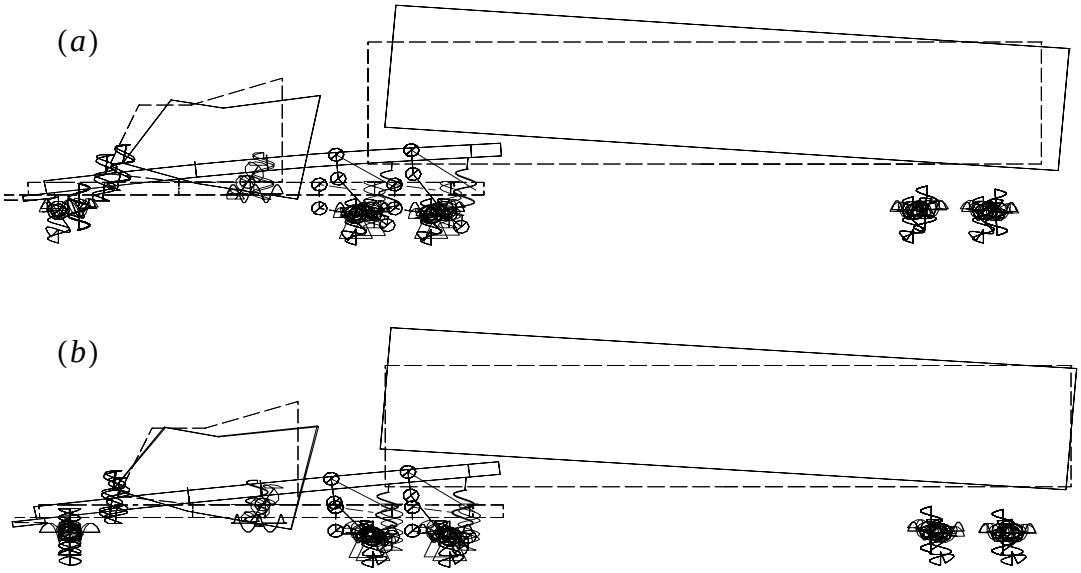

Figure 37: Bounce mode with brakes on, (a), and brakes off, (b).

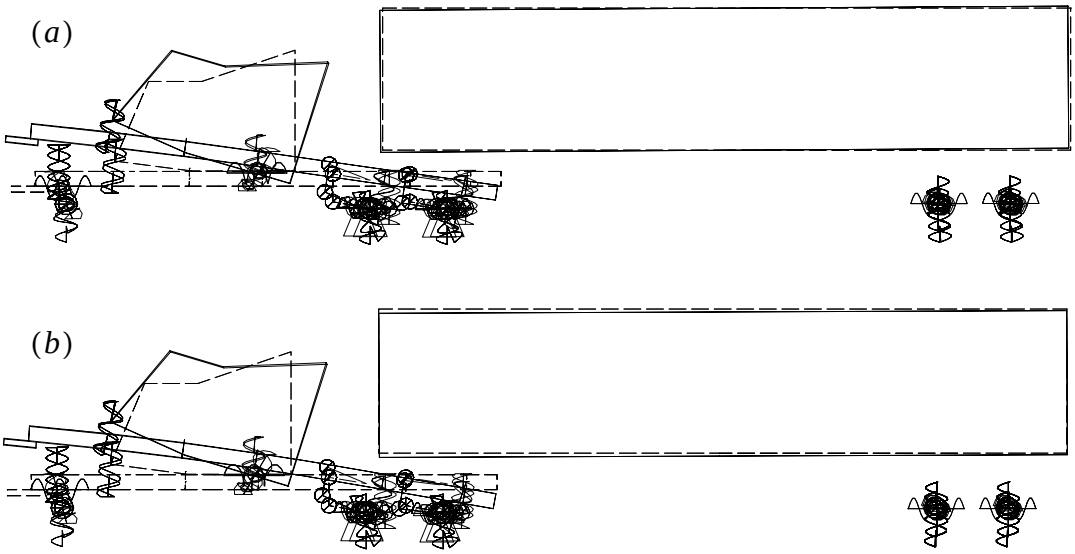

Figure 38: Pitch mode with brakes on, (a), and brakes off, (b).

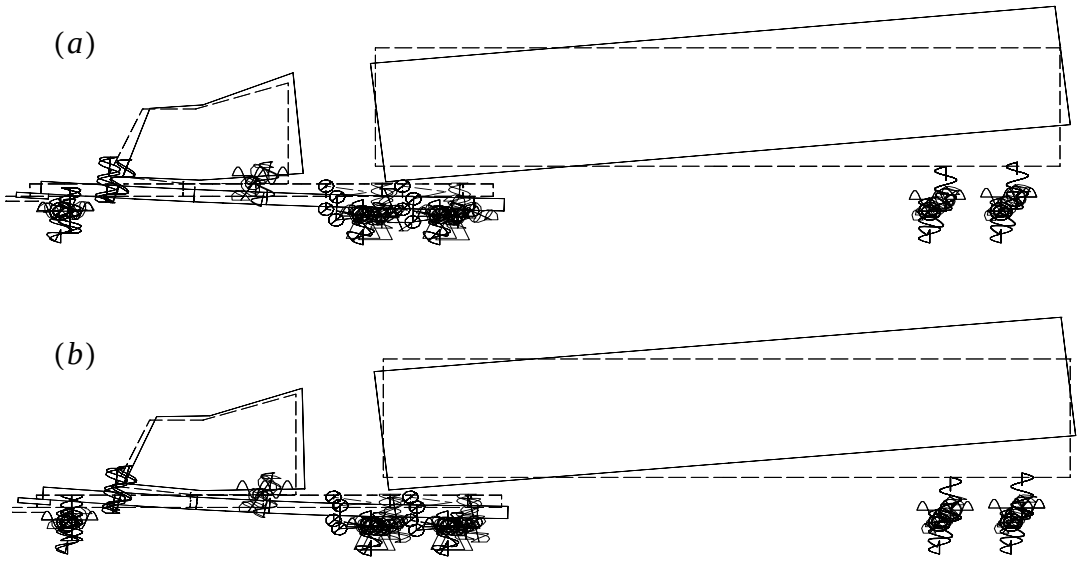

Figure 39: Counter pitch mode with brakes on, (a), and brakes off, (b).

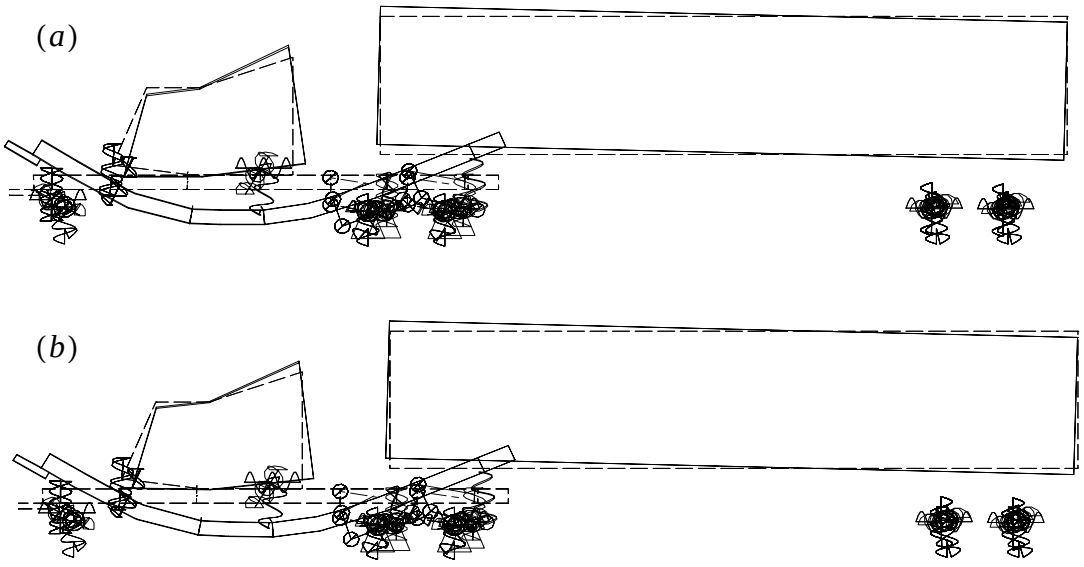

Figure 40: Frame bending mode with brakes on, (a), and brakes off, (b).

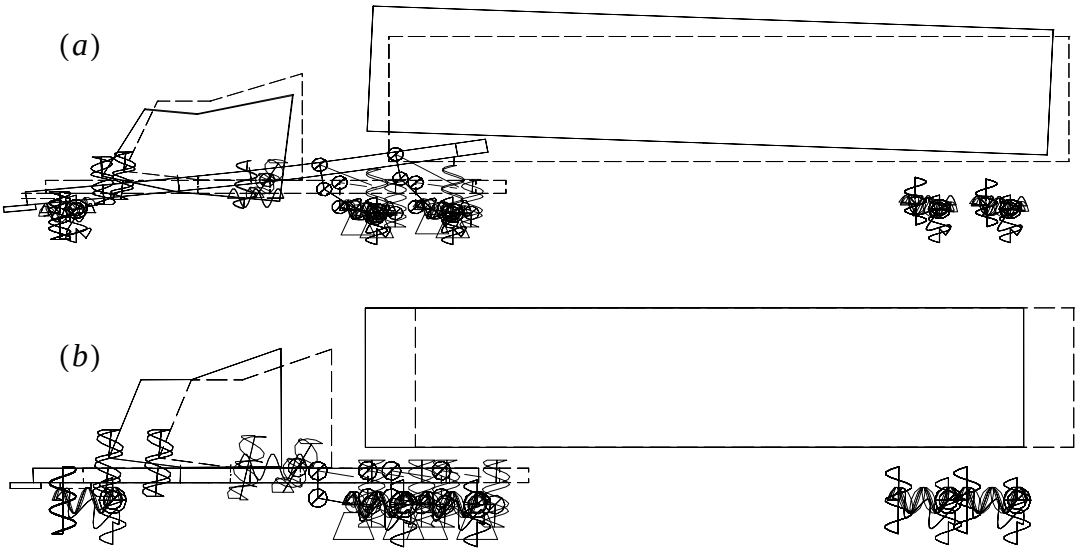

Figure 41: Fore-aft mode with brakes on, (a), and brakes off, (b).

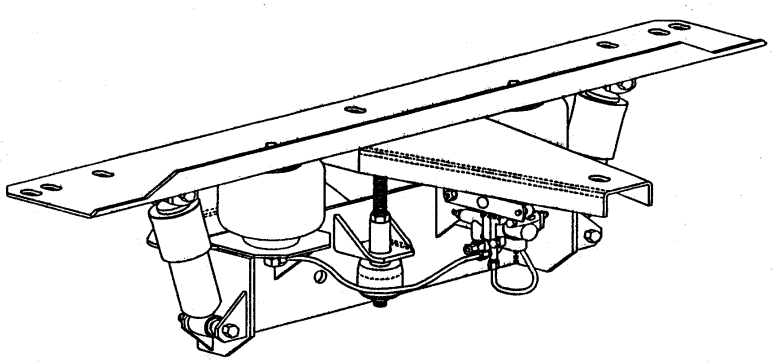

Figure 42: Link Cab-Mate™ system.

A cab suspension, such as the Link, Inc. Cab-Mate™ system shown in Fig. 42, is included in this model. For the purposes of this study, the suspension is modeled as a simple spring-damper system and is placed into the full finite element model, as shown in Fig. 43. The modal data of Table 3 include this cab suspension, with stiffness and damping values equal to what Link, Inc. would recommend for a vehicle similar to the current DOE truck. Furthermore, the stiffness and damping constants of this system are used as the design variables in the optimization problem to be discussed later. Linear springs in the three translational directions model the cab "hard-mounts" to the truck frame. The remainder of the finite element model, including the suspension systems, tires, and SST are identical to what is discussed in [19].

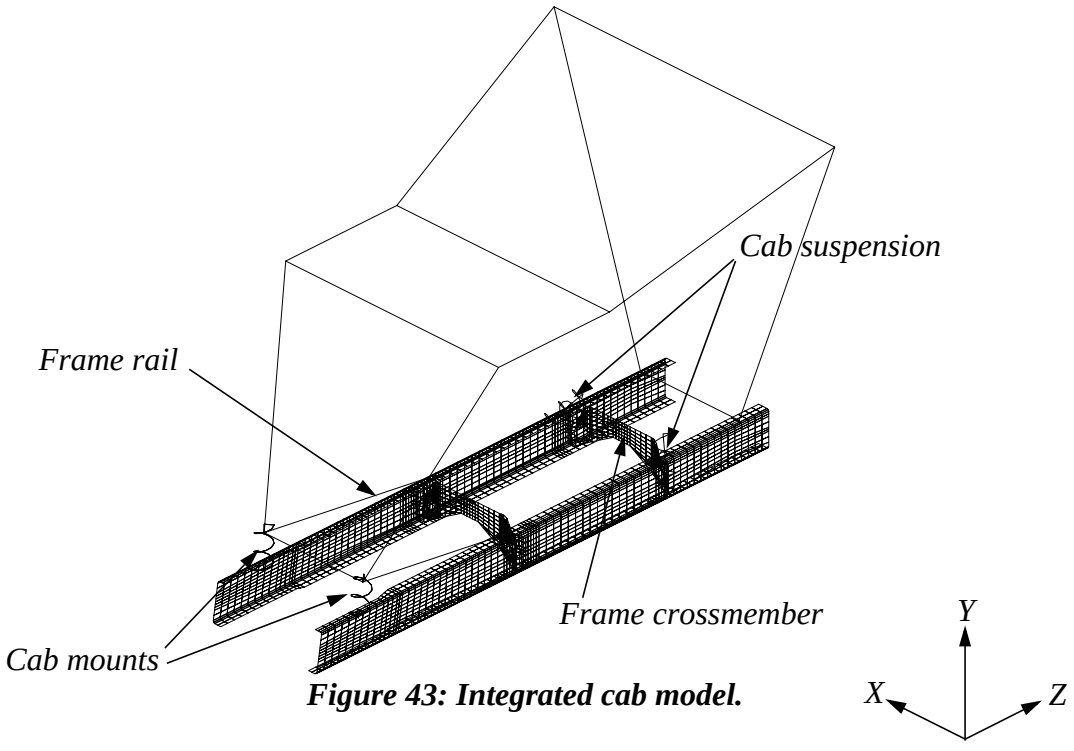

Figure 43: Integrated cab model.

3. Optimal Cab Suspension Design

The cab suspension system, placed between the rear of the integrated cab and truck frame, can be utilized to improve the ride quality of the vehicle. The ride severity index (RSI), a weighted measure of the power of the output spectrum, can be used to gauge this improvement. Consider the following relation

$$RSI = \left[\int_{f_1}^{f_2} L(f)^2 S_y(f) df\right]^{\frac{1}{2}}, \qquad \textit{(EQ 14)}$$

where $S_y(f)$ is the output power spectral density function and $f \in [f_1, f_2]$ denotes the frequency band of interest. As shown, the RSI is a scalar quantity that is just a weighted sum of the output PSD. The insertion loss factor, $L(f)$, is a quantity indicative of the human body's sensitivity to vibration. The higher the loss factor, the more sensitive the human is to the excitation.

$L(f)$ changes as the direction of the excitation changes, as shown in Fig. 44. Note that the

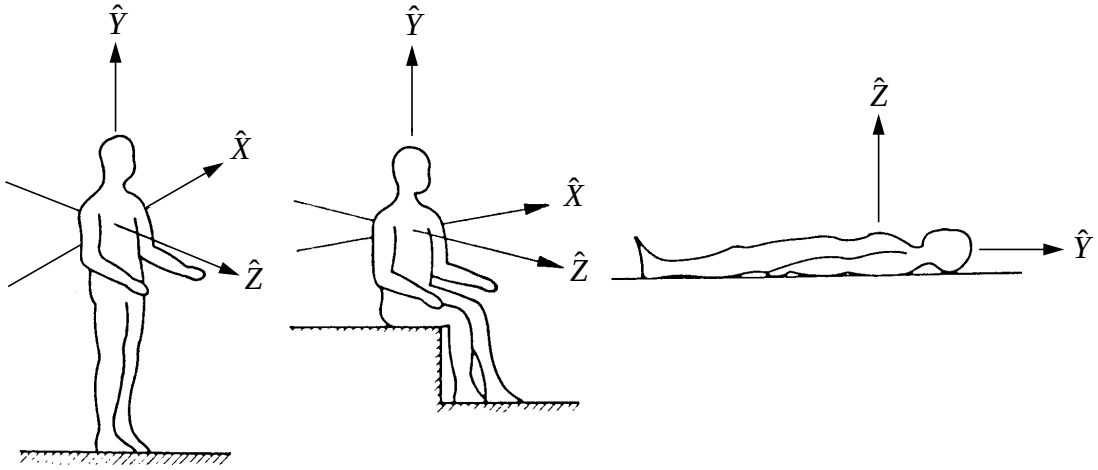

Figure 44: Insertion loss factor, $L(f)$, and the human body.

human coordinate system, $\hat{X}\hat{Y}\hat{Z}$, is identical to the global system XYZ of Fig. 33 for a seated human (*i.e.*, the driver). The insertion loss factor, normalized to have unity gain over the frequency range where the loss factor is constant, is given by the following [22]

$$L_{\hat{X},\hat{Z}}(f) = \begin{cases} 1 & f \in [1,2]\ Hz \\ \dfrac{2}{f} & f \in [2,25]\ Hz \end{cases} \textit{ and } L_{\hat{Y}}(f) = \begin{cases} \dfrac{1}{2} f^{\frac{1}{2}} & f \in [1,4]\ Hz \\ 1 & f \in [4,8]\ Hz \\ \dfrac{8}{f} & f \in [8,25]\ Hz \end{cases} \qquad \textit{(EQ 15)}$$

Hence, it is obvious that humans are most annoyed by vibrational loading between one and two *Hz* in the $\hat{X}$- and $\hat{Z}$-directions, and between four and eight *Hz* in the vertical direction,

as illustrated in Fig. 45. For the studies included here, only the vibration at the driver seat

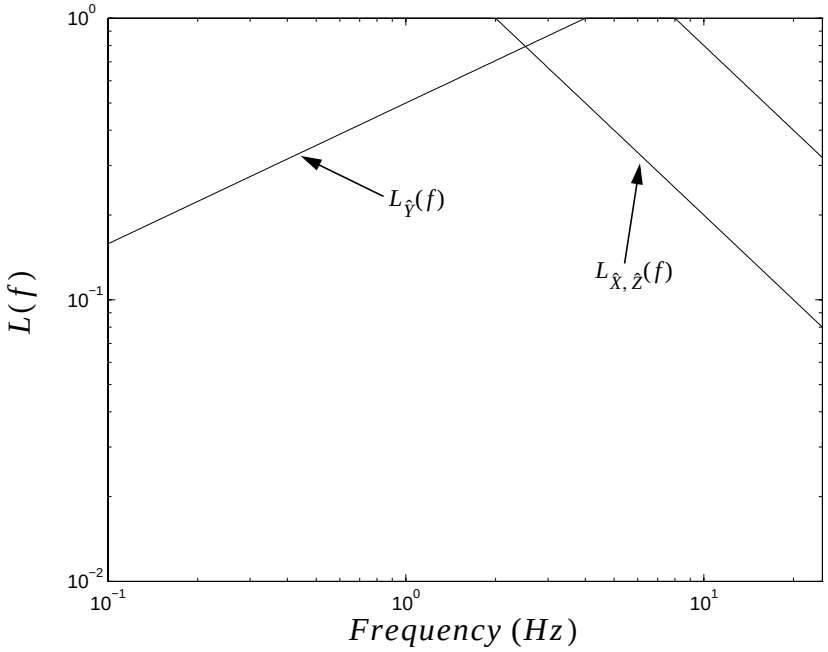

Figure 45: Insertion loss factor.

is considered, and the ride severity index is given by

$$RSI = \left(\int_1^4 \frac{f}{4} S_Y(f)df + \int_4^8 S_Y(f)df + \int_8^{25} \left(\frac{64}{f^2}\right) S_Y(f)df + 1.96\{ \int_1^2 S_Z(f)df + \int_2^{25} \left(\frac{4}{f^2}\right) S_Z(f)df \} \right)^{\frac{1}{2}} \quad \textit{(EQ 16)}$$

The terms involving $S_Z(f)$ are scaled by an additional factor of $(1.4)^2 = 1.96$ since vibration in the fore/aft direction is particularly disturbing to humans [22].

The minimization problem to be solved here can be stated as

$$\min_{k,\,c,\,z} RSI \text{ , subject to } k_{min},\, c_{min} \le k,\, c \le k_{max},\, c_{max}, \quad \textit{(EQ 17)}$$

where k, c, and z refer to the stiffness, damping, and location of the cab suspension system, respectively, and the bounds on the stiffness and damping ensure physically practical solutions. Because varying the location of the suspension system requires re-meshing the finite element model, however, Eq. (17) is solved for a fixed location, z. This location is then varied discreetly along the tractor frame to provide a qualitative estimate of the optimal location.

5. Results

The optimization capabilities of MATLAB [21] are utilized to determine optimal values of the cab suspension system at various locations along the frame. A description of the implementation is included in the Appendix. The results are shown in Table 4, where z is

Design	$k, \frac{lb}{in}$	$c, \frac{lb\text{-}s}{in}$	$RSI, mg\text{-}rms$
Current cab	N/A	N/A	20.42
Current sleeper	N/A	N/A	23.53
$z = 0.0\ in$ (Link)	245.0	100.0	11.48
$z = 0.0\ in$	333.4	105.6	11.46
$z = -12.0\ in$	420.0	125.1	11.07
$z = -24.0\ in$	287.7	128.0	9.386
$z = 12.0\ in$	410.5	101.6	11.44
$z = 24.0\ in$	416.9	95.77	11.35

Table 4: RSI of current vehicle vs. integrated cab with optimal cab suspension system.

the location of the suspension system, referenced to the location of the existing Cab-Mate™ system on the Marmon tractor. Figure 46 illustrates these discrete locations; $z = 0$ is the current location of the suspension on the Marmon vehicle, and positive and negative values of z are behind and in front of it, respectively. Note that the optimal spring-damper values are to be applied at both the passenger- and driver-side of the vehicle. Also included in the table is an indication of the ride quality of the current DOE vehicle from [20].

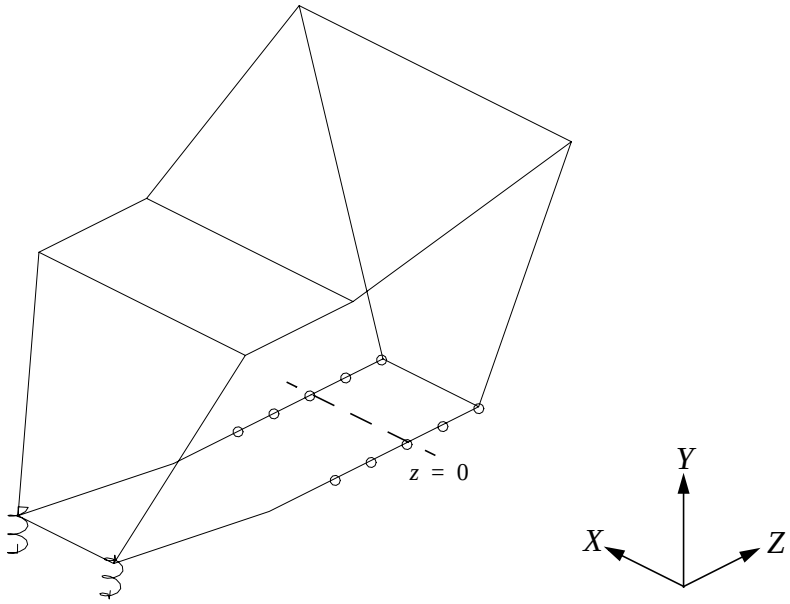

Figure 46: Cab suspension locations considered.

,

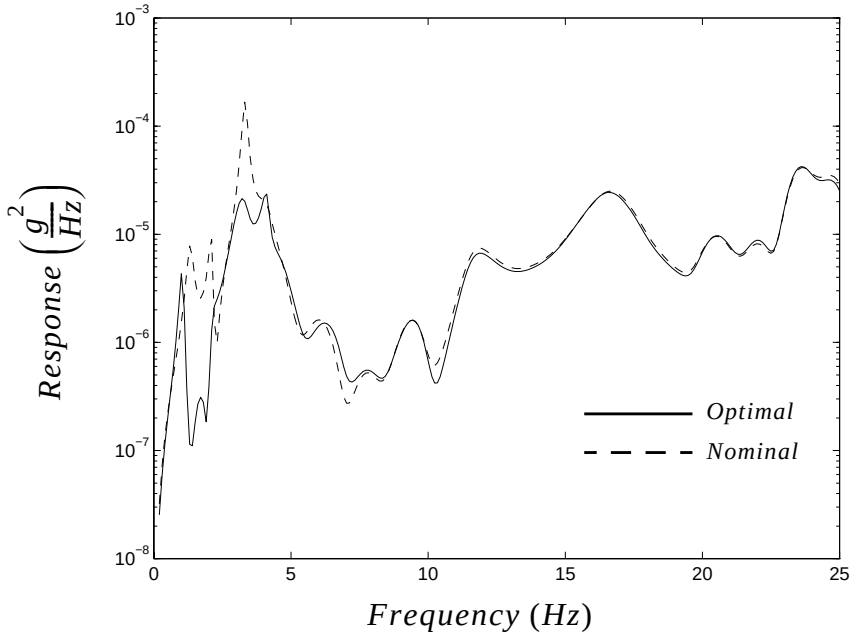

Figure 47: Output PSD response at cab in Y-direction of nominal and optimal cab suspension.

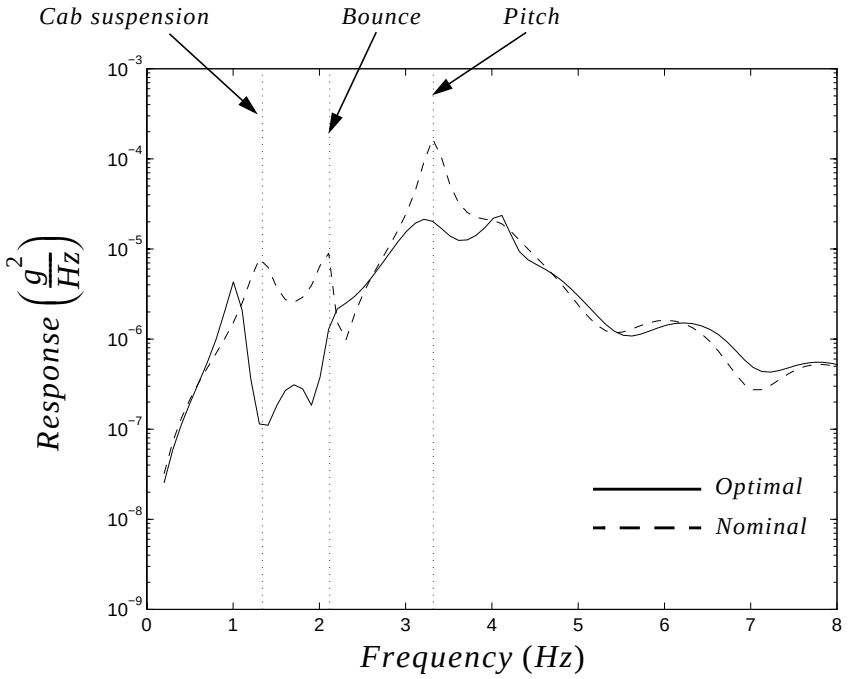

Figure 48: Close-up of response at cab in Y-direction of nominal and optimal cab suspension.

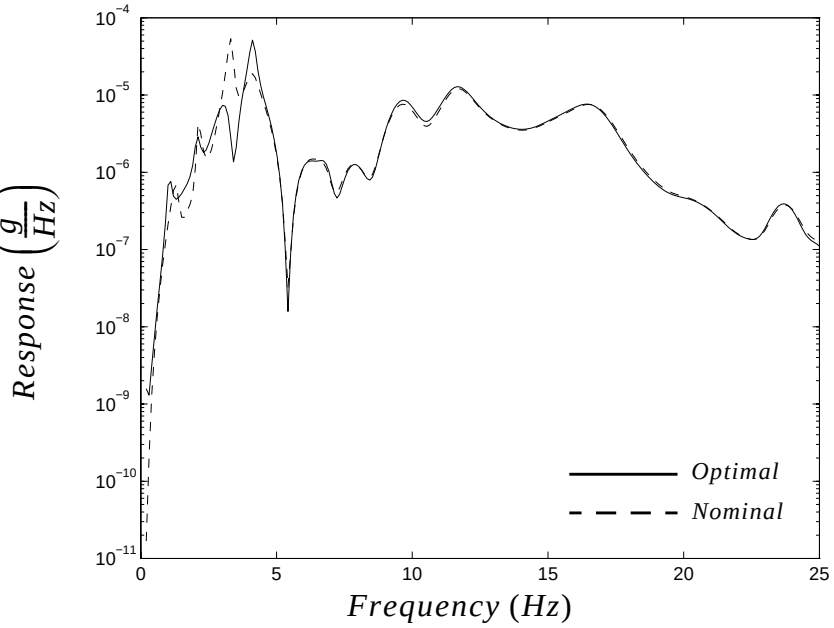

Figure 49: Output PSD response at cab in Z-direction of nominal and optimal cab suspension.

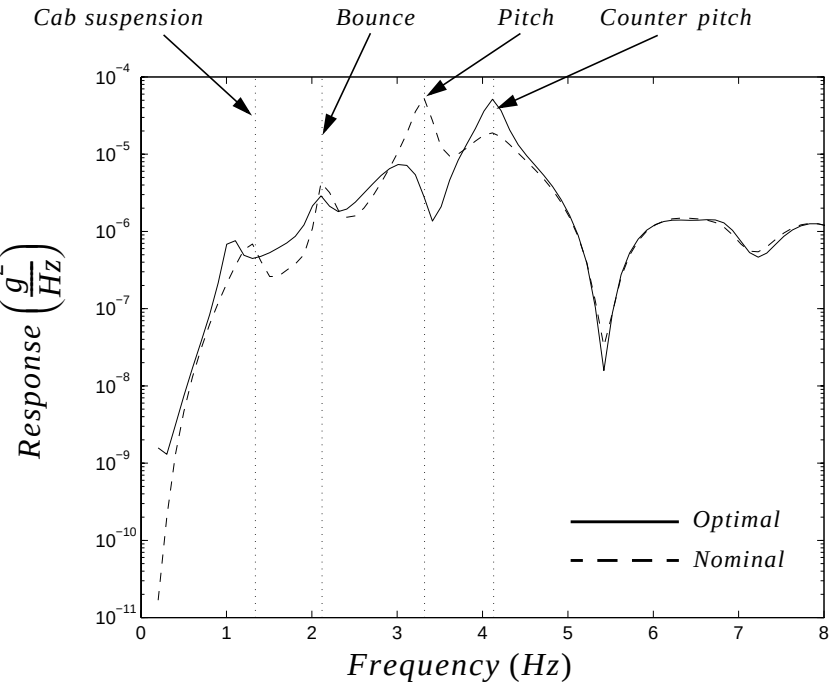

Figure 50: Close-up of response at cab in Z-direction of nominal and optimal cab suspension.

Plots illustrating the possible benefits of an optimized cab suspension are included in Figs. 47 through 50 where it is evident that changing the design of the cab suspension only has a significant effect on the response of the cab in the frequency range of 0 to 4 *Hz*. The optimal RSI occurs when the suspension is pushed 24 inches forward of its present location. The vertical response of Figs. 47 and 48 illustrate a drastic reduction in the bounce and pitch modes when using the optimal cab suspension. In addition, the vertical mode of the suspension reduces in frequency from $f = 1.34\ Hz$ to $f = 1.00\ Hz$ since, as the location of the cab suspension moves forward, it is required to carry more of the cab weight. When considering the fore/aft response of the cab, shown in Figs. 49 and 50, the optimal suspension again demonstrates reduction in the power of the bounce and pitch modes. The counter-pitch mode, however, is magnified when using the optimal cab suspension system. This makes sense, though, since the insertion loss factor of Eq. (15) weights this frequency less than that of the bounce or pitch modes.

As a general observation, it appears that the RSI will continue to decrease as the location of the cab suspension is moved forward. There are physical limits, obviously, since moving the suspension forward requires it to support a greater static load due to weight of the cab. Cab stresses are also an issue and, therefore, the location of the cab suspension cannot be chosen to minimize the ride severity index alone.

6. Conclusions

Possible design modifications to the DOE Armored Tractor with Safe Secure Trailer, namely the conversion to an integrated-type cab with a cab suspension system, have been discussed. With the addition of the integrated cab with nominal cab suspension, a 44% reduction in ride severity can be achieved over the current cab/sleeper configuration, which is hard-mounted to the truck frame (see [20]). Furthermore, once an optimized cab suspension is utilized, the RSI can be reduced by an additional 18%.

References

18. Baum, J.M., J.A. Bennett and T.G. Carne, “Truck Ride Improvement Using Analytical and Optimization Methods,” General Motors Research Laboratories, GMR-2324-R, 1978.

19. Dohrmann, C.R. and R.V. Field, Jr., “DOE Tractor Trailer Modal Test/Analysis Reconciliation,” memo to Distribution, Sandia National Laboratories, Albuquerque, NM, October, 1996.

20. Field, R.V. Jr., “DOE Tractor Trailer Rough Road Simulation,” memo to Distribution, Sandia National Laboratories, Albuquerque, NM, October 17, 1996.

21. Grace, A., “MATLAB Optimization Toolbox,” The MathWorks, 1995.

22. “Evaluation of Human Exposure to Whole-Body Vibration,” International Organization for Standardization, ISO 2631/1-1985 (E).

RVF: 9234

Copies To:

5503	E.R. Hoover	MS 0767	9234	C.R. Dohrmann	MS 0439
5512	B.D. Boughton	MS 0790	9234	G.R. Eisler	MS 0439
5513	R.G. Baca	MS 0790	9234	R.V. Field, Jr.	MS 0439
5513	J.J. Roesch	MS 0790	9234	D.R. Martinez	MS 0439
9117	H.S. Morgan	MS 0443	9741	T.G. Carne	MS 0557
9118	E.P. Chen	MS 0437	9741	L.R. Dorrell	MS 0557
9215	P.D. Heermann	MS 0318	9741	J.E. Hurtado	MS 0557
			9741	T.J. Baca	MS 0557

Appendix - Implementation

Component mode synthesis techniques were applied in NASTRAN to reduce the size of the model from over 46,000 degrees-of-freedom down to 70. Included in this reduced set are the degrees-of-freedom corresponding to the cab suspension interconnection between the frame and cab, for a fixed location. The remaining computations are computed in MATLAB.

To begin, solve the undamped eigenproblem,

$$(\mathbf{K} - \omega^2 \mathbf{M})\Phi = 0, \qquad \textit{(EQ 18)}$$

and specify modal damping

$$\tilde{\mathbf{C}} = \begin{bmatrix} 2\zeta\omega_1 & 0 & \dots & 0 \\ 0 & 2\zeta\omega_2 & & \vdots \\ \vdots & & \vdots & 0 \\ 0 & \dots & 0 & 2\zeta\omega_{70} \end{bmatrix} \qquad \textit{(EQ 19)}$$

Because the damping of the cab suspension is to be applied in physical coordinates, resolve Eq. (19) to the physical space

$$\mathbf{C} = \Phi^{-1}\tilde{\mathbf{C}}\Phi. \qquad \textit{(EQ 20)}$$

Add the variable stiffness and damping of the cab suspension system

$$\mathbf{K} = \mathbf{K} + \Delta_K \textit{ and } \mathbf{C} = \mathbf{C} + \Delta_C, \qquad \textit{(EQ 21)}$$

and solve for the impedance matrix

$$\mathbf{H}(\omega) = (-\omega^2 \mathbf{M} + j\omega\mathbf{C} + \mathbf{K})^{-1}. \qquad \textit{(EQ 22)}$$

The output PSD is then

$$\mathbf{S}_o(\omega) = \mathbf{H}(\omega)\mathbf{S}_i(\omega)\mathbf{H}(\omega)^*, \qquad \textit{(EQ 23)}$$

where the input PSD, $\mathbf{S}_i(\omega)$, is given in [20] and [18], and the RSI is given by Eq. (14). The steps involving Eqs. (21) through (23) are repeated until a minimum ride severity index is achieved.

STRUCTURAL DYNAMICS MODELING AND TESTING OF THE DEPARTMENT OF ENERGY TRACTOR/TRAILER COMBINATION

Richard V. Field, Jr.[†], John E. Hurtado[‡], Thomas G. Carne[‡], and Clark R. Dohrmann[†]

[†] *Structural Dynamics and Vibration Control*
Sandia National Laboratories
P.O. Box 5800
Albuquerque, New Mexico 87185-0439

[‡] *Experimental Structural Dynamics*
Sandia National Laboratories
P.O. Box 5800
Albuquerque, New Mexico 87185-0557

ABSTRACT*. This study presents a combined analytical and experimental effort to characterize and improve the ride quality of the Department Of Energy tractor/trailer combination. The focus is to augment the experimental test results with the use of a high quality computer model. The discussion includes an overview of the finite element model of the vehicle and experimental modal test results. System identification techniques are employed to update the mathematical model. The validated model is then used to illustrate the benefits of incorporating two major design changes, namely the switch from a separate cab/sleeper configuration to an integrated cab, and the use of a cab suspension system.*

NOMENCLATURE

c	Damping
g	Unit of acceleration
k	Stiffness
rms	Root-mean-square
$L(f)$	Insertion Loss Factor
$S(f)$	Power Spectral Density (PSD) Function
FRF	Frequency Response Function
MAC	Modal Assurance Criterion
MIF	Modal Indicator Function
RSI	Ride Severity Index

1. INTRODUCTION

Designing tractor/trailer style trucks that exhibit good ride characteristics has been a challenge to automotive engineers for many years. When attempting to improve ride quality, the response of primary interest is the vibration experienced by the driver and bunk occupants. The ride environment of the truck driver is influenced by road roughness, rotating tire/wheel assemblies, the driveline, and the engine [28]. In this study, only the ride due to external road surface excitation is considered.

Previous methods to improve cab-ride quality included altering the frame bending stiffness, introducing softer primary suspensions, and improving tire stability and driver seats [25]. The idea of a cab suspension system was first employed in heavy truck design more than three decades ago and consisted of an independent leaf spring assembly placed at each of the four corners of the cab [26]. Since then, the design of the cab suspension system has evolved into a fixed-front pivot combined with a spring/damper rear mount, and is very common on the road today.

2. FINITE ELEMENT MODEL

Figure 51 illustrates the MSC/NASTRAN finite element model of the DOE tractor/trailer combination. Currently, the cab, sleeper, and trailer are modeled as rigid body elements; each has a concentrated mass element associated with it located at the center-of-mass, and appropriate rigid element connections join these point masses to the remainder of the vehicle. One particular interface is located at the fifth wheel, where the tractor and trailer connect. The fifth wheel itself is modeled as a point mass, including the effects of the steel mounting plate that adds significant stiffness to the tractor frame. At the top of the fifth wheel is the king pin, which allows relative rotation in the X and Y directions between the tractor and trailer. Another interface occurs where linear springs model the cab and sleeper "hard-mounts" to the truck frame. These mounts exhibit stiffness in the three translational directions, and are situated in a 3-point and 4-point configuration, respectively. The tractor frame and crossmembers are modeled with a large number of QUAD elements that capture the frame elastic modes.

A detailed view of the steer axle suspension system is illustrated in Fig. 52, where the leaf spring is modeled as a simple linear spring in the vertical direction, and "very stiff" in the

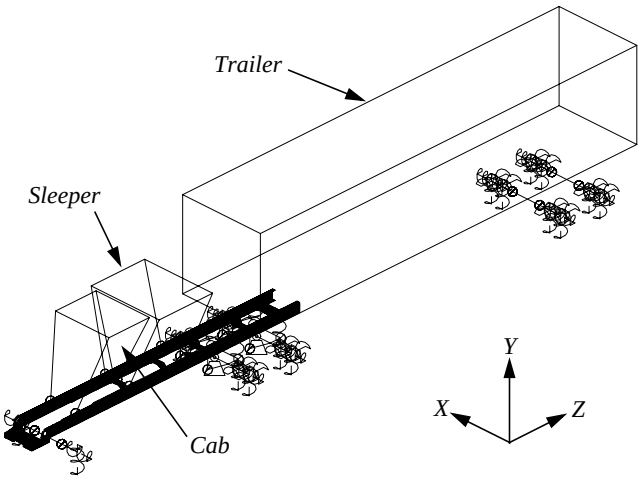

Figure 51: MSC/NASTRAN model of the DOE tractor/trailer combination.

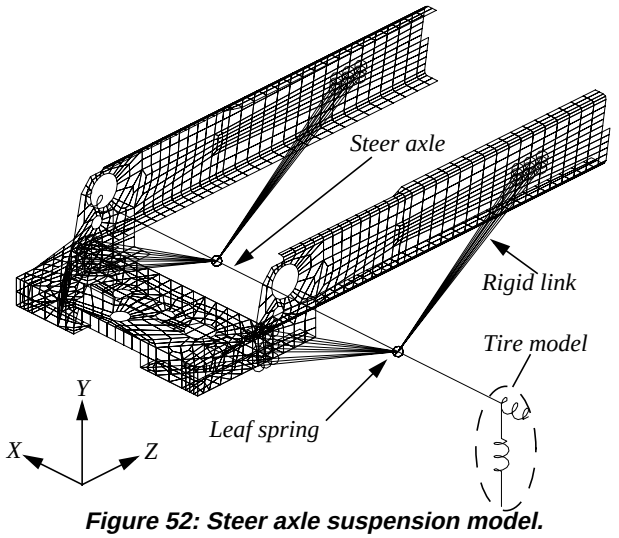

Figure 52: Steer axle suspension model.

remaining five directions. The leaf spring is rigidly connected to both the steer axle and the truck frame. A linear tire model is used here, consisting of two spring elements that represent the effective stiffness in the vertical and lateral directions. Note that this is valid because only small displacements are expected in a modal test. There is no fore/aft stiffness for the tire because there are no brakes on the steer axle. Lastly, the axle model is a series of NASTRAN BEAM elements.

Figure 53 contains a detailed view of the Neway AD-246 suspension system used on both the front and rear tractor drive axles. Each suspension system utilizes a trailing arm, modeled as a rigid link, an airbag, modeled as a linear spring in the axial direction only, and anti-roll bar, modeled as a series of BEAM elements. The AD-246 also contains two shock absorbers (just in-board of the airbags) that connect the anti roll-bar to the frame cross-members. These were not modeled, however, since the experimental modal tests were

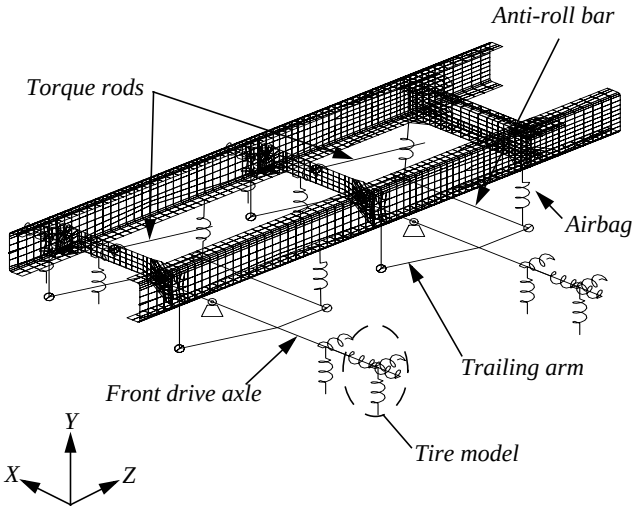

Figure 53: Drive axle suspension model.

performed with them disconnected. The tires (each axle contains four) are modeled identical to those on the steer axle, with one exception - an additional spring can be included to model the combined tire/brake stiffness in the fore/aft direction. This allows the NASTRAN model to simulate the vehicle modal response with and without the brakes applied. As before, the front and rear axles were modeled as a series of BEAM elements. The suspension systems on the trailer also utilize leaf springs, but with a much higher spring rate. Similarly, modal testing was performed with and without the brakes on the trailer, leading to a tire model identical to that on the tractor drive axles.

3. MODAL TESTING

Several modal tests were performed on the vehicle. Tests were applied with and without the brakes applied, but only the latter case is discussed herein. Electrodynamic shakers rated at 100 lb and 250 lb were used to simultaneously excite the structure. The forces were applied in the vertical direction, while a total of 101 Endevco 7751 accelerometers monitored the vibrational response of the system.

A low level, continuous-random force excitation signal was input to the vehicle through the electrodynamic shakers at two locations on the vehicle; the 100 lb shaker was located at the front/passenger side of the tractor, and the larger shaker was placed at the passenger side of the trailer, halfway back. The signals sufficiently excited the structure while keeping the dynamic response within the linear regime about the static equilibrium. Frequency response functions (FRFs) between the applied excitation forces and the measured accelerations were calculated and recorded. Modal frequencies, damping factors, and mode shapes were then estimated from the recorded FRFs.

The modal survey of the vehicle without the brakes applied was performed by releasing the applied brakes and rolling the vehicle forward to overcome any stiction in the wheels and bearings. Figure 54 shows experimental FRFs for this test

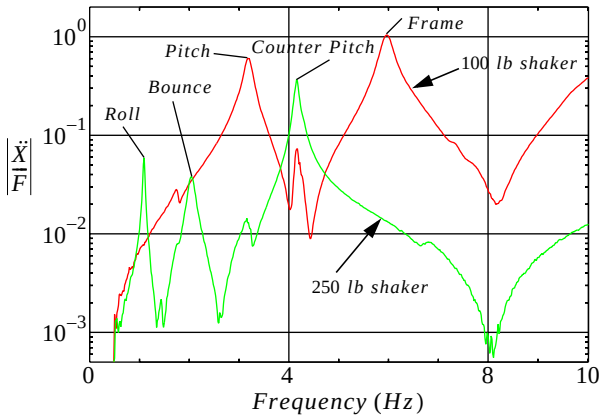

Figure 54: Experimental FRF.

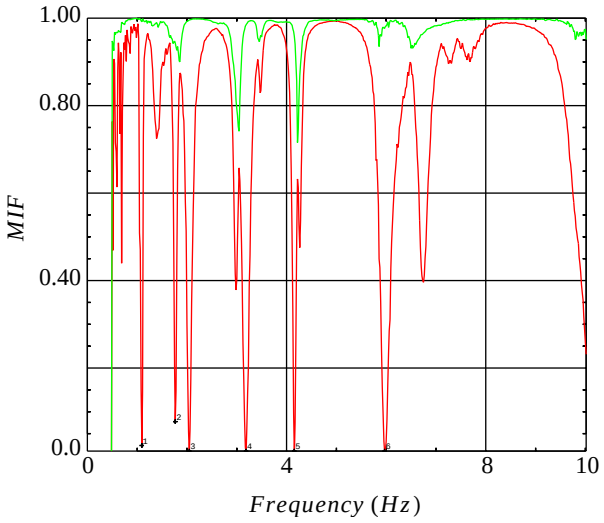

Figure 55: Experimental MIF.

configuration, and Fig. 55 shows the Mode Indicator Functions (MIFs). Table 2 lists the estimated natural frequencies from the data analysis, along with a brief description of the mode shapes. Both the experimental and analytical mode shapes are displayed in Figs. 56 through 61.

4. TEST/ANALYSIS CORRELATION

In order to obtain good agreement between the finite element model and modal test results, it was necessary to change the values of some uncertain parameters in the model. Six of the parameters that were updated are shown in Table 1. The original parameter values lead to large errors in the frequencies of the model. In addition, the mode shapes did not correlate well, as indicated by poor initial MAC values. These rather large discrepancies can be attributed to a lack of sufficient information to provide estimates for the initial stiffnesses of the various suspensions and tire/wheel assemblies.

Parameter	Original	Updated
Tire vertical stiffness	4568, $\frac{lb}{in}$	11750, $\frac{lb}{in}$
Tire lateral stiffness	1500, $\frac{lb}{in}$	2080, $\frac{lb}{in}$
Tire fore/aft stiffness	2015, $\frac{lb}{in}$	2580, $\frac{lb}{in}$
Tractor leaf spring stiffness	2050, $\frac{lb}{in}$	8340, $\frac{lb}{in}$
Air bag stiffness	2100, $\frac{lb}{in}$	1040, $\frac{lb}{in}$
Trailer leaf spring stiffness	14000, $\frac{lb}{in}$	16350, $\frac{lb}{in}$

Table 1: Parameter changes due to model update.

Updated parameter values were obtained using a Sandia in-house code PESTDY (Parameter Estimation for STructural DYnamics) and led to the improved MAC and frequency agreement shown in Table 2 and Figs. 56-61.

Mode Description	Test/Analysis Frequency (Hz)	MAC
fore/aft	N/A / 0.211	N/A
roll/twist #1	1.09 / 1.08	0.980
roll/twist #2	1.76 / 1.76	N/A
bounce	2.04 / 2.01	0.867
pitch	3.19 / 3.22	0.939
counter pitch	4.16 / 4.12	0.835
bending	5.96 / 6.06	0.830

Table 2: Results of model update.

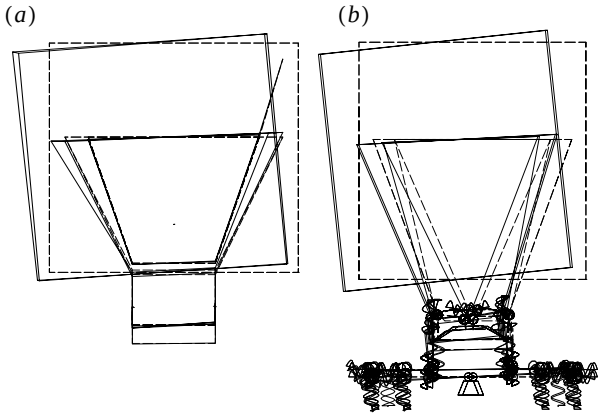

Figure 56: Roll/twist mode #1, experimental, (a), and analytical, (b).

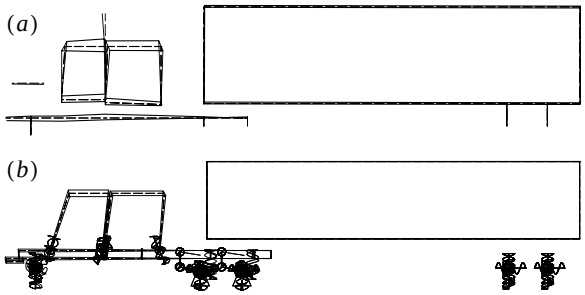

Figure 57: Roll/twist mode #2, experimental, (a), and analytical, (b).

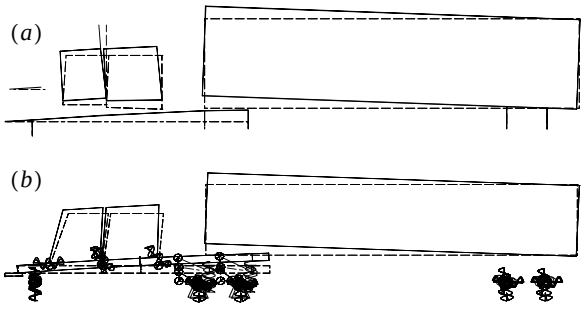

Figure 58: Bounce mode, experimental, (a), and analytical, (b).

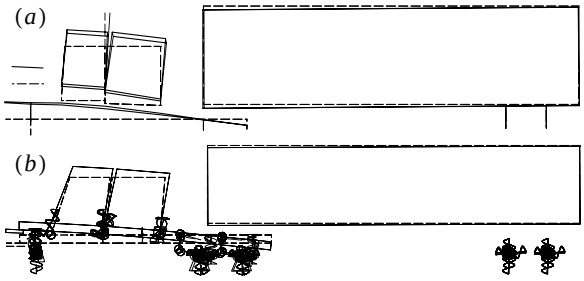

Figure 59: Pitch mode, experimental, (a), and analytical, (b).

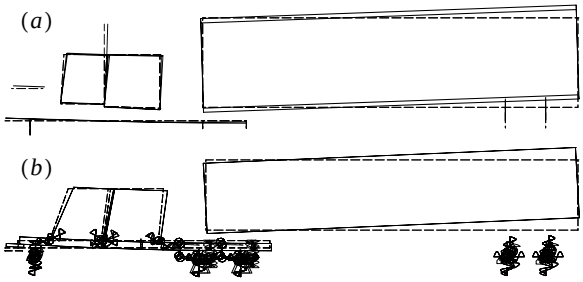

Figure 60: Counter pitch mode, experimental, (a), and analytical, (b).

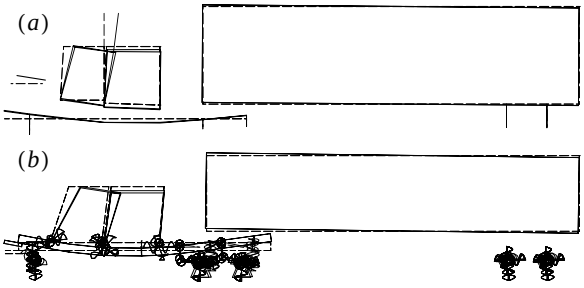

Figure 61: Frame bending mode, experimental, (a), and analytical, (b).

A few comments concerning the results of the test/analysis correlation are in order. Because the correlation was performed using modal test data, the updated parameters are associated with small amplitude motions. It is expected that some stiffnesses, such as those of the leaf springs, would be reduced in over-the-road environments where stiction effects are overcome. Efforts are currently underway to obtain stiffness and damping estimates directly from the transient response of driving the vehicle over a prescribed bump. Finally, it is noted that there remains some uncertainty in the absolute values of the tire vertical and suspension stiffnesses because they act in series.

5. DESIGN FOR RIDE QUALITY

The design of a next-generation DOE tractor is to be completed in the next few years. This new vehicle will most likely exhibit significant modifications from the current design. One such change may be a switch to an integrated cab configuration, since this provides more room to the occupants. Another might be the addition of a tractor cab suspension system to improve the vibrational response of the cab. In this paper, the authors consider the performance of a cab suspension system that is available on the market today. In addition, an optimized suspension will also be considered. This cab suspension system is optimal in the sense that it provides the maximum protection to the driver from vibration due to road surface input.

For the purposes of this study, the suspension is modeled as a simple spring-damper system and is placed into the full updated finite element model with new integrated cab, as shown in Fig. 62. Furthermore, the stiffness and damping constants of this system are used as the design variables in the optimization problem to be discussed later. Linear springs in the three translational directions model the cab "hard-mounts" to the truck frame in the front.

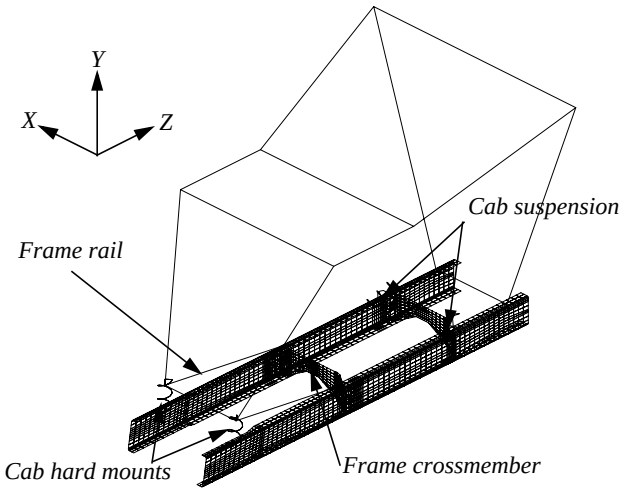

Figure 62: Integrated cab with cab suspension.

Most road surfaces have irregularities that are best described as random processes, and many can be accurately represented under an additional assumption of stationarity [27]. It is therefore relevant to study the vehicle response due to a stationary random "rough road" input at several key locations of the truck.

Frequency response and power spectral density analyses can be utilized to assess the vibratory response of automotive vehicles. Below are some results from such a study that simulates the DOE vehicle driving at 55 *m.p.h.* over a "rough road". Some theoretical concepts are presented, and analytical results using the model are discussed. Special emphasis is given to the issue of random loading and the cross-spectral density matrix that simulates the road input to an 18-wheel vehicle.

To apply this input PSD, knowledge of the cross-spectral density matrix of input forces is required. Assuming the vehicle is following a straight, constant speed trajectory, let W_1 and W_2 represent the amplitude seen by the left and right tires, respectively, due to the excitation of the road. For the studies presented here, it is assumed that the left and right tires experience the same road surface, but the two are not perfectly correlated. Define

$$\phi_{11}(\tau) = E[W_1(\tau)W_1(t+\tau)], \quad (1)$$

$$\phi_{22}(\tau) = E[W_2(\tau)W_2(t+\tau)], \quad (2)$$

$$\phi_{12}(\tau) = E[W_1(\tau)W_2(t+\tau)], \quad (3)$$

where $E[\bullet]$ is the expectation operator, $\phi_{11}(\tau)$ and $\phi_{22}(\tau)$ are the autocorrelation functions, and $\phi_{12}(\tau)$ is the crosscorrelation function representing the interaction between the left and right sides of the vehicle.

The schematic shown in Fig. 63. illustrates the 10 locations in which the "rough road" will excite the vehicle, assuming the dual wheel locations at stations 3 through 10 act together. The complete input power spectra is therefore characterized by a ten-by-ten matrix, where the elements of this matrix involve the Fourier transforms of Eqs. (1)-(3). Specifically, the two-by-two blocks on the diagonal of this matrix are of the form

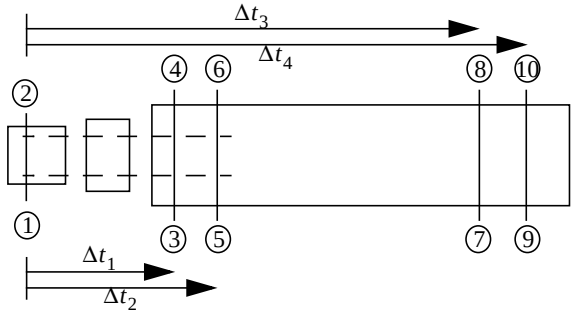

Figure 63: Input stations for the DOE tractor/trailer combination.

$$\Phi_{2x2}(f) = \begin{bmatrix} k_{eff}^2\phi_{11}(f) & k_{eff}^2\phi_{12}(f) \\ k_{eff}^2\phi_{12}(f) & k_{eff}^2\phi_{22}(f) \end{bmatrix}, \quad (4)$$

where k_{eff} is the effective stiffness at the particular station of interest (*i.e.*, the collective vertical tire stiffness), and $\phi_{11}(f)$, $\phi_{12}(f)$, and $\phi_{22}(f)$ are the Fourier transforms of Eqs. (1)-(3). Note that by scaling Eq. (4) by the stiffness terms, the input is now a *force* power spectral density.

The remaining terms of Φ involve various degrees of correlation between the different axles. Because the vehicle is at a constant speed, this can be accomplished by delaying the input to the tractor front drive axle, as well as those behind it [30], as illustrated in Fig. 63.

It has been found that terrain roughness can be represented in the frequency domain by power spectral density functions of the form

$$\Psi(\Omega) = c\Omega^{-n}, \quad (5)$$

where Ω is the spatial frequency, in units of *cycles/length*, and n and c are constants. As discussed in [27], $n = 2.0$ is typical. Therefore, for a vehicle traveling at a constant speed of v_o, the power spectral density that describes the input displacement seen at the road surface can be given by

$$\Phi(f) = \frac{1}{v_o}\Psi(\frac{2\pi f}{v_o}) = \frac{v_o c}{(2\pi f)^2}, \quad (6)$$

where f is now the temporal frequency, in units of *cycles/sec*. In addition, plots of Ψ *vs.* Ω are presented in [23], [30] and [31] for several road surface types. Assuming a "rough road" terrain, $c = 3.24e\text{-}6$ *in-cycles*.

Figure 64 illustrates $\phi_{11}(f)$, $\phi_{22}(f)$, and $\phi_{12}(f)$ vs. frequency, where plot (a) is directly from Eq. (6) for $v_o = 55\ mph$. To estimate the correlation of the terrain between the left and right tire tracks of the vehicle, consider the coherency function

$$g^2(\Omega) = \frac{|\Psi_{12}(\Omega)|^2}{\Psi_{11}(\Omega)\Psi_{22}(\Omega)}, \ 0 \le g^2(\Omega) \le 1 \quad (7)$$

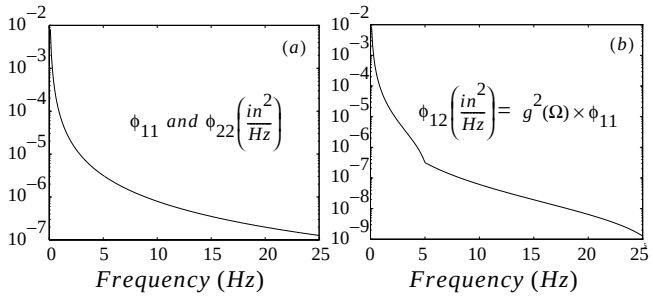

Figure 64: Input autopower and crosspower spectral density functions.

Typically, as discussed in [31], the coherency function is near unity at low frequencies (*i.e.*, high correlation for hills or dips in the road surface), and much lower at the higher frequencies (*i.e.*, low correlation for cracks in the pavement, potholes, etc.). Utilizing this assumption, Eq. (7) can be used to determine $\phi_{12}(f)$ shown in Fig. 64(b).

The cab suspension system, placed between the rear of the integrated cab and truck frame, can be utilized to improve the ride quality of the vehicle. The ride severity index (RSI), a weighted measure of the power of the output spectrum, can be used to gauge this improvement. Consider the following relation

$$RSI = \left[\int_{f_1}^{f_2} L(f)^2 S_{out}(f) df\right]^{\frac{1}{2}}, \tag{8}$$

where $S_{out}(f)$ is the output power spectral density function and $f \in [f_1, f_2]$ denotes the frequency band of interest. As shown, the RSI is a scalar quantity that is simply a weighted sum of the output PSD. The insertion loss factor, $L(f)$, is a quantity indicative of the human body's sensitivity to vibration. The higher the loss factor, the more sensitive the human is to the excitation.

For the studies included here, only the vibration at the driver seat is considered, and the ride severity index is given by

$$RSI = \left(\int_1^4 \frac{f}{4} S_Y(f) df + \int_4^8 S_Y(f) df + \int_8^{25} \left(\frac{64}{f^2}\right) S_Y(f) df + 1.96\left\{\int_1^2 S_Z(f) df + \int_2^{25} \left(\frac{4}{f^2}\right) S_Z(f) df\right\}\right)^{\frac{1}{2}} \tag{9}$$

The terms involving $S_Z(f)$ are scaled by an additional factor of $(1.4)^2 = 1.96$ since vibration in the fore/aft direction is particularly disturbing to humans [24].

The minimization problem to be solved here can be stated as

$$\min_{k,\,c,\,z} RSI, \text{ subject to } k_{min}, c_{min} \le k, c \le k_{max}, c_{max}, \tag{10}$$

where k, c, and z refer to the stiffness, damping, and location of the cab suspension system, respectively, and the bounds on the stiffness and damping ensure physically practical solutions. Because varying the location of the suspension system requires re-meshing the finite element model, however, Eq. (10) is solved for a fixed location, z. This location is then varied discreetly along the tractor frame to provide a qualitative estimate of the optimal location.

The optimization capabilities of MATLAB [29] are utilized to determine optimal values of the cab suspension system at various locations along the frame. The results are shown in Table 3, where z is the location of the suspension system, referenced to the location of truck's third frame crossmember

Design	k, $\frac{lb}{in}$	c, $\frac{lb\text{-}s}{in}$	RSI, $mg\text{-}rms$
Current cab	N/A	N/A	20.42
Current sleeper	N/A	N/A	23.53
z = 0.0 in	333.4	105.6	11.46
z = -12.0 in	420.0	125.1	11.07
z = -24.0 in	287.7	128.0	9.386
z = 12.0 in	410.5	101.6	11.44
z = 24.0 in	416.9	95.77	11.35

Table 3: RSI for current design (cols. 1 and 2) vs. integrated cab with optimal suspension.

(where a typical cab suspension would be located due to structural considerations). $z = 0$ is the typical location of the suspension, and positive and negative values of z are behind and in front of it, respectively. Note that the optimal spring-damper values are to be applied at both the passenger- and driver-side of the vehicle.

Plots illustrating the possible benefits of an optimized cab suspension are included in Figs. 65 and 66, where it is evident that changing the design of the cab suspension only has a significant effect on the response of the cab in the frequency range of 0 to 6 *Hz*.

The optimal RSI occurs when the suspension is pushed 24 inches forward of its present location. The vertical response in Fig. 65 illustrate a drastic reduction in the bounce and pitch modes when using the optimal cab suspension. In addition, the vertical mode of the suspension reduces in frequency

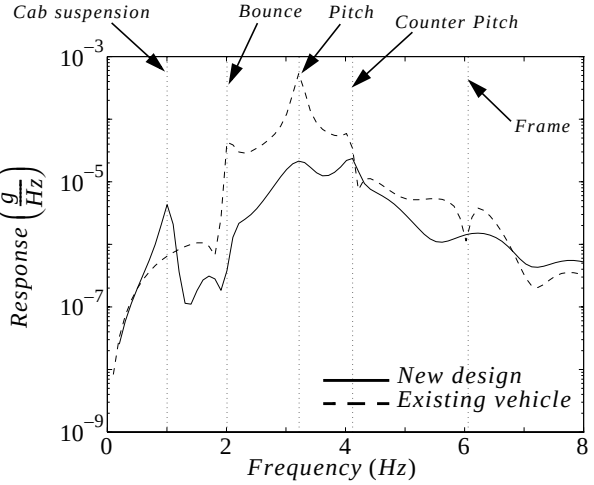

Figure 65: Vertical response at the cab of existing vehicle and new design.

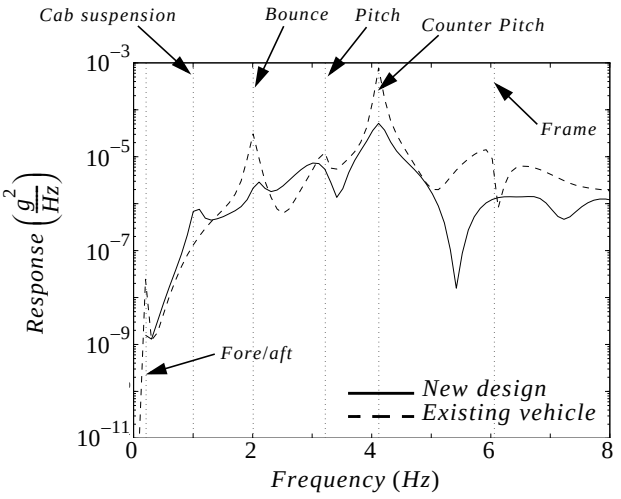

Figure 66: Fore/aft response at the cab of existing vehicle and new design.

from $f = 1.34\ Hz$ to $f = 1.00\ Hz$ since, as the location of the cab suspension moves forward, it is required to carry more of the cab weight. When considering the fore/aft response of the cab, shown in Fig. 66, the optimal suspension again demonstrates reduction in the power of the bounce, pitch, and counter-pitch modes.

As a general observation, it appears that the RSI will continue to decrease as the location of the cab suspension is moved forward. There are physical limits, obviously, since moving the suspension forward requires that it support a greater static load due to weight of the cab. Cab stresses are also an issue and, therefore, the location of the cab suspension cannot be chosen to minimize the ride severity index alone.

6. CONCLUSIONS

The preliminary dynamic model of the DOE tractor/trailer combination correlates well with the characteristics seen during the experimental modal tests. As the model is refined, it is clear that it will be an integral tool in determining the design of the next-generation tractor. Any possible benefits to be gained from the use of available passive cab vibration suppression methods will be researched. In addition, the computer model can be used to examine any improvements utilizing active vibration control techniques.

Possible design modifications to the vehicle, namely the conversion to an integrated-type cab with a cab suspension system, have been discussed. With the addition of the integrated cab with nominal cab suspension, a 44% reduction in ride severity can be achieved over the current cab/sleeper configuration, which is hard-mounted to the truck frame. Furthermore, once an optimized cab suspension is utilized, the RSI can be reduced by an additional 18%. Finally, the results shown here indicate that the cab suspension system should be located as far forward as structural considerations will allow.

7. ACKNOWLEDGEMENTS

The authors would like to acknowledge the help of Rob Pirtle and Hoden Farrah of Marmon Motors and Ken Vande Brake of Link Manufacturing, Inc.

8. REFERENCES

[23] Baum, J.M., J.A. Bennett and T.G. Carne, “Truck Ride Improvement Using Analytical and Optimization Methods,” General Motors Research Laboratories, GMR-2324-R, 1978.

[24] “Evaluation of Human Exposure to Whole-Body Vibration,” International Organization for Standardization, ISO 2631/1-1985(E).

[25] Flower, W., “Analytical and Subjective Ride Quality Comparison of Front and Rear Cab Isolation Systems on a COE Tractor,” *Society of Automotive Engineers*, No. 780411, pp. 1917-1929, 1978.

[26] Foster, A.W., “A Heavy Truck Cab Suspension for Improved Ride,” *Society of Automotive Engineers*, No. 780408, pp. 1899-1916, 1978.

[27] Gillespie, T.D., *Fundamentals of Vehicle Dynamics*, Society of Automotive Engineers, 1992.

[28] Gillespie, T.D., “Heavy Truck Ride, Society of Automotive Engineers, The Thirty-First L. Ray Buckendale Lecture, SP-607, 1985.

[29] Grace, A., “MATLAB Optimization Toolbox,” The MathWorks, 1995.

[30] Healy, A.J., “An Analytical and Experimental Study of Automobile Dynamics with Random Roadway Inputs,” *ASME Journal of Dynamic Systems, Measurement, and Control*, December, pp. 284-292, 1977.

[31] Soong, T.T. and M. Grigoriu, *Random Vibration of Mechanical and Structural Systems*, Prentice-Hall, Inc., 1993.

Sandia National Laboratories

Albuquerque, New Mexico 87185

date: October 29, 1997

to: Distribution

from: R. V. Field, Jr., Dept. 9234, MS0439, J.E. Hurtado and T.G. Carne, Dept. 9741, MS0577

subject: Analytical and Experimental Assessment of Heavy Truck Ride

ABSTRACT

This study is the second phase in a combined analytical and experimental effort to characterize and improve the ride quality of the Department Of Energy tractor/trailer. The discussion includes a brief overview of the finite element model of the vehicle and experimental road and modal test results. A novel system identification approach is used, employing both lab-based modal tests, and modal data derived using the Natural Excitation Technique (NExT), a scheme that utilizes the roadway surface as a natural forcing function. The use of a cab isolation system is investigated with the computer model for purposes of improving the ride quality of the vehicle. To validate these analytical predictions, an engineering prototype vehicle was developed, which included a cab isolation system, to experimentally assess ride quality. Ride quality improvements due to the addition of the isolation system are then assessed both experimentally and analytically, and the results are compared.

1. INTRODUCTION

The Department of Energy (DOE) is committed to researching ideas for improved heavy truck ride, because a smoother ride is less fatiguing to the operators and, hence, safer to everyone on the road. Previous work funded by the DOE in this area [34], demonstrated that the addition of a cab isolation system may provide considerable ride improvements to DOE's existing fleet of tractor/trailers.

Designing tractor/trailer style trucks that exhibit good ride characteristics has been a challenge to automotive engineers for decades [38]. Hence, the use of a cab isolation system is not a new concept. Previous methods to improve cab-ride quality have included: altering the frame bending stiffness, introducing softer primary suspensions, and improving tire stability and driver seats [35]. The idea of a cab suspension system was first employed in heavy truck design more than three decades ago and consisted of an independent leaf spring assembly placed at each of the four corners of the cab [36]. Since then, the design of the typical cab suspension system has evolved into a fixed-front pivot combined with a spring/damper rear mount. It is this configuration that is commonly seen on the road today.

Previous conclusions about the possibilities of ride improvement discussed in [34] were based solely upon a model that was validated with laboratory-based modal tests. These tests used a very low level of excitation; it was known at the time that the tires and leaf springs added nonlinear behavior to the overall dynamics of the vehicle and would react quite differently when subject to the much larger level of excitation provided by the road surface. Hence, it was expected that the truck would behave much differently when exposed to an operational level of excitation. Laboratory modal tests, however, were the only means available to validate the computer model at the time. Dynamic modes of the vehicle have since been extracted using the Natural Excitation Technique (NExT) [40]; this dynamic state is more representative of the truck's operational environment. Correlating the computer model to these test results will allow a much more realistic prediction of the vehicle's ride characteristics.

The purpose of this work is threefold: (1), to illustrate the combined use of laboratory modal test results, modes extracted from the operating environment of the vehicle using NExT, and the truck's PSD response to validate the computer model, (2), to make a comparison between analytical predictions and experimental measurements of ride quality, and (3), to broaden the knowledge base in the areas of vehicle dynamics and proper testing techniques.

2. VEHICLE DESCRIPTION

Figure 67 illustrates a schematic of the DOE tractor, including some of the terminology commonly used in the heavy truck community. The driver is located in the cab, and any off-duty personnel lie on the bunk in the sleeper compartment. The vehicle is configured in a separate cab / sleeper arrangement, as compared to an integrated cab / sleeper design.

The MSC/NASTRAN finite element model of the DOE tractor is shown in Fig. 68. A standard, two-axle trailer connected to the tractor at the fifth wheel is also modeled, but not shown in the figure. See [34] for a detailed description of the finite element model development.

3. EXPERIMENTAL TESTING

In an effort to characterize the ride characteristics of the vehicle, two sets of experimental tests were performed. The first was the typical laboratory-based modal test, indicative of how the vehicle responds to low-level excitation. The second set of tests using NExT, were performed under the truck's normal operating conditions. The following two sections provide detailed descriptions of the two tests.

3.1 Modal testing

A low level, continuous-random force excitation signal was input to the vehicle through electrodynamic shakers at two locations on the vehicle; a 100 lb shaker was located at the front/passenger side of the tractor, and a larger 250 lb shaker was placed at the passenger side of the trailer, halfway back. The signals sufficiently excited the structure while keeping the dynamic response within the linear regime about the static equilibrium. Frequency response functions (FRFs) between the applied excitation forces and the measured

accelerations were calculated and recorded. Modal frequencies, damping factors, and mode shapes were then estimated from the recorded FRFs. Prior to each test, the vehicle was rolled forward and back to overcome any stiction in the wheels and bearings. Figure 69 contains experimental FRFs for this test configuration.

3.2 Natural excitation testing

The tractor was instrumented with thirty one accelerometers, the majority of which were placed along the passenger side of the vehicle. Five displacement sensors were located along the passenger side of the vehicle at each of the five axle locations. These sensors measured the relative displacement between an axle and the frame directly above it. During all road testing, the vehicle was driven along Interstate 25 (I-25) south of Albuquerque at a constant velocity of 55 *mph*.

The cross spectral densities (CSD's) of the accelerometers were computed for various choices of reference accelerometers. A total of 1024 spectral points were used in the computation, along with a Hanning window function and overlap processing. Treating the CSD's as transfer functions, the Complex Mode Indicator Function (CMIF) was computed and is shown in Fig. 70 for several reference accelerometer choices. Here, the largest singular value is plotted along the y-axis, illustrating that there are relatively lightly damped structural modes at frequencies of 2.75 Hz, 3.75 Hz, and 5.50 Hz. There is a very heavily damped structural mode at 1.25 Hz, and a periodic response near 8.0 Hz, which is related to the tire rotation frequency.

A peak-picking strategy was adopted and applied to the CSD's to determine frequency and mode shape information. Specifically, it is the magnitude and phase information of the CSD's that lead to the frequency and shape information. To illustrate, consider the mode at 3.75 Hz. Clearly from Fig. 70, the CMIF has the largest amplitude at 3.75 Hz when channel 22 is selected as the reference channel. Thus, at 3.75 Hz, the magnitude and phase information of the CSD's associated with channel 22 selected as the reference channel are used to determine the associated mode shape. This process is repeated with a different reference channel to obtain the magnitude and phase information related to the other frequencies. The magnitude gives the nodal amplitudes, and the phase is used to determine the sign of the amplitude: if the amplitude is near $0°$ then the amplitude is taken as positive; if the amplitude is near $\pm 180°$, then the amplitude is taken as negative. A judgement call must be made for phase angles that significantly deviate from either of these extremes.

4. TEST/ANALYSIS CORRELATION

Before the computer model can be utilized to predict ride characteristics, correlation between measured test data and predicted analysis data is required. Comparing the model predictions to laboratory-based modal test results is the usual procedure, but this proved to be inadequate due to a number of nonlinear elements evident in the vehicle. One such element, the leaf spring suspension assembly located at the steer axle and trailer axles, is known to exhibit hysteretic behavior. In addition, a typical tire produces less spring rate when rotating than when motionless [39]. As a result, correlating the model to laboratory-based modal test results alone is not an acceptable approach due to the presence of these and other nonlinear qualities. Furthermore, using NExT test data as the only information to

verify the computer model is not a viable alternative. Cross-spectra were measured between different locations on the vehicle using the road surface as the input. The unknowns in the computer model cannot be determined, however, because these data sets do contain sufficient information. The solution is to treat the vehicle as a quasi-linear system, behaving linearly in one regime under laboratory-level excitation, and linearly in a second regime under normal operating levels of excitation.

The computer model, correlated to the modal test results, is used as a starting point. Herein it is assumed that only those parameters behaving in a highly nonlinear manner will deviate from how they behave during laboratory modal tests. As a result, the NExT procedure is used to *complement* the modal tests, providing sufficient information to validate the model so it can predict responses due to natural operating conditions.

4.1 Correlating to modal tests

In order to obtain good agreement between the finite element model and modal test results, it was necessary to adjust the values of some uncertain parameters in the model. These included stiffnesses of the tires, airsprings, and leaf spring assemblies.

Updated parameter values were obtained using a Sandia in-house code PESTDY [32] (Parameter Estimation for STructural DYnamics). Refer to [34] for a more detailed discussion of this procedure. The corresponding modal assurance criteria (MACs) and frequency agreement are shown in Table 1. Because the correlation was performed using modal test data, the updated parameters are associated with small amplitude motions. It is expected that some stiffnesses, such as those of the leaf springs, would be reduced in over-the-road environments where stiction effects are overcome.

4.2 Correlating to natural excitation tests

Because the NExT method also provides modal frequency, damping, and shape information, the techniques discussed in §4.1 can be employed to the road data. However, and as noted above, neither the laboratory or road test data can be used alone to update the model. Therefore, using the model correlated to the modal test as a starting point, certain parameters were adjusted until the entire model matched the NExT results. Those elements in the model suspected of highly nonlinear behavior (*i.e.*, tire and leaf spring stiffnesses) were the only parameters changed in the effort to correlate to NExT results.

Mode Description	Test/Analysis Frequency (Hz)	Measured damping (%)	MAC
bounce	2.04 / 2.01	3.36	0.867
tractor pitch	3.19 / 3.22	2.91	0.939
counter pitch	4.16 / 4.12	1.15	0.835
frame bending	5.96 / 6.06	2.10	0.830

Table 1: Results of model / modal test reconciliation.

Mode Description	Test/Analysis Frequency (Hz)	Measured damping (%)	MAC
bounce	1.25 / 1.98	26.0	0.661
tractor pitch	2.75 / 2.75	9.1	0.934
counter pitch	3.75 / 3.75	3.5	0.986
frame bending	5.50 / 5.50	3.1	0.783

Table 2: Results of model / NExT test reconciliation.

Table 2 illustrates the results of the model / NExT test reconciliation effort. Note that there is a large discrepancy in the modal frequency of the bounce mode. As illustrated by Fig. 70, the bounce mode was not sufficiently excited by the road surface, thereby making the extraction of the modal frequency, damping, and shape not a well defined task. The level of excitation is directly related to the vehicle's speed. Therefore, future road tests will be conducted at different speeds to ensure that all dynamic modes are sufficiently excited. For all the tests discussed here, the vehicle was operated at 55 *mph*; little effort went into correlating the computer model to the test results for the bounce mode for this reason.

The test and analytical mode shapes characterizing the vehicle under operating-level excitation are included in Figs. 71-74. An interesting concept to notice is how the model parameters change when correlating to modal or NExT tests. As illustrated by Table 3, the leaf springs on both the tractor and trailer are much stiffer when subject to the low-level excitation of a modal test. When the level of excitation increases, however, the leaves start sliding with respect to one another, and the stiffness of the entire assembly decreases. In addition, the slight decrease in the vertical tire stiffness shown in Table 2 is expected, because a rotating tire is slightly less stiff than a stationary one [39].

5. ENGINEERING PROTOTYPE VEHICLE

For experimental ride quality studies, an engineering prototype vehicle was established by modifying one tractor in the current DOE fleet. A drawing of the prototype is included in Fig. 75. As illustrated in Fig. 76, a sub-frame assembly was added beneath the cab and

Parameter	Correlated to modal tests ($\frac{lb}{in}$)	Correlated to NExT tests ($\frac{lb}{in}$)
Tire vertical stiffness	6342	6131
Tire lateral stiffness	1988	1982
Tractor leaf spring stiffness	27320	8063
Air bag stiffness	1141	1124
Trailer leaf spring stiffness	47190	23900

Table 3: Parameter changes due to model update.

sleeper. This approximates an integrated cab configuration, because the sub-frame ties the cab and sleeper together; they behave as a single unit on top of the vehicle's main frame.

The Cab-mate™ cab isolation system, provided by Link Manufacturing, Inc., is also shown in Fig. 76. The objective of this system is to isolate the cab occupants as much as possible from vibrations due to road surface roughness. Typically, a $2\ dB$ reduction in the vibrational response of the cab has been observed. To help determine how vital the location of this system is, the sub-frame was assembled so as to allow the fore/aft position of the Cab-mate™ to vary between the aft end of the sub-frame and 33 inches forward. This vehicle was then used for all ride quality studies that follow. Specifically, the ride characteristics of three configurations were assessed: (1), *nominal* (cab is hard mounted to the frame), (2), *isolation #1* (cab isolation system is installed at the rear of the sleeper), and (3), *isolation #2* (cab isolation system is installed 33 inches forward of the rear of the sleeper).

Because it is this prototype vehicle that is to be used for all ride quality studies, appropriate changes were made to the finite element model to accurately represent all three configurations of this prototype vehicle. Analytical predictions of the dynamic modes of the prototype (*isolation #1* configuration) under operational-level excitation are shown in Figs. 78-81. A summary of the modal frequencies is shown in Table 4.

Mode description	Iso #1 analysis frequency	Iso #2 analysis frequency
cab pitch	1.90	1.80
bounce	2.55	2.30
tractor pitch	3.04	2.89
counter-pitch	3.77	3.75
frame bending	6.29	6.28

Table 4: Predictions of the prototype vehicle's over-the-road response.

6. RIDE QUALITY ASSESSMENT

The ride severity index (RSI), a weighted measure of the power of the output spectrum, was introduced in [34] and can be used to gauge the ride quality of the vehicle. Consider the following relation

$$RSI = \left[\int_{f_1}^{f_2} L(f)^2 S(f) df\right]^{\frac{1}{2}}, \qquad \text{(EQ 24)}$$

where $S(f)$ is the output power spectral density function and $f \in [f_1, f_2]$ denotes the frequency band of interest. Note that the RSI is a scalar quantity that is simply a weighted sum of the output PSD. The insertion loss factor, $L(f)$, is a quantity indicative of the human body's sensitivity to vibration and is applied as a filter to the output response. The higher the loss factor, the more sensitive the human is to the excitation [33].

	RSI at driver seat mg_{rms}	RSI at bunk mg_{rms}
Analytical	57.69	49.73
Experimental	59.32	50.99

Table 5: Ride quality for nominal configuration.

6.1 Experimental results

Three different tests were conducted, and within each test, eight different runs were performed. In the odd numbered runs of each test, data was collected as the vehicle traveled southbound along I-25, from mile marker 175 to 141. In the even numbered runs, data was collected as the vehicle traveled northbound along I-25, from mile marker 141 to 174. In each run of a particular test, time series ensembles of the sensor signals were averaged to obtain auto and cross correlation functions. The auto correlation functions were then used to compute power spectral densities (PSD's), from which a measure of the ride quality at the driver seat and bunk were determined.

6.2 Analytical results

To assess the ride characteristics of the prototype vehicle, the procedure discussed in [34] was employed here. The mass, damping, and stiffness matrices representing the vehicle from the finite element model were imported into the MATLAB environment. Transfer functions representing the output accelerations at the driver seat and bunk due to input excitation from the road surface at the axles were then computed.

An analytical model of the frequency spectrum of the road surface at a constant speed v_o, given by

$$\Phi(f) = \frac{v_o c}{(2\pi f)^2}, \qquad \text{(EQ 25)}$$

was then applied to recover PSD responses at the output locations of interest [37,41]. There was some discrepancy in the literature, however, about the value of the scale factor, c, for a paved road surface. In addition, the amount of correlation between the excitation at the left and right tracks of the vehicle was also an unknown quantity. This must be determined, because it dictates how much asymmetrical behavior will occur while the vehicle is in operation. In short, model validation can be inexact when the form of the input is unknown. Therefore, part of the reconciliation effort went into identifying the form of the road surface input so that it matched the measured road surface of I-25.

The ride severity was calculated both experimentally and analytically, for the three vehicle configurations. The results are tabulated in Tables 5-7. Experimentally, it is evident that the ride quality at the driver seat has improved by approximately 20% due to the addition of the cab isolation system, but remains unchanged at the bunk. Furthermore, the location of the isolation system does not affect the experimental measurements. Similar results are

	RSI at driver seat mg_{rms}	RSI at bunk mg_{rms}
Analytical	57.49	55.26
Experimental	50.05	48.30

Table 6: Ride quality for Iso #1 configuration.

	RSI at driver seat mg_{rms}	RSI at bunk mg_{rms}
Analytical	51.18	49.01
Experimental	50.50	47.86

Table 7: Ride quality for Iso #2 configuration.

predicted by the computer model only when the isolation system has been moved forward. While the isolation system is positioned at the rear of the integrated cab, no improvement in ride is predicted.

Figures. 82 and 83 illustrate the vertical PSD response at the driver seat from the measured test results and analytical predictions, respectively. There are several discrepancies between the experimental results shown in Fig. 82 and the analytical results shown in Fig. 83. First, the predicted bounce mode occurs at a higher frequency than measured in the test. As discussed above, this is because the test results for this mode were somewhat suspect, due to insufficient excitation of the bounce mode for accurate measurement. Second, all predicted dynamic modes increased in frequency when the isolation system was introduced (see Table 4). This was not the case, however, for the experimental test results. As illustrated in Fig. 82, the cab isolation system reduces the tractor pitch mode at 2.75 Hz, but leaves the other modes unaffected, implying that the response of the cab isolation system is uncoupled from the dynamics of the rest of the vehicle. In addition, the experimental frequencies appear independent of the physical location of the isolation system. In the model, the modes near 2 Hz shift down in frequency as the isolation system is moved forward; this makes sense because as the system moves forward, the resultant load on the isolation system increases. Third, the experimental results reveal a 5 dB reduction in the amplitude of the tractor pitch mode due to the cab isolation system. The analytical model, however, only predicts a 3 dB reduction.

7. CONCLUSIONS

A computer model of the DOE tractor/trailer has been validated using a combination of modal and road test data. Experimental results from each test were shown to be quite different due to the high degree of nonlinearity present in the dynamics of heavy trucks. As a result, model reconciliation efforts proved to be anything but straightforward. Even so, the computer model proved invaluable in explaining many complex features of heavy truck dynamics.

Ride quality has been measured both experimentally and analytically, with and without the use of a cab isolation system. When considering ride quality, the pitch mode at 2.75 *Hz* is the only major contributor, as evidenced by the magnitude of the PSD response in Fig. 82. The analytical model does a good job of predicting the over-the-road response of this mode, leading to an adequate prediction of ride quality. However, while the computer model predicts an overall ride severity index comparable to what was experimentally measured, it has limitations when predicting the overall PSD response. This can be attributed to: uncertainty in the road input, inadequate excitation of the bounce mode during road testing, and the presence of nonlinearities in the vehicle response.

As a general observation, the work presented here makes a strong argument about the need for operational testing. Without it, the only means of verifying a computer model would be the laboratory-based modal tests. The level of disparity shown here between responses due to low- and high-level excitations makes this approach to model validation clearly inadequate. Moreover, this observation should not be confined to the study of heavy truck dynamics. Automobiles, rockets, missiles, *etc*. are subject to the same degree of nonlinearity; this should be addressed in the modeling effort of these systems as well.

8. REFERENCES

32. Dohrmann, C.R., "User's Manual for PESTDY," memo to Distribution, Sandia National Laboratories, April 22, 1996.

33. Evaluation of Human Exposure to Whole-Body Vibration," International Organization for Standardization, ISO 2631/1-1985(E).

34. Field, R.V. Jr., J.E. Hurtado, T.G. Carne, and C.R. Dohrmann, "Structural Dynamics Modeling and Testing of the Department of Energy Tractor/Trailer Combination," *Proceedings of the 15th International Modal Analysis Conference*, Orlando, FL, February, 1997, pp. 1994-2000.

35. Flower, W., "Analytical and Subjective Ride Quality Comparison of Front and Rear Cab Isolation Systems on a COE Tractor," *Society of Automotive Engineers*, No. 780411, pp. 1917-1929, 1978.

36. Foster, A.W., "A Heavy Truck Cab Suspension for Improved Ride," *Society of Automotive Engineers*, No. 780408, pp. 1899-1916, 1978.

37. Gillespie, T.D., *Fundamentals of Vehicle Dynamics*, Society of Automotive Engineers, 1992.

38. Gillespie, T.D., "Heavy Truck Ride, Society of Automotive Engineers, The Thirty-First L. Ray Buckendale Lecture, SP-607, 1985.

39. Gillespie, T.D., "Mechanics of Heavy-Duty Trucks and Truck Combinations", *University of Michigan Transportation Research Institute course notes*, July, 1992.

40. James, G.H., T.G. Carne, and J.P. Lauffer, "The Natural Excitation Technique (NExT) for Modal Parameter Estimation for Operating Structures," *International Journal of Analytical and Experimental Modal Analysis*, Society of Experimental Mechanics, Vol. 10, No. 4, October, 1995.

41. Soong, T.T. and M. Grigoriu, *Random Vibration of Mechanical and Structural Systems*, Prentice-Hall, Inc., 1993.

RVF: 9234

Copies to:

6300	D.E. Ellis	MS0766
6303	A.K. Moonka	MS0767
6312	H.J. Abeyta	MS0767
6313	R.G. Baca	MS0790
6313	J.J. Roesch	MS0790
6314	B.D. Boughton	MS0767
6314	B.W. Marshall	MS0767
9117	H.S. Morgan	MS0443
9234	C.R. Dohrmann	MS0439
9234	R.V. Field, Jr.	MS0439
9234	D.R. Martinez	MS0439
9741	T.J. Baca	MS0557
9741	P.S. Barney	MS0557
9741	T.G. Carne	MS0557
9741	J.E. Hurtado	MS0557

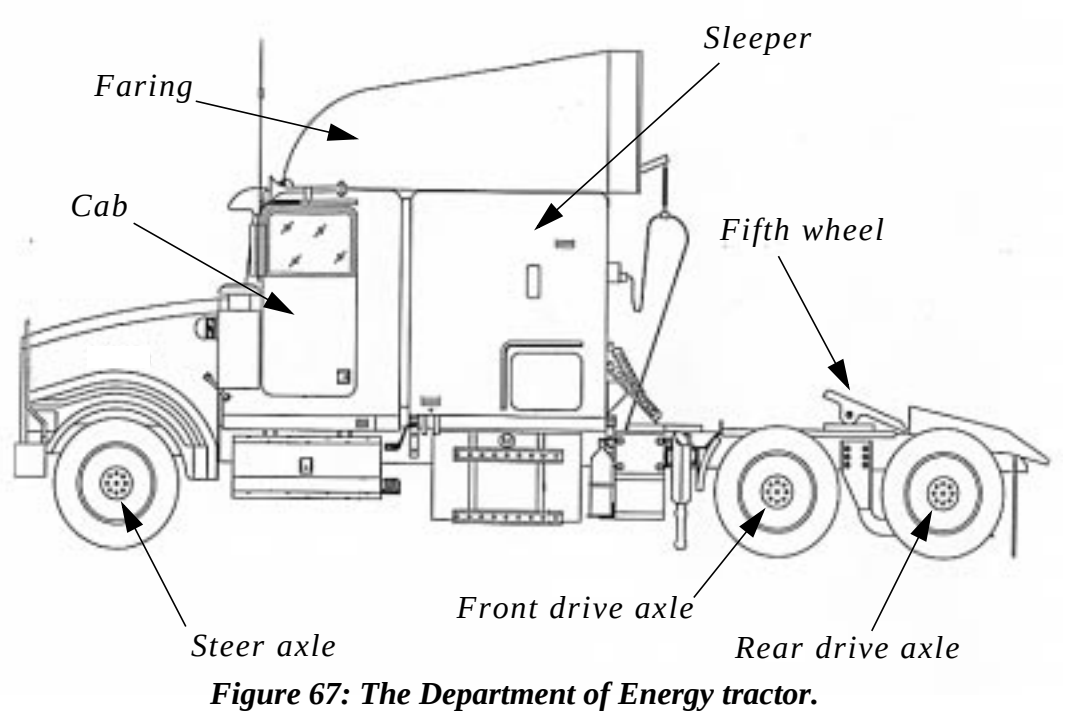

Figure 67: The Department of Energy tractor.

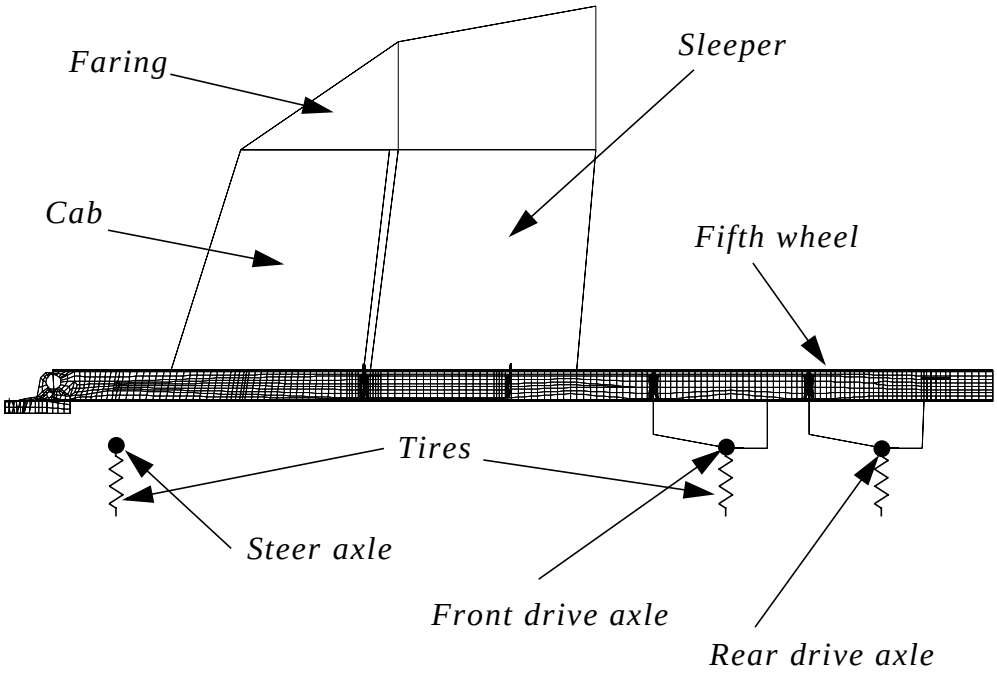

Figure 68: MSC/NASTRAN model of the DOE tractor.

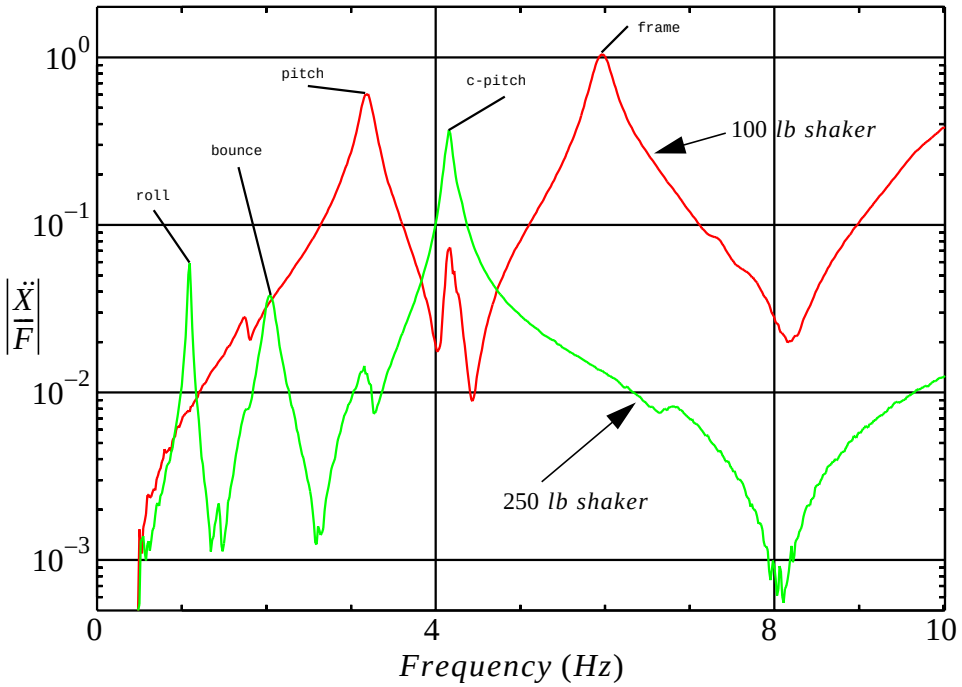

Figure 69: Experimental FRF from modal tests.

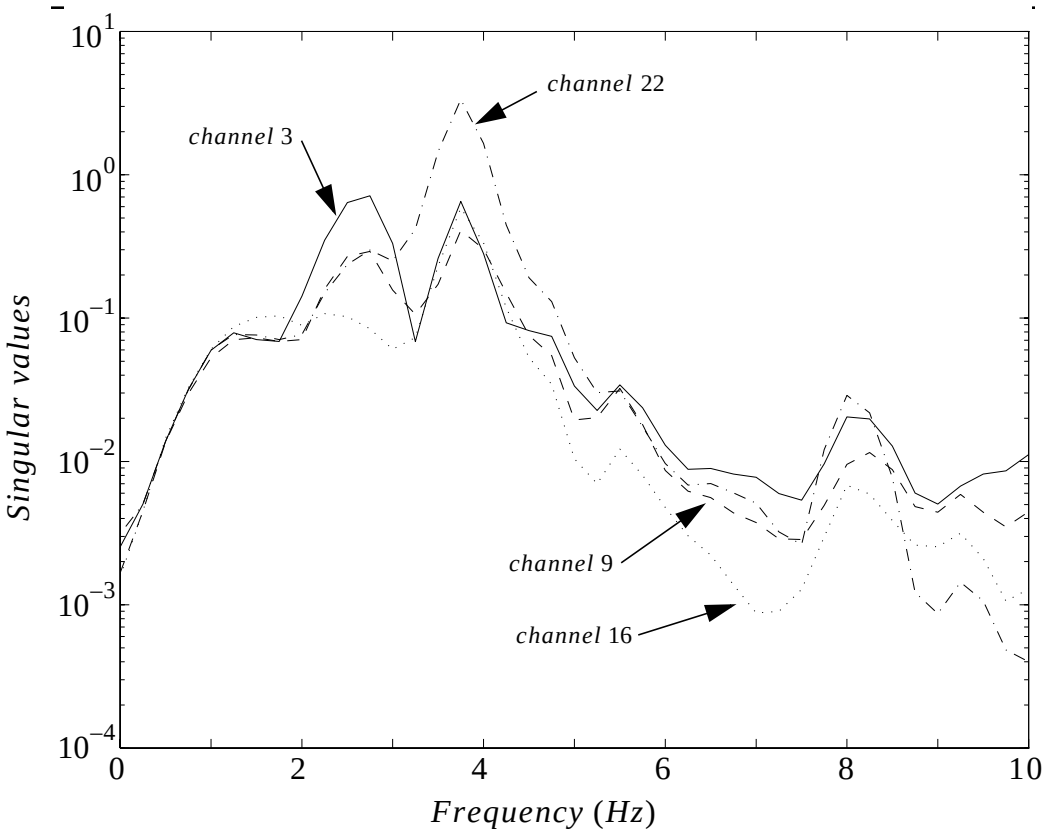

Figure 70: Experimental complex mode indicator function from natural excitation tests.

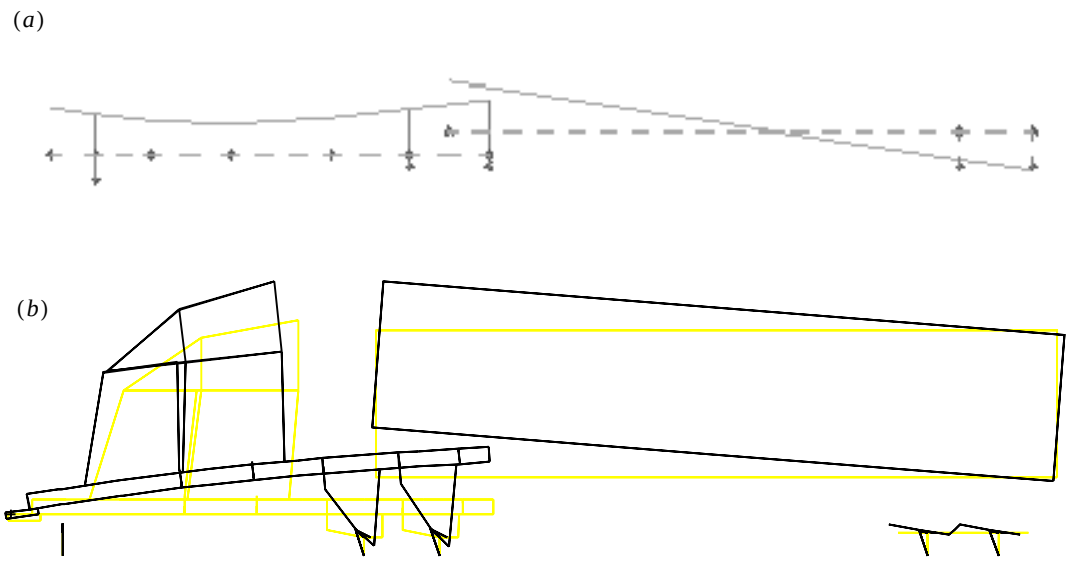

Figure 71: Bounce mode, experimental, (a), and analytical, (b).

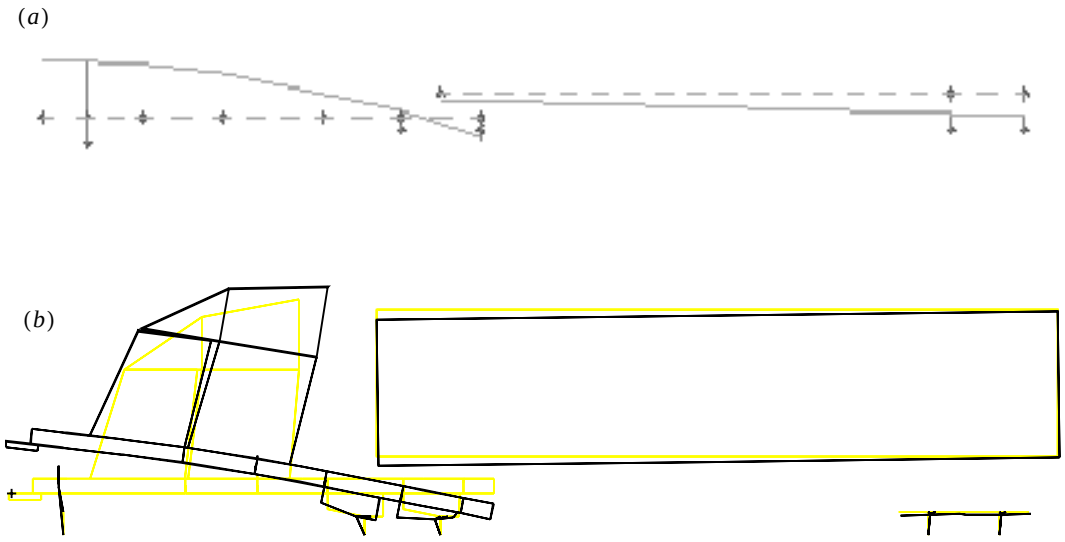

Figure 72: Tractor pitch mode, experimental, (a), and analytical, (b).

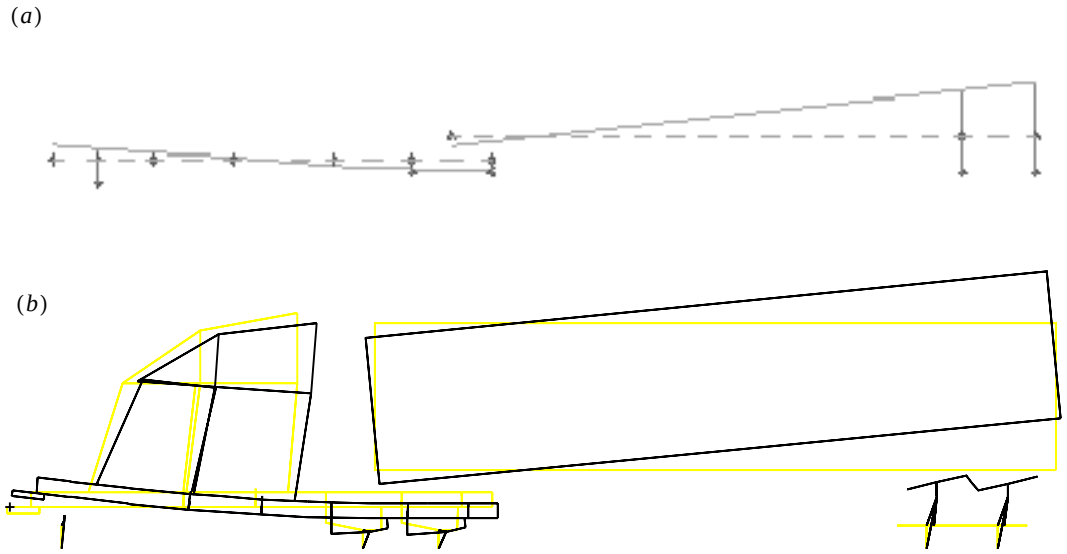

Figure 73: Counter-pitch mode, experimental, (a), and analytical, (b).

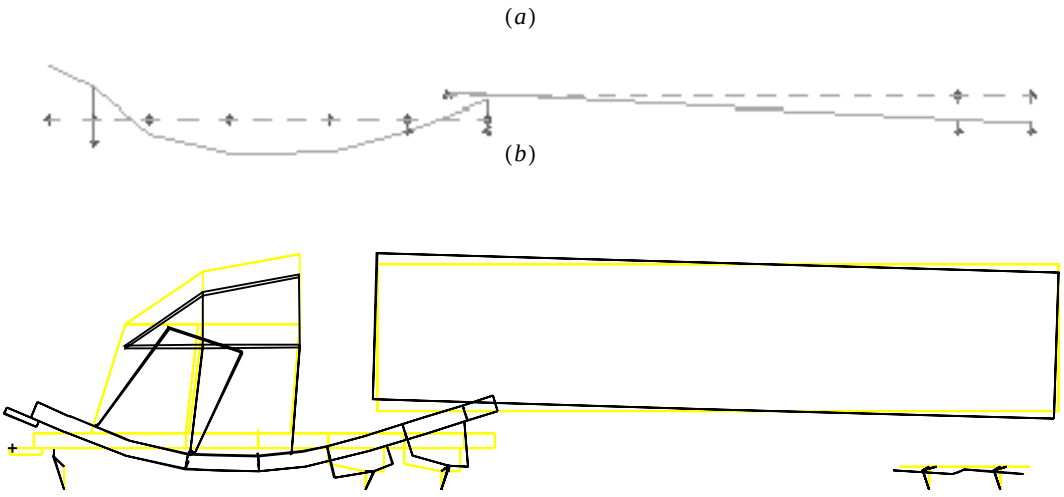

Figure 74: Frame bending mode, experimental, (a), and analytical, (b).

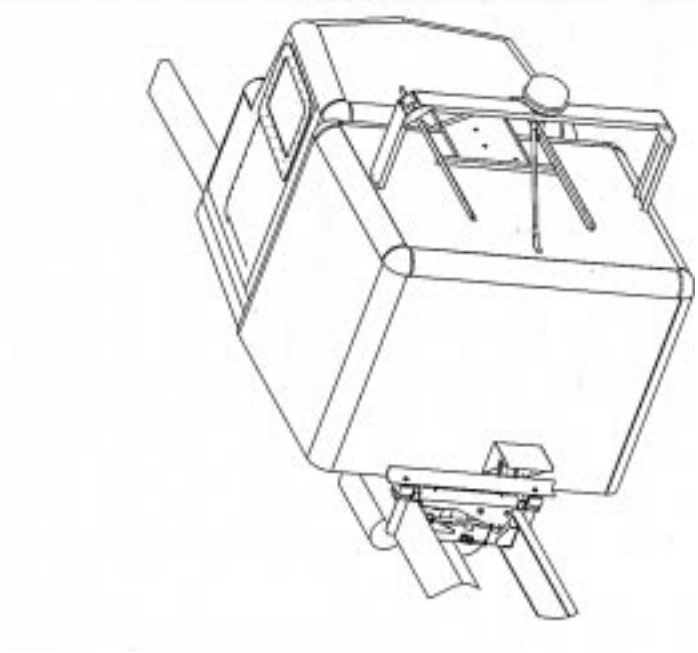

Figure 75: The engineering prototype.

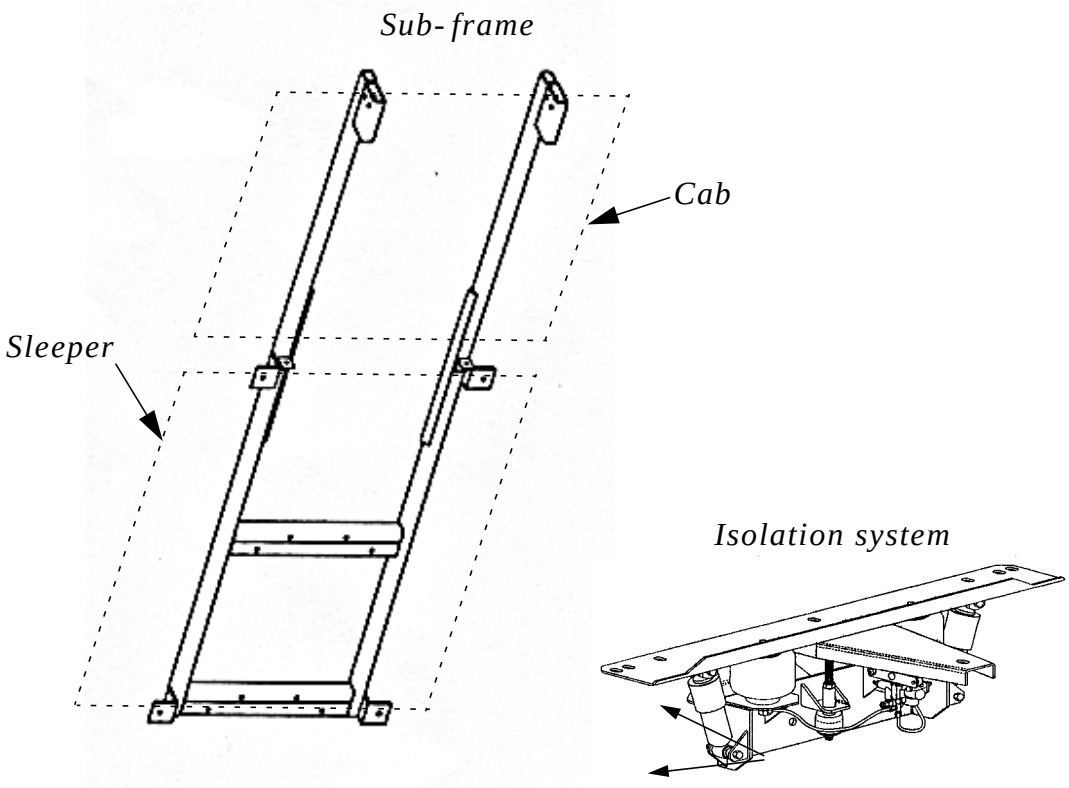

Figure 76: The cab sub-frame and isolation system.

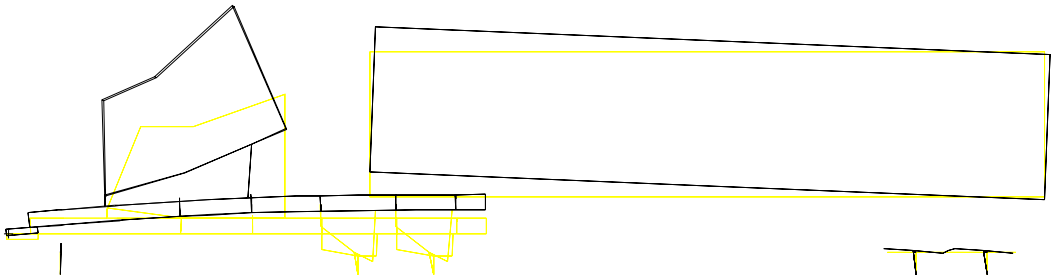

Figure 77: Predicted cab pitch mode of prototype vehicle.

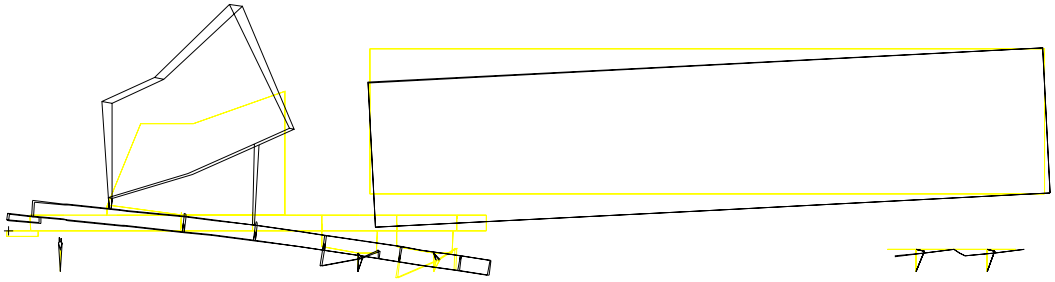

Figure 78: Predicted bounce mode of prototype vehicle.

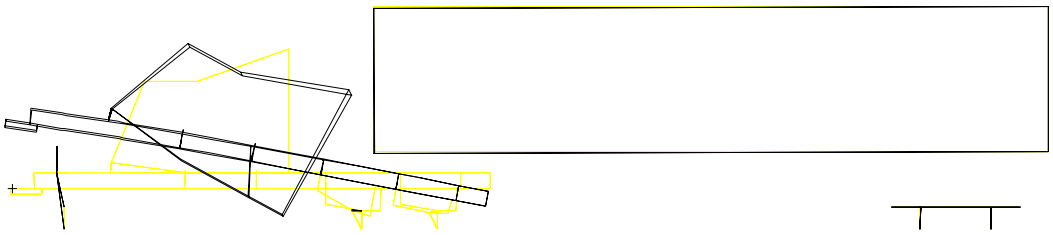

Figure 79: Predicted tractor pitch mode of prototype vehicle.

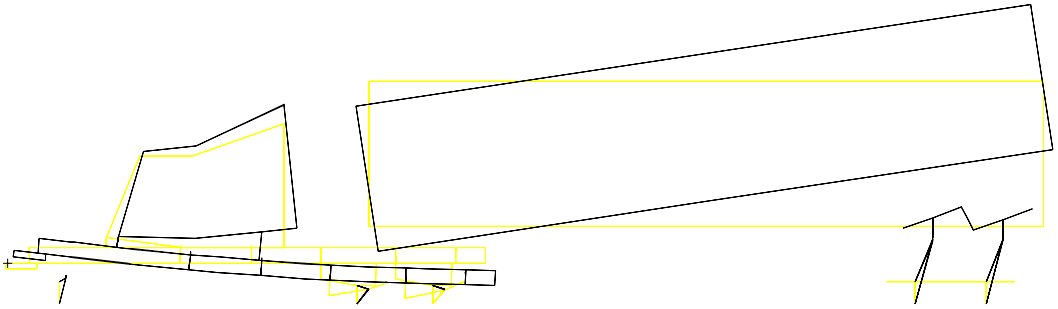

Figure 80: Predicted counter-pitch mode of prototype vehicle.

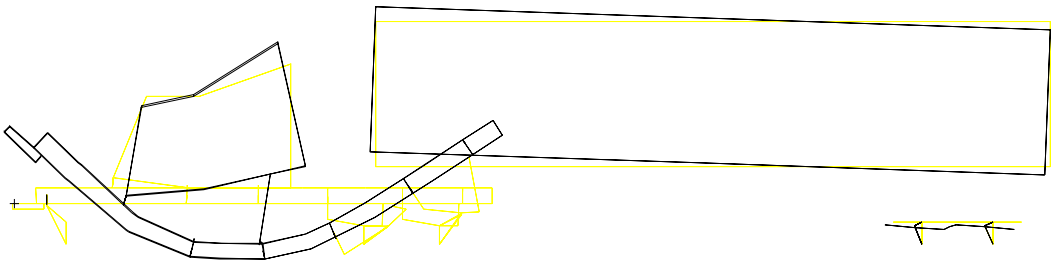

Figure 81: Predicted frame bending mode of prototype vehicle.

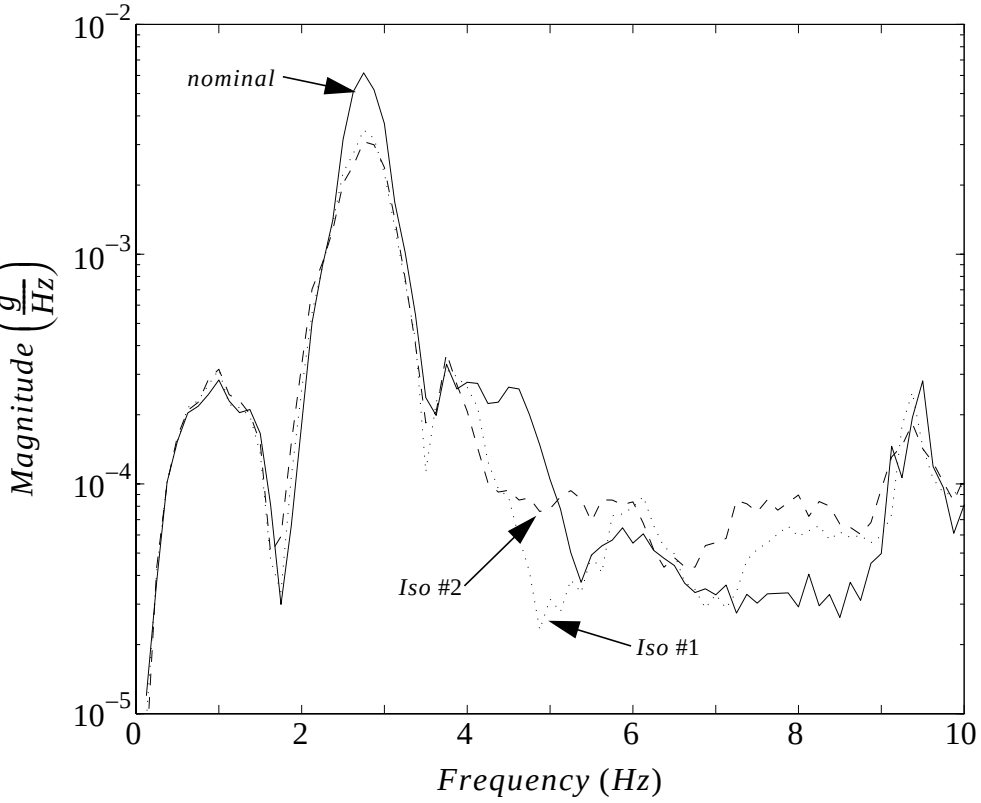

Figure 82: Measured PSD response at driver seat.

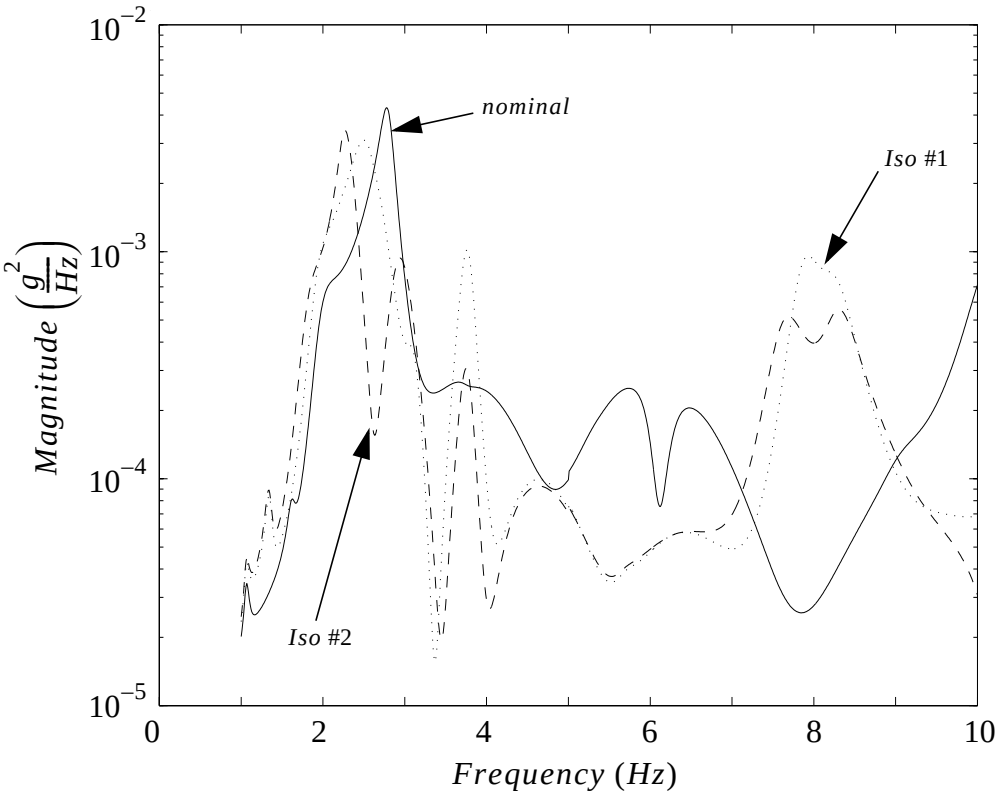

Figure 83: Predicted PSD response at driver seat.

Sandia National Laboratories

date: January 13, 1998

Albuquerque, New Mexico 87185

to: Distribution

from: R. V. Field, Jr.
Org. 9234, MS 0439

subject: Analytical assessment of proposed four-point cab isolation system

1. Summary

During the past two years, Sandia has constructed finite element computer models capable of predicting ride characteristics of tractor/trailer vehicles [42-45]. This information has proved invaluable in the design process for the next-generation fleet of DOE vehicles to be constructed in the following years. Link Manufacturing, Ltd., has asked Sandia to perform a similar ride assessment study to help examine the potential of their four-point cab isolation system for improved truck ride. The preliminary work presented here illustrates that the proposed design for a four-point isolation system will not improve the ride quality of the vehicle. Recommendations based on analysis are made, however, that may help improve the design.

2. Finite Element Model

The finite element model of Link's tractor, coupled with a typical trailer, is shown in Fig. 84. The only differences between this model and previous DOE models are the mass

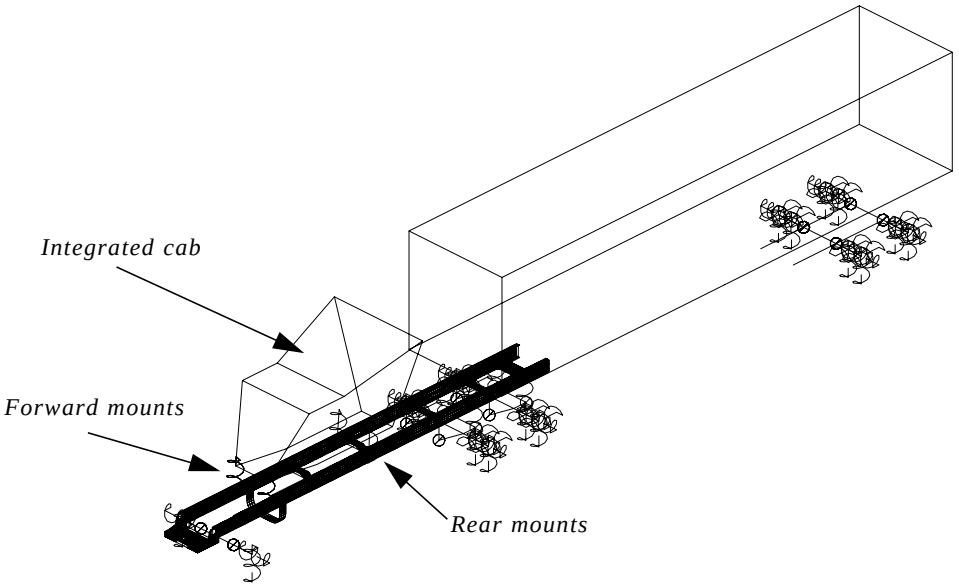

Figure 84: MSC/NASTRAN model of tractor/trailer.

	Rear mount		Front mount	
cab mass	stiffness	damping	stiffness	damping
2850 *lbs*	306.4 *lb/in*	12.2 %	516.4 *lb/in*	12.2 %

Table 1: Cab mass and isolation system parameters used.

properties of the integrated cab and the isolation systems used to mount the cab to the vehicle frame. These differences are listed in Table 1. Individuals interested in the details of the development of the model are referred to [44].

Spring rates for the front and rear mounts were determined through a combination of data supplied by Link, Firestone Industrial Products (the airspring manufacturer), and engineering judgement. To determine the stiffness value, apply

$$k = P_{a1}\left[A_c\left(\frac{V_1}{V_c}\right)^{1.38} - A_e\left(\frac{V_1}{V_e}\right)^{1.38}\right] - 14.7(A_c - A_e), \qquad \text{(EQ 26)}$$

where P_{a1} and V_1 are the absolute pressure and volume of air in the airspring at equilibrium, A_c and A_e are the cross-sectional areas of the spring during compression and extension, respectively, and V_c and V_e represent the volume of air in the airspring during compression and extension, respectively [46].

The damping characteristics of the mounts were deduced through judgement alone. Assume a damped sinusoidal response

$$y = e^{-\zeta\omega_n t_o}\sin\omega_d t = e^{-\zeta 2\pi f_n t_o}\sin\omega_d t = e^{-\zeta 2\pi \frac{t_o}{T}}\sin\omega_d t, \qquad \text{(EQ 27)}$$

where ζ is the critical damping ratio, ω_n is the natural frequency of oscillation in *rad/sec*, and t_o is the time at which the system response is "damped out". Typical isolation systems appear to damp out after 3 oscillatory cycles, so let $t_o / T = 3$. Assuming "damped out" to mean when the response reaches 1/10th of its starting value, solve for the damping ratio

$$\zeta = \frac{-\ln(0.1)}{6\pi} = 0.122. \qquad \text{(EQ 28)}$$

Before proceeding into the ride assessment section, it is important to investigate the modal response of the vehicle, since the over-the-road response is a linear combination of the modes. As shown in Table 2, the vehicle with a hard-mounted cab exhibits four fundamental low-frequency modes: (1) the *vehicle bounce mode* where the entire truck bounces together on the tires and suspensions, (2) the *tractor pitch mode* where the tractor pitches about the fifth wheel (the trailer is motionless) and bounces on the steer axle, (3) the *counter-pitch mode* where the tractor and trailer are both bouncing on the tires and suspensions, but out of phase with one another, and (4) the *frame bending mode* where the cab oscillates on top of a bending frame. When the hard cab mounts are replaced with the isolation systems, new modes are introduced (one for the 2-point system and two for the

Mode	Hard mounts (*Hz*)	2-point system (*Hz*)	4-point system (*Hz*)
Vehicle bounce	2.01	1.96	1.96
Cab pitch #1	n/a	2.66	2.85
Tractor pitch	2.93	3.15	2.61
Counter-pitch	3.75	3.77	3.77
Cab pitch #2	n/a	n/a	4.31
Frame bending	5.88	6.31	6.36

Table 2: Modal frequencies of the Link vehicle.

four-point system) where the governing motion is the cab bouncing or pitching on top of the frame. Note that in general, when these cab modes are added, the other four fundamental modes are shifted slightly in frequency.

3. Ride Assessment

It has been shown both analytically and experimentally in [45] that the use of a cab isolation system at the rear of the cab can provide improvement in ride quality. Therefore, for completeness, a simulation of the Link vehicle with only the rear isolation system installed was also completed. In addition, the vehicle with no isolation effects whatsoever was also considered. All in all, three vehicle configurations were investigated: (a) hard (stiff) mounts at both the front and rear of the cab, (b) soft mounts at the rear and hard mounts at the front, and (c) soft mounts at both the front and rear. Ride assessment studies were performed of the Link vehicle using the MATLAB software package. In all cases, modal reduction techniques were applied to the full model to make it manageable in MATLAB.

Frequency response functions (FRFs), quantities illustrating the input/output characteristics of a system, were then computed. For purposes of the vehicle simulations, the inputs are located at each of the tires and the outputs are the driver seat and bunk. In order to present the data in a meaningful way for purposes of ride quality studies, the vehicle's velocity was figured into the calculations; the FRFs due to each input are weighted by a phase quantity and then summed together to form a composite FRF. For example, the response due to input at the drive axle cannot be simply added to the response due to input at the steer axle because the velocity of the moving truck causes the inputs to be out of phase with one another. In fact, they are out of phase by Δt, the time it takes for the two axles to cross over the same point on the road surface. Composite FRFs illustrating the vertical acceleration response at the driver seat are shown in Fig. 85. It is evident that while the 2-point system (isolation at the rear only) appears to reduce the vibration level at the driver seat, this four-point system actually amplifies it.

This is further illustrated in Fig. 86 where the power spectral density (PSD) response at the driver seat is plotted. This result is even more representative of the road environment

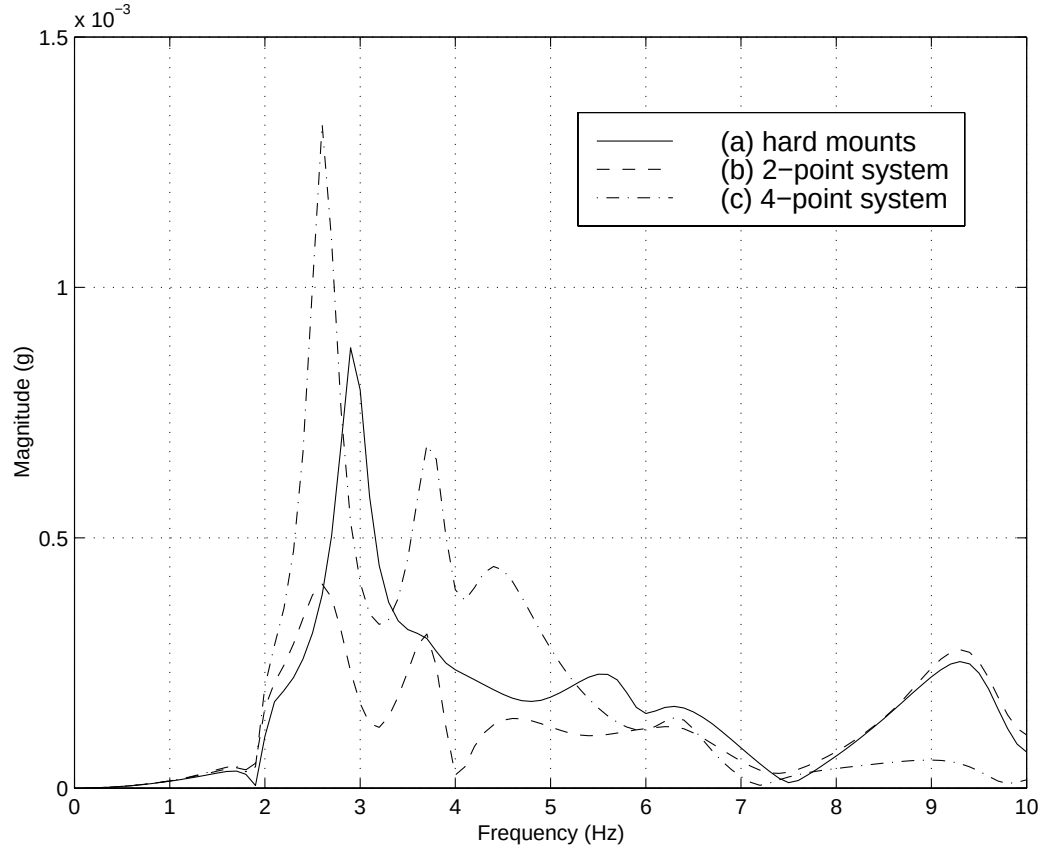

Figure 85: Composite FRF at driver seat, vertical direction.

because the actual road surface is now included in the calculations. Specifically, the PSD response is calculated as

$$S_{out}(f) = H(f)S_{in}(f)H(f)^{*}, \qquad \text{(EQ 29)}$$

where $S_{out}(f)$ is the output PSD shown in Fig. 86, $H(f)$ is the FRF matrix representing all input locations, $S_{in}(f)$ is the input PSD matrix of the road surface, and $(\cdot)^{*}$ denotes complex conjugate transpose. The derivation of $S_{in}(f)$ is tedious and discussed in detail in [43], but can be generally characterized as [47]

$$\phi(f) = \frac{v_o}{(2\pi f)^2}, \qquad \text{(EQ 30)}$$

for a vehicle traveling at a constant velocity v_o.

From the work contained in [42-45], a metric was derived to give an overall measure of ride quality. This metric has been termed the ride severity index (RSI) and is given by

$$RSI = \left[\int_{f_1}^{f_2} L(f)^2 S_{out}(f)df\right]^{\frac{1}{2}}, \qquad \text{(EQ 31)}$$

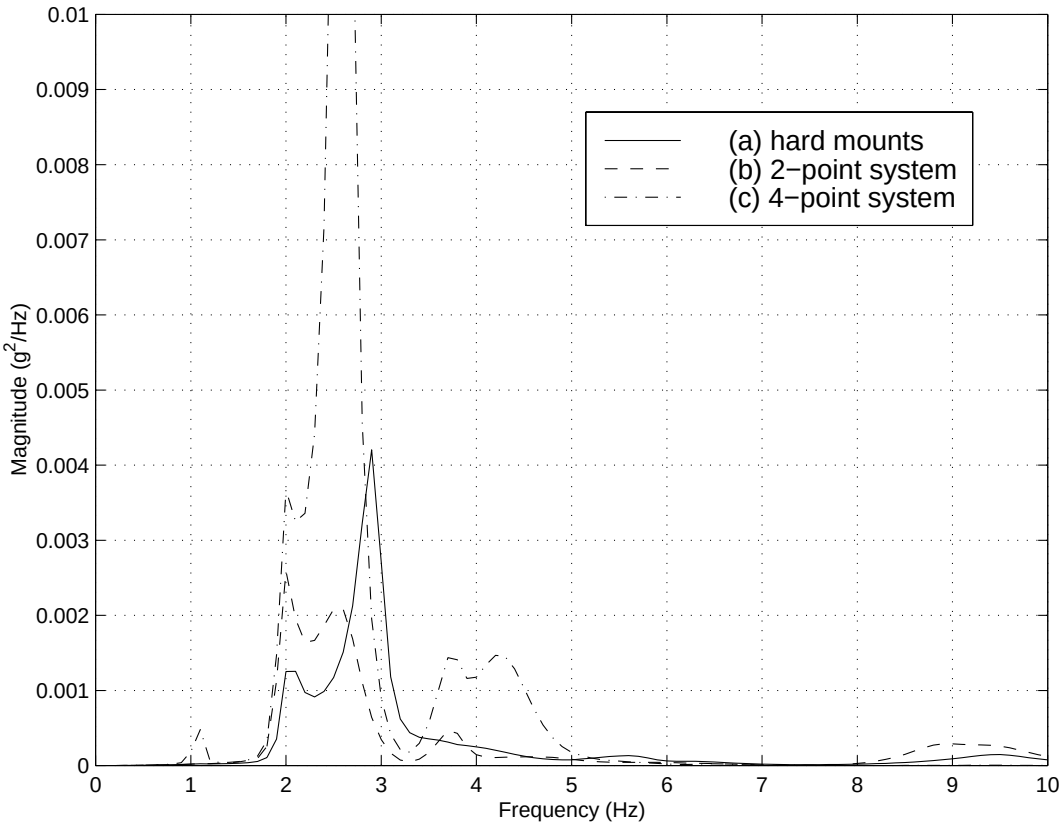

Figure 86: PSD at driver seat, vertical direction.

where $f \in [f_1, f_2]$ denotes the frequency band of interest and the insertion loss factor, $L(f)$, is a quantity indicative of the human body's sensitivity to vibration. The higher the loss factor, the more sensitive the human is to the excitation [48]. Listed in Table 3 are the RSI values for each of the three configurations. This data illustrates that the ride has improved about 12% with the introduction of the rear cab isolation system, but reiterates the fact that the ride is worse when the four-point system is introduced.

During the course of the analysis, it was apparent that the peaks of the output PSD changed dramatically with changing stiffness and damping of the isolation systems. This is expected because these peaks represent contributions from each of the modes of Table 2. As a general rule, softer airsprings will drive the cab isolation modes down in frequency, while stiffer ones will drive them up in frequency. In addition, the closer these new modes are to the four fundamental modes, the more they alter the fundamental response. Specifically, if a mode is placed between (in frequency) two of the fundamental modes, it will cause the

Hard mount	2-point system	4-point system
52.3 *mg rms*	50.7 *mg rms*	84.1 *mg rms*

Table 3: Ride severity indices (RSI) for Link vehicle.

lower fundamental mode to drop in frequency and the higher fundamental mode to raise in frequency.

When considering ride quality, it is important to keep as much of the system's energy out of the frequency range where vibration is most irritating to the human body (between 2 *Hz* and 8 *Hz* - see [48]*).* Unfortunately, the dynamics of most heavy trucks are such that the fundamental vehicle modes occur right in the middle of this. In addition, the characteristics of the cab isolation systems studied here were such that additional modes were introduced into this same frequency range. One possible solution to improve the performance of the four-point system is to make the suspension as soft as possible, leaving the four fundamental vehicle modes unchanged. In addition, the modes introduced will not add energy into the system in that same frequency band. If soft enough, the isolation system will truly isolate the cab - all higher-frequency response will be isolated. While it may be possible to set the stiffness of the cab suspensions so that the cab modes lie between the fundamental vehicle modes *and* the ride is improved, this is not recommended because it is very vehicle-specific; the designer would need accurate *a priori* knowledge of where these fundamental modes are in frequency - a luxury he may not have.

4. Conclusions and Recommendations

A finite element computer model of the Link tractor/trailer has been constructed and used to predict the potential changes in ride quality due to the addition of cab isolation systems. It has been shown that about 15% improvement in ride quality can be expected when the hard mounts are replaced with a rear isolation system. Adding the proposed isolation system to the front, however, degrades the ride of the vehicle. Although it may be possible to choose a suspension design that will improve the ride, this is vehicle-specific and therefore will not be robust to manufacturing uncertainty, choice of vehicle suspension systems, cargo weight, etc. To avoid this, the analyst recommends the designers look to make the four-point suspension system as soft as possible to let it behave as a true isolation system.

5. References

42. Field, R.V. Jr., "Optimal Cab Suspension for Next-Generation Tractor," October 17, 1996.

43. Field, R.V. Jr., "DOE Tractor Trailer Rough Road Simulation," October 17, 1996.

44. Field, R.V. Jr. and C.R. Dohrmann, "DOE Tractor Trailer Modal Test/Analysis Reconciliation." October 22, 1996.

45. Field, R.V. Jr., J.E. Hurtado, and T.G. Carne, "Analytical and Experimental Assessment of Heavy Truck Ride," October 15, 1997.

46. Notes from Ken Vande Brake.

47. Gillespie, T.D., *Fundamentals of Vehicle Dynamics*, Society of Automotive Engineers, 1992.

48. Evaluation of Human Exposure to Whole-Body Vibration," International Organization for Standardization, ISO 2631/1-1985(E).

RVF

Distribution

6313	R.G. Baca	MS0790
6314	B.D. Boughton	MS0767
9234	R.V. Field, Jr.	MS0439
9234	D.R. Martinez	MS0439
9741	T.G. Carne	MS0557

K. Vande Brake
S. Vander Kooi
Link Manufacturing, Ltd.
223 15th St. NE, Box 68
Sioux Center, IA 51250

Distribution

MS0321	09200	Camp, William J.
MS0437	09118	Thomas, Robert K.
MS0439	09234	Dept. Archive
MS0439	09234	Martinez, David R.
MS0439	09234	Dohrmann, Clark R.
MS0439	09234	Field, Richard V. (5)
MS0443	09117	Morgan, Harold S.
MS0557	09119	Baca, Thomas J.
MS0557	09119	Barney, Patrick S.
MS0557	09119	Boughton, Barry D.
MS0557	09119	Carne, Thomas G.
MS0766	06301	Abeyta, Henry J.
MS0766	06300	Ellis, Doris E.
MS0766	06303	Moonka, Ajoy K.
MS0790	06313	Baca, Robert G.
MS0790	06313	Roesch, Joseph J.
MS0841	09100	Hommert, Paul J.
MS1003	09611	Hurtado, John E.

MS9018	Central Technical Files, 8940-2 (1)
MS0899	Technical Library, 4916 (2)
MS0619	Review & Approval Desk, 12690 (2) For DOE/OSTI

Richey, Richard H.
Sandoval, Nick A.
U.S. Department of Energy
Albuquerque Operations Office
Pennsylvania & H Street
Kirtland Air Force Base
Albuquerque, NM 87116